Targeting Downstream Effectors of IGF/Insulin Signaling System in Human Breast Cancer

A DISSERTATION
SUBMITTED TO THE FACULTY OF
UNIVERSITY OF MINNESOTA
BY

Yuzhe Yang

IN PARTIAL FULFILLMENT OF THE REQUIREMENTS
FOR THE DEGREE OF
DOCTOR OF PHILOSOPHY

Douglas Yee, Advisor

August 2015

Acknowledgements

First and foremost, I want to thank my advisor Dr. Douglas Yee, for his continuing and fatherly encouragement, tremendous guidance, and financial support throughout my entire Ph.D. training at the University of Minnesota. During the five years that he has been my advisor, he has served as an incredible inspiration and talented mentor in my scientific endeavors. He has also provided a lot of guidance and advice on my career development. As a student of him, I not only have developed expertise in several areas, but also have learned some important skills in research. I am very grateful to have had the opportunity to know and work with such an excellent physician, scientist, and professor.

I also would like to thank Dr. Carol Lange, Dr. Sundaram Ramakrishnan, Dr. Gibson Wood, and Dr. Peter Bitterman at the University of Minnesota, for taking time from their busy schedules to review my proposal and thesis, participate in my annual committee meetings and final defense, and offer valuable suggestions towards my research and career progress.

I want to express my sincere thanks to a number of individuals supported my progress and gave me valuable advice throughout my research training. Thank you to all Yee lab members, both past and present. I also would like to thank Dr. Deepali Sachdev, Dr. Todd Knutson, Caroline Diep, Dr. Wenqi Han, and Dr. Siyan Cao for their help and support in my Ph.D. life. I would like to extend a special thank you to Dr. Hua Zhang for both your technical and professional guidance. Without your assistance and encouragement, I would not be where I am as a scientist today.

Last but not least, I would like to thank all of the people who have supported me behind the scenes. To my parents and grandfather, thank you for your love, continuous support, encouragement, and understanding throughout this process. To my parents in-law, thank you for your wonderful care of Clover. I would like to express my dearest thanks to my husband Yingjie for always being there for me, to listen, encourage, and motivate me.

Finally, I would like to thank my little daughter Clover for bringing so much happiness and joy into our life. My career and life are more meaningful because of the love and care that I have been privileged to receive from my whole family.

Dedication

This thesis is dedicated to my daughter Clover, my mother Yajun, my father Guolin, and my husband Yingjie.

Abstract

Transmembrane growth factor receptors mediate signaling through multiple intracellular pathways. In breast cancer cells, the type I insulin-like growth factor receptor (IGF-IR) has been implicated of tumorigenicity, proliferation, and metastasis. However, clinical trials with anti-IGF-IR monoclonal antibodies have generally been disappointing, partially due to lack of predictive biomarkers or adaptive compensational pathways activated when IGF-IR is blocked. To determine whether IGF-IR inhibition could be enhanced by disrupting other pathways, here we sought to investigate novel molecular targets downstream of IGF-IR signaling system and evaluate combination efficacy in estrogen receptor (ER) positive, basal-like, and endocrine resistant human breast cancer cell lines *in vitro*.

The first part of this dissertation focuses on characterization of the mechanism of action and evaluation of therapeutic efficacy of a novel insulin receptor substrate 1 and 2 (IRS1/2) targeting compound NT157 in multiple breast cancer types. IRS1/2 transduce signaling from IGF-IR and insulin receptor (InR) to mediate the IGF effects on breast cancer cell biology. IRS-1 plays a critical role in cancer cell proliferation in ER positive breast cancers while IRS-2 is the predominate isoform in many basal-like breast cancers and is associated with motility and metastasis. NT157, a small-molecule tyrphostin, has been shown to downregulate IRS proteins in several model systems. In ER positive and basal-like breast cancer cells, NT157 treatment suppressed IRS protein expression in a dose dependent manner. NT157 treatment did not affect IGF-I, IGF-II, and insulin

induced activation of phosphatidylinositol-4,5-bisphosphate 3-kinase (PI3K) and mitogen-activated protein kinase (MAPK) in the short term, but longer exposure to NT157 inhibited the activation of these signaling pathways. The ability of NT157 to induce serine phosphorylation of IRS proteins was dependent on MAPK activation. Serine phosphorylation resulted in disassociation between IRS proteins and their receptors resulting in IRS degradation. In ER positive breast cancer cells, NT157 also resulted in cytoplasmic ERα downregulation likely because of disruption of an IRS-1-IGF-IR/InR/ERα complex. NT157 decreased S phase fraction after IGF/insulin treatment in ER positive breast cancer cells with inhibition of monolayer and anchorage-independent growth. NT157 downregulation of IRS protein expression also sensitized ER positive breast cancer cells to rapamycin. Moreover, NT157 inhibited the growth of tamoxifen resistant ER positive breast cancer cells. In basal-like breast cancer cells, NT157 repressed the proliferation (G2/M abrogation) and migration through downregulation of IRS1/2 protein. Given that both IGF-IR and InR play a role in cancer biology, targeting of IRS adaptor proteins may be a more effective strategy to inhibit these receptors.

In the second part of this dissertation, we highlight an amino acid transporter – xC^- to be a novel co-target in addition to IGF-IR targeted therapies in ER positive breast cancer cells. IGF-I stimulates growth of normal and malignant cells. Increased uptake of amino acids after activation of IGF-IR signaling has been well characterized. xCT (*SLC7A11*) encodes the functional subunit of the heterodimeric plasma membrane

transport system xC^- critical for the cellular uptake of cystine, generation of glutathione, and modulation of cellular redox control. Here, we show that IGF-I induced xCT mRNA, protein expression, and function in ER positive breast cancer cell lines in an IRS-1 dependent manner. IGF-I further controlled cellular redox level through the xC^- transporter. IGF-I-stimulated monolayer and anchorage-independent growth was suppressed by reducing xCT expression or by treating cells with the xC^- chemical inhibitor sulfasalazine (SASP). Anchorage-independent growth assays showed that disruption of xC^- function by SASP sensitized cells to anti-IGF-IR inhibitors (monoclonal antibody huEM164 and tyrosine kinase inhibitor NVP-AEW-541). The growth suppressive effects of SASP were reversed by the ROS scavenger N-acetyl-L-cysteine. Thus, IGF-I promotes the proliferation of ER positive breast cancer cells by regulating xC^- transporter function to protect cancer cells from ROS in an IRS-1 dependent manner. Our findings also imply that inhibition of xC^- transporter function combined with anti-IGF-IR agents may have synergistic therapeutic effect.

The third part of this dissertation aims at thoroughly investigating the IGF's regulation on Nuclear factor-erythroid 2-related factor 2 (Nrf2) in ER+ breast cancers and evaluating Nrf2 as a target in triple negative / basal-like (TNBC) breast cancers. Nrf2 is a key transcriptional activator that mediates cellular antioxidant response by initiating expression of various anti-oxidative and anti-inflammation genes. Constitutive stabilization of Nrf2 has been observed in many human cancers and confers chemo- and radio-resistance of cancer cells. We examined Nrf2 expression and function in a panel of

breast cancer cell lines. mRNA expression of Nrf2 was higher in the TNBC/basal-like cell lines MDA-MB-231 and MDA-MB 436 compared to immortalized breast epithelial cells and other types of breast cancers. In estrogen receptor positive (ER+) breast cancer cells MCF-7 and T47D where basal level of Nrf2 were low, IGF signaling system regulated Nrf2 expression, nucleus translocation and ARE-binding capability. Downregulation of Nrf2 sensitized ER+ cells' response towards irradiation in the presence of IGF-I ligand. shRNA knock-down of Nrf2 in MDA-MB-231 and MDA-MB-436 TNBC cells showed decreased mRNA expression of multiple Nrf2 regulated anti-oxidant and pentose phosphate pathway genes, enhanced basal levels of cellular reactive oxygen species, impaired mitochondrial function and reduced S phase entry. Cells with decreased Nrf2 had reduced cell growth in monolayer, anchorage independent, and 3-dimensional growth assays. In addition, Nrf2 suppression reduced cell migration. Nrf2 down-regulated MDA-MB-231 cells also showed increased response towards ionizing radiation in clonogenic and soft agar assays. Furthermore, reduced Nrf2 expression decreased the number of stem-like ($CD44^+/CD24^-$) population in MDA-MB-231 cells possibly through xC^- transporter regulation. Thus, IGF signaling induces Nrf2 expression and function, which suggests Nrf2 could be a therapeutic co-target in combination to anti-IGF treatment. Nrf2 regulates various aspects of the malignant phenotype in TNBC that inhibition of Nrf2 might be a therapeutic option for TNBC.

Taken together, the data in this thesis demonstrate that IGF-IR activation stimulates multiple downstream effectors important for breast cancer cell biology. Inhibition of

selected downstream signaling molecules alone or in combination with anti-IGF-IR drugs is likely to better therapeutic outcomes in breast cancers.

Table of Contents

List of Figures

List of Tables

Chapter 3

Chapter 4

Chapter 1

Introduction

Yuzhe Yang and Douglas Yee
Targeting insulin and insulin-like growth factor signaling in breast cancer.
J Mammary Gland Biol Neoplasia. 2012; 17**:** 251-261.

Introduction

Breast cancer is the most common cancer and the second leading cause of cancer death among women in the US. In 2015, about 231,840 breast cancer cases will be newly diagnosed and about 40,290 women will die from this disease (www.cancer.org). In the past decade the death rate from breast cancer is decreasing, even though breast cancer incidence remains high. The wider use of adjuvant therapy for operable breast cancer partially accounts for this improvement. Targeting the estrogen receptor-α (ERα) has proven to be one of the most useful methods to decrease breast cancer death mortality [1]. Targeting human epidermal growth factor receptor 2 (Her2) with trastuzumab (Herceptin®) has also been an important advance [2, 3]. The clinical success of targeting receptors critical in breast cancer biology has underlined the importance of identifying and understanding the regulatory pathways involved in breast cancer growth and metastases. Furthermore, with the awareness of the complexity and heterogeneity of breast cancer [4], developing additional targeted therapies is critical to further improve breast cancer outcomes.

The insulin-like growth factor/insulin (IGF/insulin) system possesses potent mitogenic and pro-migratory properties and has been extensively implicated in many malignancies including breast cancer [5-7]. The type I insulin-like growth factor receptor (IGF-IR) is a component of the complex IGF/insulin signaling network. IGF-IR has been shown to deregulate cell metabolism, enhance transformation, stimulate proliferation, and promote metastasis in breast cancer [5, 6, 8-10]. Numerous lines of evidence suggest that blockade of the IGF/insulin signaling pathway inhibits growth and metastasis in multiple cancer types including breast cancer both in vitro and in vivo [8, 11-14]. Collectively, IGF-IR has been viewed as a potentially valuable target for breast cancer treatment.

The IGF/insulin system consists of three ligands, IGF-I, IGF-II, and insulin; six ligand-binding proteins, IGFBP 1-6; and 2 half transmembrane tyrosine kinase receptors (RTK), half IGF-IR and half insulin receptor (IR), that are capable of forming various types of holo or hybrid full receptors (Figure 1.1). These functional receptors are

composed of two extracellular α subunits covalently linked to two intracellular β subunits, which contain the tyrosine kinase domains. Following ligand binding to the extracellular α subunits, the IGF-IR undergoes a conformational change resulting in activation of its tyrosine kinase activity and trans-phosphorylation of the intracellular β subunits. The activated receptors then recruit and phosphorylate adaptor proteins including insulin receptor substrates (IRS 1-6) and Shc. This couples the initial ligand-binding event and further triggers multiple downstream signaling pathways, including phosphatidylinositol 3'-kinase (PI3K) and the mitogen-activated protein kinase (MAPK). These secondary messenger molecules result in stimulation of specific cellular functions, such as proliferation, apoptosis, metastasis, metabolism, angiogenesis, and drug resistance [15, 16] (Figure 1.1).

The closely related insulin receptors are expressed as two isoforms, insulin receptor A (IR-A) and insulin receptor B (IR-B) with a 12 amino acid difference in exon 11 [17]. IR-B is the major form expressed in adults and has high affinity for insulin, while IR-A, which is abundantly expressed during fetal development and is commonly overexpressed in tumors [17], can transmit signals by binding to both insulin and IGF-II [18]. Since deregulation of cellular energy metabolism has been considered as an emerging hallmark of cancer [19], IR and its related metabolic syndromes have become another major focus in the breast cancer research and treatment field. Both obesity and type 2 diabetes mellitus could lead to hyperinsulinemia, which has been reported to overactivate insulin receptors in normal breast epithelial cells [20] and in neoplastic tissues [21], increase the risk of developing breast cancer in patients with metabolic syndromes [22], promote metastatic progression, and associate with poor prognosis in breast cancer patients [23].

Strategies targeting the IGF-I/insulin system

Blockade of ligand binding

In normal physiology, insulin is produced by pancreatic β-islet cells and arrives at target tissues through the blood circulation. For IGFs, the liver is the major producer for the circulating IGF-I, but normal tissue and tumor tissue can frequently secrete both IGF-

I and IGF-II. Therefore, IGF-I and IGF-II could affect tumor biology via autocrine, paracine, and endocrine mechanisms. As mentioned above, IGF-IR and IR require ligand binding for receptor activation, thus reducing ligands levels becomes a reasonable and practical strategy to control the IGF-I/insulin signaling in neoplastic tissue. In normal physiology, reduction of insulin level is not practical because of the resultant metabolic effects on glucose control. In contrast, low levels of IGFs appear to be well tolerated in humans [24]. Since IGF-I is regulated by the hypothalamic-pituitary axis, via secretion of growth hormone, growth hormone-releasing hormone antagonists (e.g. JV-1-38 [25]) disrupting this pathway could be used to affect IGF-I levels. In addition, pegvisomant, a direct antagonist of the growth hormone receptor, has been developed to treat acromegaly and is also able to inhibit IGF-I levels in normal human subjects [26].

Another approach to reduce the levels of unbound ligands involves the use of monoclonal antibodies to neutralize extracellular IGFs. MEDI-573, a monoclonal antibody with high binding affinity for both IGFs selectively inhibits the activation of both the IGF1R and IR-A signaling pathways in vitro and in mouse models without disrupting glucose metabolism mediated by insulin and IR interaction [27]. MEDI-573 is now involved in several phase I clinical trials for different types of tumors (clinicaltrials.gov, identifier no. NCT01446159, NCT00816361). Another novel IGF ligand neutralizing antibody, BI 836845 (Boehringer Ingelheim Pharmaceuticals), was recently shown to improve preclinical antitumor efficacy of rapamycin by suppressing IGFs' bioactivity and inhibiting rapamycin-induced PI3K/AKT activation. This drug is currently in a phase I clinical trial (NCT01317420).

IGFBPs regulate IGFs' bioactivity by sequestering the peptides from binding to the receptors. Most of the IGFBPs can also act in an IGF-independent fashion. IGFBP3, in particular, has been shown to directly associate with cell surface and nuclear receptors thereby inducing antiproliferative effects and apoptosis (extensively reviewed in [28]). Thus, other approaches to reduce the ligands bioactivity may include recombinant IGFBPs, namely IGFBP3 [29, 30].

Targeting the receptors

As noted above, IGF/insulin system consists of multiple receptor tyrosine kinases and nearly all of them are targetable by either dominant negative constructs or pharmacological approaches. Traditionally, IR has not been considered the primary target due to its central role in glucose metabolism. However, accumulated data suggests IR-A may play important roles in breast cancer progression and survival [31, 32]. IR-A signaling has also been suggested as a possible mechanism of resistance to IGF-IR targeted therapies [33, 34]. Thus, developing safe therapies to control IR signaling is urgently needed. Indirectly targeting IR-A activation by downregulation of one of its ligands, IGF-II, has been shown to inhibit cancer cell growth [34]. It is possible that ligand neutralization, as opposed to receptor inhibition, could result in less disruption of glucose metabolism.

In the past several years, major effort has been directed toward targeting IGF-IR. Anti-IGF-IR monoclonal antibodies have been developed and several trials using such antibodies as single agents or in combination with other antitumor drugs are in phase I/II clinical trials. The antibodies are designed specifically to bind the α subunit of IGF-IR with high affinity, thus they do not directly affect IR-A or IR-B. This class of drugs shares similar mechanisms of action by interfering with ligand binding to both holo-IGF-IR and hybrid receptors [35], and causing receptor endocytosis and subsequent degradation in the endosome thereby inhibiting cancer cell proliferation and metastasis [36].

Figitumumab (CP-751, 871, Pfizer), a fully human IgG2 α-IGF-IR monoclonal antibody, generated enthusiasm in a randomized phase II clinical study (NCT00147537). The study showed that combined figitumumab with carboplatin and paclitaxel enhanced response rate and prolonged progression-free survival and overall survival in non-small-cell lung cancer (NSCLC). However, Pfizer discontinued two phase III figitumumab clinical trials (NCT00673049, NCT00596830) due to a failure to confirm the promising

phase II results and also observed substantial toxicity. Treatment of breast cancer patients with an aromatase inhibitor with or without figitumumab was studied but showed no benefit for the antibody. AVE1642 (sanofi-aventis), a humanized IgG1 antibody, showed promising data in preclinical studies [37, 38] but failed in its phase II clinical trials in breast cancer patients (NCT00774878). One reason for the failure might be the lack of molecular markers that predict IGF-IR sensitive tumors.

Despite these failures, there are still several currently active trials primarily aimed to evaluate IGF-IR antibody as an adjuvant agent to other antitumor drugs in many types of cancer. Ganitumab (AMG 479, Amgen), a fully humanized IgG1 antibody, is being tested in combination with cytotoxic chemotherapy, mTOR inhibitors, and hormonal therapies in various diseases including NSCLC, colorectal, pancreatic, ovarian, and breast cancer. Similar trials have been completed with the fully humanized IgG1 IGF-IR antibody cixutumumab (IMC-A12, Imclone).

Dalotuzumab (MK 0646, Merck), another humanized IgG1 antibody with promising preliminary profiles [39, 40], is currently being studied with aromatase inhibitors and the mTOR antagonist in advanced breast cancer.

The anti-IGF-IR monoclonal antibodies also share a common effect on the disruption of normal endocrine feedback systems that might have implications for phase III clinical trials. One of the common side effects using the antibodies is disruption of the negative feedback of IGF-I on growth hormone secretion by the pituitary. Administration of the antibodies results in upregulation of the growth hormone serum levels resulting in increased circulating IGF levels, hyperglycemia, and hyperinsulinemia [6]. Since the antibodies do not block IR signaling, this could explain the failure to demonstrate clinical activity when only IGF-IR signaling is disrupted. Furthermore, subsequent development of refectory tumors in IGF-IR antibody treated patients might be due to both hyperinsulinemia [41] and high free IGF [41, 42]. Certainly, activation of IR signaling could initiate pro-survival signaling to blunt the effects of cytotoxic chemotherapy. A

recent clinical trial for women with ER-positive breast cancer reported combined IGF-IR antibody with the aromatase inhibitor exemestane trended toward benefit only in patients with normal hemoglobin A1C levels, which is an indicator for insulin resistance. In IGF-IR antibody clinical trials design, patients with pre-existing insulin resistance may need to be excluded or have their hyperinsulinemia better controlled. It would be important to state that in preclinical model systems as seen with rodents, the effect of hyperinsulinemia is not seen after exposure to IGF1R monoclonal antibodies as these antibodies do not generally cross-react with murine IGF1R. Adult rodents also do not have significant level of circulating IGF-II [43], thus mouse models might not accurately model the human endocrine milieu and the effects of endocrine disruptors designed to target human receptors.

Another major class of drugs to target IGF-IR activation is small-molecule tyrosine kinase inhibitors (TKI), which compete for the ATP binding site in the catalytic domain of the β subunit of IGF-IR and IR. Most TKIs show limited selectivity of IGF-IR over IR in vitro or in vivo [44, 45]. The high degree of homology of the intracellular β subunits of the IGF-IR and IR may account for this relative lack of selectivity of the TKIs. However, this dual targeting might have some benefits given the potential role for IR in cancer. Specifically, upregulated levels of insulin after IGF1R monoclonal antibody treatment might not have as much effect on the tumor if both IGF1R and IR are blocked by a TKI. Studies showed that these TKIs inhibited IGF-IR/IR phosphorylation and AKT activation, enhanced apoptosis, decreased in vitro cell proliferation, and tumor suppression in xenograft models [40, 46, 47]. A dual IGF-IR/IR dual tyrosine kinase inhibitor BMS-754807 (BMS) showed better antitumor efficacy in combination with hormonal therapies in hormone sensitive breast cancer model systems [47]. BMS-754807 and OSI-906 are two promising examples of small molecule inhibitors, being tested in several breast cancer clinical trials.

The cyclolignan picropodophyllin (AXL1717 or PPP, Axelar) is reported to specifically inhibit IGF-IR specific tyrosine kinase activity, although the exact

mechanism is uncertain. The compound reportedly possesses both signal inhibitory properties and downregulates IGF-IR in vitro [48]. A phase I trial of this drug has been completed showing favorable safety and pharmacokinetics profiles of PPP in patients with advanced cancer (NCT01062620).

Other novel approaches to target IGF/insulin system at the receptor level include using small interfering RNA (siRNA) and microRNA to suppress IGF-IR expression and function. Recently, an interesting preclinical study showed that 2'-O-methyl modified IGF-IR specific siRNA are able to downregulate IGF-IR expression, block IGF-IR signaling, and suppress tumor growth in vivo by triggering antitumor immune responses [48]. siRNA-based therapies face two major barriers: the delivery of the large and highly charged molecules to the targets [49] and the transient effects of the downregulation of the target gene. In pre-clinical in vivo studies, the latter could be solved by developing in vivo stable and inducible long-term expression of target short hairpin RNA under the control of doxycycline, tetracycline, or other dimerizing drugs [50]. Specific microRNAs inhibited cancer cell proliferation, motility, invasion, xenograft tumor growth, and metastasis in different cancers by downregulation of IGF-IR expression [51, 52]. Typically these microRNAs have approximately 22 nucleotides and usually have more than one target; potential drug candidates need to be carefully examined to exclude off-target effects before evaluation in clinical trials. Introduction of kinase deficient mutation into IGF-IR as a gene transfer strategy could also be an alternative approach to suppress IGF-IR signaling pathway and result in tumor suppression [53].

Targeting IGF/insulin downstream signaling pathways

As noted, PI3K/AKT and Ras-MAPK axis are two well-established intracellular signal networks downstream of IGF/insulin signaling. Therefore, several key molecules in these pathways might be relevant targets for drug development including mammalian target of rapamycin (mTOR), a serine/threonine protein kinase. Activation of mTOR upon growth factor stimulation subsequently induces the activation of ribosomal p70 S6 kinase (S6K1). Phosphorylated eukaryotic initiation factor 4E-binding protein-1 (4EBP1)

releases eIF4E, the latter recruits elF4G to form eIF4F complex, which then binds to the 5' mRNA cap and initiates cap-dependent mRNA-protein translation, thereby regulating cell growth and proliferation (Figure 1.1). Rapamycin and its analogs, everolimus (Novartis), temsirolimus (Pfizer) and ridaforolimus (Merck), have been developed to inhibit mTOR. Based on preclinical data using breast cancer cell lines [54-57] and mouse tumor models [58], both temsirolimus and everolimus have been approved for cancer treatment. Two recently published reports showed that everolimus combined with endocrine therapies were of benefit. In hormone refractory patients, tamoxifen plus everolimus resulted in increased clinical benefit compared to tamoxifen alone with improved time to progression and overall survival in hormone receptor (HR)-positive, human epidermal growth factor receptor (EGFR) 2-negative metastatic breast cancer patients [59]. In a similar patient population, everolimus combined with the aromatase inhibitor exemestane showed improved progression-free survival in HR positive advanced breast cancer patients [60].

These promising clinical studies provide important evidence that anti-ER therapies can be combined with anti-signaling strategies. However, some caution is warranted in using mTOR inhibitors with the IGF system. Normally, IGF stimulation results in activation of S6K1, which negatively regulates adaptor protein insulin receptor substrate-1 (IRS-1) function by phosphorylation. IRS-1 phosphorylation results in degradation of IRS1 protein and suppression of IRS-1 gene expression [61]. mTOR inhibitors disrupt this negative feedback loop and enhance IGF/insulin signaling and subsequent PI3K/AKT activation [62].

Combination therapy with anti-IGF-IR agents might be needed to address this problem and will be discussed later. Beyond mTOR inhibitors, other small molecule inhibitors of the downstream pathways, such as PI3K inhibitor LY294002 [63], S6K1 inhibitor H89 [54], MAPK inhibitor U0126 [54, 64], and dual PI3K/mTOR inhibitor NVP-BEZ235 [65] are currently in preclinical and clinical studies. The important

translation initiation protein 4EBP1 could also be a potential drug target to terminate IGF/insulin signaling induced cap-dependent translation.

Crosstalk and combination therapies

IGF-IR monoclonal antibodies and mTOR inhibitors

As noted above, mTOR inhibitors affect the S6K1-IRS1 negative feedback loop and result in enhanced PI3K- AKT activation through IGF-IR signaling [66]. If this pathway represents a resistance mechanism for the mTOR inhibitors, then co-targeting IGF-IR and mTOR might result in enhanced clinical benefit over mTOR inhibitor monotherapy. Studies showed that dual inhibition of IGF-IR and mTOR improved antitumor activity in vitro and in breast cancer and other cancer patient tumor samples [66, 67]. Currently, Merck is determining the benefits of IGF-IR monoclonal antibody (dalotuzumab) and mTOR inhibitor (ridaforolimus) combination therapy in breast cancer patients with ER-positive tumors (NCT01220570, NCT01234857). Amgen is evaluating the clinical benefits of combining ganitumab with everolimus in patients having advanced cancers (NCT01061788, NCT01122199). The results of these clinical trials are expected to reveal the benefits of co-targeting IGF-IR and mTOR. It is worth noting that drugs acting as dual inhibitors of PI3K and mTOR, such as NVP-BEZ235, also demonstrated improved antitumor efficacy compared to mTOR inhibitors alone [65, 68, 69].

Targeting IGF-IR/IR and ERα

Cross talk between IGF/insulin system and estrogen receptor signaling pathway is well established [40, 54, 70]. IGF/insulin signaling activates ERα via PI3K/AKT and/or MAPK pathways respectively by phosphorylating ERαserine167 and/or ERαalanine118 [54, 71-73]. Estrogen increases expression of several key genes in the IGF signaling pathway including IGF-II [74], IGF-IR, and IRS1 [75], while decreasing expression of other genes, such as IGFBP-3 [76] and IGF-IIR [77]. Thus, the overall effect of estrogen on the IGF/insulin system is to positively regulate signaling.

Acquired resistance to anti-estrogen therapies is an important clinical problem. Since ERα may function together with IGF-IR signaling to enhance cell survival [78], targeting both pathways may have value. More recently, microarray data suggest that a gene signature co-regulated by IGF-I and estrogen correlated with poor prognosis in human breast cancer [64], which also implies dual inhibition of IGF-IR and ER pathway may be necessary in certain breast cancer subtypes.

However, the clinical trials using the combination therapy for patients with endocrine-resistant breast cancer have been disappointing. In these trials, most women had already developed resistance to anti-ER therapies. In most of the reported trials, the anti-IGF-IR strategies were tested as the second or third line endocrine therapies.

We have recently shown that tamoxifen-resistant (TamR) cells and tumors lose expression of IGF-IR while maintaining IR expression. These findings suggest IGF-IR is a poor target in tamoxifen resistant tumors and IR might be an alternative option in treating TamR breast cancer [40]. Patients with tamoxifen resistant tumors also show loss of IGF-IR at the time of progression on tamoxifen [79]. Thus, endocrine resistant patients might not be the best candidates for anti-IGF-IR therapies. However, there are other ways to target IGF-IR and IR with small molecule TKIs, ligand neutralizing antibodies, or even growth hormone receptor antagonists, so the final word about the clinical relevance of these cross talk pathways is not yet settled.

Targeting IGF-IR and human epidermal growth factor receptor (EGFR)

About 30% of the patients with invasive breast cancers have amplification or overexpression of EGFR2 (Her2), which is associated with poor prognosis breast cancer [80-82]. Trastuzumab is a recombinant humanized monoclonal antibody that targets the extracellular domain of RTK Her2 [83]. Trastuzumab initially showed outstanding anti-tumor efficacy in patients with Her2 positive breast cancer in combination with cytotoxic chemotherapy. However, not all patients benefit from this regimen and in advanced breast cancer, resistance develops in about one year [84, 85]. IGF-IR and Her2 are

reported to form heterodimers in trastuzumab-resistant breast cells [81]. Further, IGF-I was shown to activate Her2 signaling in trastuzumab-resistant breast cancer cells but not parental cells. Inhibition of IGF signaling resulted in restoration of trastuzumab sensitivity to resistant cells [81, 86, 87]. These preclinical findings led to several clinical trials aimed at evaluating the benefits of co-targeting IGF-IR and Her2 in trastuzumab-resistant breast cancer patients (NCT01479179, NCT00788333, NCT00684983, and NCT01111825).

Other combination therapy strategies

IGF/insulin signaling and chemotherapy:

Combining either IGF-IR monoclonal antibodies or IGF-IR TKI could enhance doxorubicin drug efficacy [37, 88]. We demonstrated that giving cytotoxic chemotherapy first or concurrently with IGF-IR inhibitors resulted in a better tumor response. In contrast, IGF-IR prior to cytotoxic chemotherapy did not improve the benefits of doxorubicin and may represent an interference pathway between cytotoxic chemotherapy and IGF-IR inhibitors. These results suggest a combination of IGF-IR blockade and chemotherapy works in a sequencing-dependent fashion [37].

IGF/insulin system therapy and metformin:

As noted above, IGF-IR blockade is predicted and proven to result in compensational upregulation of circulating IGFs and insulin. These effects may cause hyperinsulinemia and be clinically manifested as metabolic syndrome or frank type-2 diabetes [6, 56, 89-91]. Therefore, combining insulin-sensitizing drugs to decrease serum levels of insulin with metformin might be necessary to attenuate the metabolic effects of the anti-IGF-IR/IR drugs. The I-SPY2 trial of neoadjuvant breast cancer therapy will test the therapeutic value of combining ganitumab, metformin and paclitaxel. The metformin will help to manage any acquired insulin resistance induced by ganitumab [92]. Metformin also reduces reactive oxygen species in mitochondria, which potentially would be important to inhibit tumorigenesis independent of the effects on glucose metabolism [6, 93]. Thus metformin combined with IGF-IR blockades may not only

attenuate the drug-induced hyperglycemia and hyperinsulinemia, but may also exhibit antitumor efficacy.

Future Directions

In order to maximize patient response to the emerging anti-IGF/insulin signaling therapies and accelerate developments of these antitumor drugs, the identification of therapeutic predictive biomarkers will need great attention.

The 'figitumumab downfall' raises an important question: what molecular attributes will likely be predictive of tumor dependence on IGF-IR? In these figitumumab clinical trials patients were not selected based upon any molecular markers. Microarray analysis has been used to determine sarcoma and neuroblastoma cell lines either sensitive or resistant to a TKI of IGF1R/IR, (BMS-536924). These data show that the mRNA levels of IGF-I and IGF-II highly correlated with cell response to BMS-536924 [94, 95]. Interestingly, the mRNA level of IGF1R did not meet the stringent statistical significance threshold to serve as an independent predictive biomarker, suggesting hybrid receptor mediated some of the IGF-I/IGF-II effects in these cells. Similarly, in a report addressing the sensitivity profile of another anti-IGF1R TKI, OSI-906 in colorectal cancer, the level of the phosphorylation status of IGF1R alone did not have positive correlation with cell sensitivity to OSI-906 [96]. These findings suggest a more complete definition of the IGF system signaling components is likely to assist in the clinical evaluation of anti-IGF1R therapies. Distinct receptor composition on the cell surface may influence cancer cell biology and predict sensitivity to anti-IGF1R therapy. Many studies have supported the important role of holo-IGF1R in cancer [9, 10, 97], yet the function of the IGF1R/IR hybrid receptor has not been well studied. The function of hybrid receptor signaling [18, 34]compared to holo-IGF1R and holo-IR receptors needs further characterization in order to serve as predictive biomarkers in breast cancer patients.

In addition, the IGF/insulin downstream signaling effectors may be important to predict a patient's response to the anti-IGF1R therapy. As adaptor molecules are

important components to transduce IGF1R signaling, the preferential expression of specific IRS isoforms in breast cancer cells has been linked to distinct signal transduction pathways and shown to mediate distinct biological behavior [98-101]. Our laboratory studied the gene expression profiles of a series of T47D variant cell lines with differential IRS adaptor protein expression to develop predictive IGF-I pathway biomarkers in breast cancer cells (submitted, Becker et al.). The results have suggested IGF-induced gene expression is IRS-dependent and highly conserved. In addition, this previous study has revealed several genes regulated specifically by either IRS-1 or IRS-2.

Besides cell surface composition of the receptors and preferential expressions of IRS adaptor proteins, other components of the IGF/insulin system may serve as predictive biomarkers for therapeutic outcomes and disease prognosis. Pre-treatment level of free IGF-I has been shown to predict NSCLC patients' benefit from IGF-IR monoclonal antibody [102]. IGF-IR nuclear staining has been reported to associate with a better progression-free survival and overall survival in a small group of soft tissue sarcoma patients treated with IGF-IR antibody [103]. A recent report suggested IGFBP5 expression was associated with resistance to IGF-IR/IR targeted therapy. Furthermore, increased IGFBP5/IGFBP4 ratio is associated with decreased sensitivity to IGF-IR/IR inhibition and worse prognosis in breast cancer patients [104].

In sum, the IGF/insulin system is complex. Simply targeting one receptor may not be sufficient enough to completely inhibit tumor biology. Additional preclinical data are needed to unravel the true clinical benefit of the anti-IGF/insulin targeted agents in breast cancer patients. This thesis suggesting three novel ways to target the IGF/insulin system: adaptor protein, gene products, and transcription factors activated by IGF signaling.

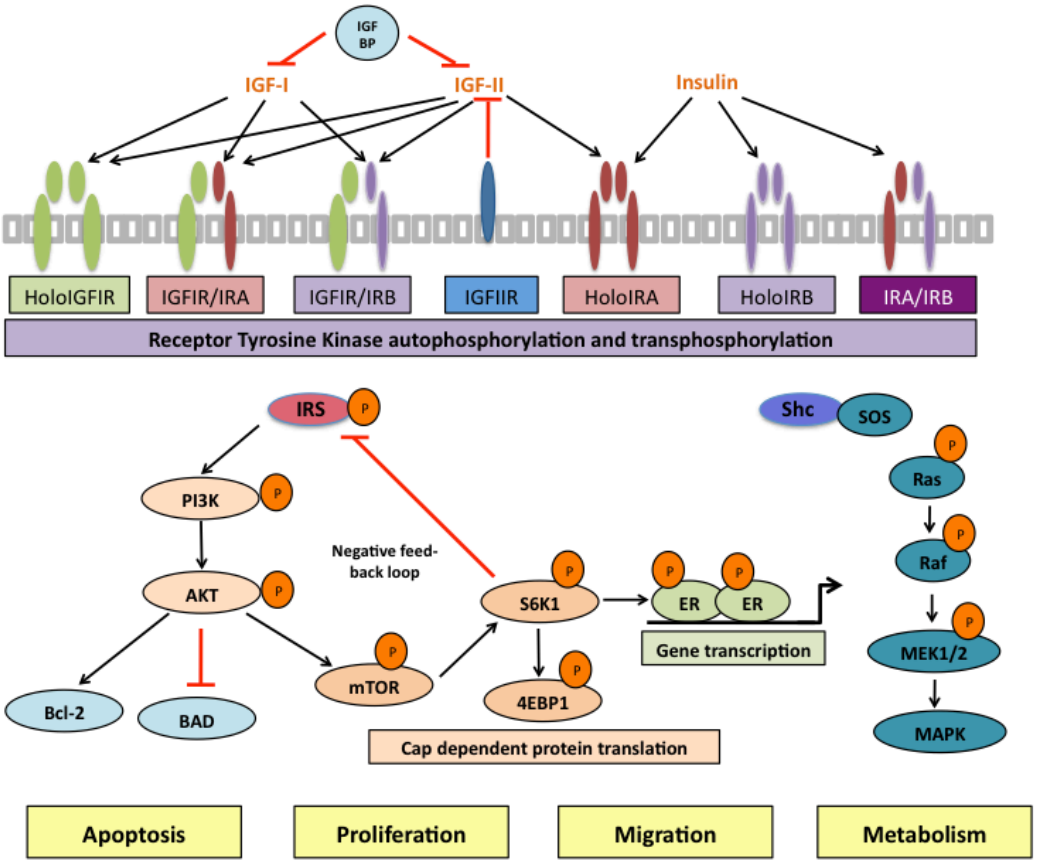

Figure 1.1 Schematic representation of the IGF/insulin system.
In the extracelluar environment, ligands IGF-I, IGF-II and insulin bind to distinct members of the IGF-IR and IR receptor family (as indicated by arrows). These transmemberane tetrameric receptors (three types of holo-receptors and three types of hybrid receptors) are composed of two extracelluar α-subunits, which function as binding domains; and membrane-spanning β-subunits, which possess tyrosine kinase activity. The bioactivity if IGF-I and IGF-II are negatively influenced by IGFBPs and IGF-IIR. Following the ligand binding and receptor activation, the phosphorylated adaptor proteins IRS and Shc provide a platform to initiate multiple downstream signaling pathways, namely PI3K/Akt and MAPK axis, ultimately influence tumor cell biology.

Chapter 2

Targeting insulin receptor substrates in various types of breast cancer cells

Yuzhe Yang, Nuri A Temiz, Alexander Levitzki, and Douglas Yee.
Insulin receptor substrate suppression by the tyrphostin NT157 inhibits responses to insulin-like growth factor-I and insulin in breast cancer cells.
Submitted to ***Oncotarget*** for peer review

Introduction

The insulin-like growth factor (IGF)/ insulin signaling pathway has been implicated in the proliferation, migration, and survival of many human malignancies[6, 105]. Upon ligand binding, the type I IGF receptor (IGF-IR) and insulin receptor (InR) recruit the insulin receptor substrate (IRS) adaptor proteins to transduce signals to downstream signaling molecules and thereby regulate cellular biology. In breast cancers, IRS-1 and IRS-2 are the two major isoforms that mediate IGF/insulin signaling. The role of IRS-1/2 proteins in breast malignancies has been well documented: IRS-1 promotes tumor growth [100, 101], whereas IRS-2 stimulates motility[99, 101].

The clinical trials for targeting IGF-IR have generally been disappointing. While several factors may account for the limited clinical activity the disruption of endocrine homeostasis with resultant hyperinsulinemia could abrogate the effect of only inhibiting IGF-IR[106]. Targeting of InR could be difficult due to disruption of glucose homeostasis. However, targeting key signaling pathways downstream of both receptors, such as the IRS proteins, has appeal and could be another strategy for cancer treatment.

NT157 is a novel small molecule tyrphostin targeting the IRS-1/2 proteins. Its efficacy and mechanism of action have been studied in models of melanoma [107] and prostate cancer[108]. In our current study, NT157 caused IRS protein degradation by inducing serine phosphorylation of IRS and disassociation from IGF-IR and InR in breast cancer cells. Treatment NT157 did not affect short-term phosphatidylinositol-4,5-bisphosphate 3-kinase (PI3K) and mitogen-activated protein kinase (MAPK) activation induced by IGF-I or insulin. However, prolonged treatment NT157 inhibited PI3K activation after prolonged ligand stimulation resulting in cell cycle S phase arrest and growth suppression. In estrogen receptor positive (ERα+) breast cancer cell lines where IRS-1 is the predominately-activated isoform, the serine phosphorylation of IRS-1 induced by NT157 compound also promoted the dissociation of ERα from IRS-1-IGF-IR/InR complex resulting in ERα degradation, cell cycle arrest, and growth inhibition. In basal-like breast cancer cells, NT157 inhibited cell proliferation and was associated with

suppression of the mesenchymal markers N-cadherin [109] and vimentin [110] and inhibition of ligand-induced migration. Since NT157 inhibited IGF1R and InR signaling, substrate inhibition may be exploited as a cancer therapy.

Results

NT157 induced IRS protein degradation through serine phosphorylation of IRS-1/2 in multiple breast cancer cell lines

To evaluate the ability of NT157 to downregulate IRS-1 and IRS-2 protein expression breast cancer cell lines were incubated with increasing doses of NT157. NT157 reduced IRS1/2 levels while inducing serine phosphorylation of IRS-1/2 (serine 636/639). IGF-IRβ expression was not affected in ERα+ (Figure 2.1 A top panels) and basal-like (Figure 2.1 B left) breast cancer cell lines. NT157 induced IRS protein downregulation occurred after 4 hours of drug exposure (Figure 2.8 A). To evaluate the mechanism of IRS downregulation and phosphorylation, cells were pre-treated with small molecule inhibitors of downstream signaling pathways (Figure 2.1 A bottom panels, B right). Only MEK inhibition by UO126 inhibited NT157's ability to phosphorylate IRS proteins. Inhibition of PI3K (LY294002) or IGF-IR (HuEM164 and BMS-754807) did not reverse the serine phosphorylation of IRS by NT157.

NT157 promoted dissociation of IRS-1 and ERα with IGF-IR/InR in breast cancer cells resulting in IRS-1 and ERα degradation

Since previous studies showed that IRS-1 and ERα formed a complex in the cytosol[111], we examined the effect of NT157 on ERα expression. In ERα+ cell lines, NT157 treatment down-regulated total ERα expression (Figure 2.1 A top panels). Subcellular fractionation analysis further confirmed that NT157 specifically down-regulated cytoplasmic ERα (Figure 2.2 A). Whether downregulation of ERα further affected gene expression was then examined. After NT157 treatment, in ERα+ breast

cancer cell lines, the ERα coding gene *ESR1* and its regulated gene *IRS-1* [75, 112] and *CCND1* [111] were significantly suppressed, while *IRS-2* expression levels were maintained (Figure 2.2 B, Figure 2.4 B). 17β-estradiol (E_2) mediated *CCND1* and *IRS-1* expression was further analyzed. qRT-PCR results suggested that NT157 treatment abrogated E_2 stimulation of *CCND1* mRNA expression in MCF-7 cells (Figure 2.2 C).

In ERα+ breast cancer tumors and patient-derived cell lines, *IRS-1* was positively correlated to *ESR1* expression [113] (Figure 2.9) suggesting a role for NT157 in responses to E2. In basal-like cell lines where ERα was not expressed, *IRS-1* mRNA was not affected by NT157 (Figure 2.10 B). To prove the mRNA level suppression was due to NT157's effects on ERα, ERα+ breast cancer cells were transfected with both IRS-1 and IRS-2 siRNAs. Genetic downregulation of IRS proteins did not affect ERα protein, mRNA expression, or ERα regulated genes expressions (Figure 2.10 A) suggesting that NT157 resulted in ERα protein degradation by interfering with its interaction with IRS-1.

IRS-1 protein forms complexes with IGF-IR/InR and ERα at the cell membrane [111] in normal mammary epithelial cells and breast cancer cell lines[78]. To determine if NT157 affected this complex, cell lysates were immunoprecipitated with IGF1R or InR antibodies. NT157 promoted the dissociation of IRS-1 from IGF-IR/IR as well as induced the dissociation of ERα from the IRS-1-IGF-IR/IR (Figure 2.3 A). The data above suggested a novel function of NT157 compound in ERα+ breast cancer cells.

Down-regulation of IRS proteins in ERα+ cancer cells does not affect short-term IGF-I treatment-induced signaling transduction

In the presence of IGF-I, NT157 treatment eliminated the tyrosine phosphorylation of IRS1/2 (Figure 2.11 A). Interestingly, neither down-regulation of IRS proteins in ERα+ cells by NT157 treatment nor siRNA transfection attenuated activation of short-term IGF-I-induced signaling cascades (PI3K and MAPK) (Figure 2.3 B, 2.11 B). Despite this lack of efficacy on signaling, data indicated that NT157 treatment suppressed

cyclin D1 and induced p21 protein and mRNA expression in ERα+ breast cancer cell lines (Figure 2.4 A and B, and Figure 2.12). Cyclin D1 is an estrogen regulated gene, thus the degradation of ERα induced by NT157 reduced cyclin D1 expression. IGF-I stimulated cyclin D1 was abolished by NT157 treatment in ERα+ cells (Figure 2.4 D). Down-regulation of IRS proteins by siRNA did not affect IGF-I regulated cyclin D1 (Figure 2.10 A bottom panel), which indicated that suppression of IRS protein expression alone was not sufficient to inhibit IGF-I regulation of cyclin D1. NT157 disruption of the complex was required for maximal effect on cell cycle progression. Cell cycle analysis also revealed that NT157 treatment caused S phase arrest upon IGF/insulin system ligand stimulation (Figure 2.4 C). The unaltered upstream signaling pathway in ERα+ cancer cells may due to compensation of other adaptor proteins, such as shc (Figure 2.2 and 2.4 A).

NT157 inhibited IGF/insulin and 17β-estradiol (E_2) induced cell proliferation in ERα+ breast cancer cells

To investigate the specificity and toxicity of NT157 towards IRS proteins, immortalized breast epithelial cell line MCF10A, MCF-7L, and MCF-7L tamoxifen resistant (TamR) cell lines were studied. MCF-7L TamR cells expressed significantly lower level of IRS-1 when compared to its parental cell line[40, 114]. The dose-response curves showed that MCF-7L cells were significantly more sensitive to NT157 treatment (Figure 2.13 A) than TamR cells. Concentrations of NT157 up to 2μM did not affect MCF10A cells while this concentration suppressed monolayer growth of MCF-7L cells (Figure 2.13 A left). These data indicated that NT157 potently downregulates IRS proteins in multiple breast cancer cell lines and growth effects are associated with the level of IRS expression.

NT157 growth inhibitory effects in ERα+ breast cancer cell lines were further assessed. Both monolayer and anchorage independent growth experiments showed that NT157 abolished IGF/insulin system ligands (IGF-I, IGF-II, and insulin) as well as E_2

induced monolayer (Figure 2.5 A, 2.13 B) and anchorage independent growth (Figure 2.5 B). Moreover, parallel signaling experiments revealed that prolonged NT157 treatment resulted in suppressed PI3K signaling, down-regulation of cyclin D1 expression, increased p21 expression, and enhanced activation of $p38^{MAPK}$ after ligand stimulation (Figure 2.5 C). Genetic suppression of IRS1/2 proteins also resulted in partial inhibition of ligand-induced growth (Figure 2.14 A) and attenuated PI3K pathway activation upon prolonged ligand stimulation but did not affect the cell cycle machinery (Figure 2.14 B). These data indicated that IRS proteins play a role in maintaining persistent activation of PI3K pathway. NT157 treatment induced ERα degradation and further suppressed ligand-stimulation of the cell cycle regulatory machinery in addition to IRS protein suppression. Therefore, NT157 inhibited ERα+ breast cancer cells by several different mechanisms and was more effective than genetic suppression methods.

NT157 effects in two tamoxifen resistant ERα+ breast cancer cell lines – MCF-7L TamR and T47D TamR [40, 114] were also evaluated. These cells have reduced IRS-1 expression due to ERα functional suppression but retained similar expression levels of IRS-2 expression. Monolayer and anchorage independent growth assays both indicated that NT157 blocked ligand-induced proliferation in TamR cells (Figure 2.15). Thus, targeting IRS proteins by NT157 may also have therapeutic potential in treating endocrine resistant breast cancers.

NT157 compound sensitized ERα+ breast cancer cells to mTOR inhibition

The mammalian target of rapamycin (mTOR) is a downstream effector of PI3K signaling. Inhibitors of mTOR are experimentally and clinically proven to have therapeutic effects in breast cancer[115, 116]. However, mTOR inhibitors suppress S6K1 activity. S6K1 functions to phosphorylate IRS proteins at serine sites resulting in IRS downregulation. Thus, mTOR inhibition results in disruption of a negative feedback loop to enhance levels of IRS expression[117], increase upstream receptor tyrosine kinase activation[66], and may result in resistance to this class of drugs. Therefore, NT157 could

overcome the consequences of rapamycin upregulation of IRS and might improve cancer cell growth inhibition.

NT157 sensitized ERα+ cellular response to rapamycin treatment in both monolayer and anchorage independent growth in full media or IGF-I treated conditions (Figure 2.6 A and B top panels). Immunoblot data also showed that rapamycin treatment alone caused up-regulation of IRS proteins while NT157 suppressed this effect of rapamycin on IRS expression (Figure 2.6 B bottom panel). These data implicated that NT157 could be combined with rapalogs in the treatment of ERα+ breast cancers to avoid monotherapy induced resistance.

NT157 compound inhibited proliferation and migration in basal-like breast cancer cells

Basal-like breast cancer patients do not express ER and express lower levels of both *IRS-1* and *IRS-2* when compared to ERα+ breast cancers (Figure 2.9). However, in patients with ER- tumors, high levels of *IRS-1* mRNA expression are correlated with poor prognosis (overall survival, refractory free survival, and distant metastasis free survival) (Figure 2.16). In basal-like cell lines, NT157 treatment also inhibited cell growth (Figure 2.7 A). NT157 did not affect *CCND1* but still up-regulated *p21* protein and mRNA expression (Figure 2.7 B). In cell cycle analysis, NT157 caused G2/M phase abrogation in basal-like cells (Figure 2.7 C), which was distinct from the mechanism found in ERα+ breast cancer cells.

In basal breast cancer cell lines, IRS-2 was shown to be the predominant adaptor molecule for IGF/insulin signaling and was required for ligand-induced cell motility (Figure 2.1 B, 2.7 E)[99, 101, 118]. NT157 also suppressed MDA-MB-231 cells migration possibly by affecting epithelial-mesenchymal transition and reversing MDA-MB-231 mesenchymal morphology through the suppression of IRS-2, N-cadherin and vimentin (Figure 2.7 D, F).

Discussion

Preclinical and population data implicated IGF-IR's critical roles in cancer biology and encouraged the development of anti-IGF-IR targeted therapies. However, almost all IGF-IR monoclonal antibody (monotherapy or in combination with other therapies) clinical trials have failed due to not show clinical benefit in a significant number of patients[105, 119]. Because the IGF-IR inhibitors upregulate systemic insulin levels, disruption of InR signaling might be necessary to inhibit this highly homologous pathway[106]. Our previous work showed that IRS proteins were the predominant adaptor proteins downstream of both IGF-IR/InR in breast cancer cells[99, 100] and IGF-IR/IR required the IRS proteins to transduce signaling as well as mediate biological outcomes in breast cancer models[101]. Disruption of IRS proteins might be a better strategy to inhibit both receptors' signaling pathways. NT157 downregulation of IRS proteins resulted in dual receptor intracellular signaling inhibition in melanoma[107], prostate[108], and breast cancers.

In the current study, we tested NT157's efficacy and mechanism of action in multiple types of breast cancer cells. In the ERα+ breast cancers, we showed that NT157 induced the serine phosphorylation of IRS proteins, which resulted in the degradation of IRS. We also found that NT157 promoted the dissociation of ERα from IRS-IGF-IR/InR complex and resulted in ERα degradation (Figure 2.17). The cytoplasmic degradation of ERα further resulted in the *ESR1*-regulated gene suppression and inhibitory effects of the S-phase cell cycle regulatory machinery. These findings were unique in ERα+ breast cancers. In the tamoxifen-resistant ERα+ breast cancer cells (details described previously [40]), NT157 also had inhibitory effects. Dual targeting of upstream signaling pathways and ERα might be superior to targeting a single pathway alone. The clinical approval of palbociclib and everolimus for treatment of ERα expressing breast cancer demonstrates the value of developing inhibitors of these pathways in hormone sensitive and resistant cells. These encouraging results suggested that in hormone resistant TamR cancers, targeting IRS proteins could be a therapeutic option.

Our study showed that rapamycin treated ERα+ breast cancer cells had elevated IRS protein expression levels. Co-targeting IRS by NT157 resulted in improved growth inhibitory effects. A recent study showed that IGF-IR and IRS-1 were increased in crizotinib treated anaplastic lymphoma receptor tyrosine kinase (ALK) fusion protein positive lung cancer patients and co-targeting IGF-IR axis with ALK tyrosine kinase inhibitor resulted in therapeutic enhancement[120]. Another study demonstrated that targeting PI3K in hormone receptor breast tumors resulted in up- regulation of ER function, which suggested that the necessity of co-targeting PI3K signaling pathway and ER in ER+ breast cancer patients[121]. NT157's ability to disrupt IGF-IR/IR-IRS-1-ERα complex might make it a better drug to overcome hormone resistance.

We also evaluated NT157 in basal-like breast cancer cell lines. To date, basal-like cancers are generally not sensitive to targeted therapies. Our previous and current studies suggested that IRS proteins might be a target. IRS-1 expression levels served as indicator of poor prognosis in basal-like cancers and IRS-2 mediated the IGF-I induced motility in basal-like cell lines. NT157 treatment showed both growth and motility inhibitory effects in basal-like cells. This study implicated that targeting IRS protein in breast cancers have broad therapeutic spectrum.

Overall, our study emphasized the NT157 therapeutic potential as mono- and combination therapy in various breast cancer models. In addition, we, for the first time, revealed that NT157 also targeted ERα in ERα+ breast cancer cells. Targeting IRS protein could be useful alone or in combination with other therapies in many different subtypes of breast cancer.

Materials and Methods

Reagents and antibodies Growth media and supplements were purchased from Invitrogen (Grand Island, NY). IGF-I was purchased from Gro*Pep* (Adelaide, Australia). IGF-II was purchased from Gemini (Woodland, CA). Insulin was purchased from Eli

Lilly (Indianapolis, IN). LY294002, U0126, and actin antibody were purchased from Sigma-Aldrich (St. Louis, MO). Humanized anti-IGF-IR monoclonal antibody huEM164 was provided by Immunogen Inc. (Norwood, MA). BMS-754807 was provided by Bristol Myers Squibb (New Jersey, Marco Gottardis). Antibodies for phosphorylated AKT serine 473, total and phospho-IGF-IR, total and phosphorylated p44/42 (MAPK), phospho-p38 ^{MAPK}, total and phospho-IRS-1 (serine 636/639), phospho-S6K1, p21, p18, CDK2, CDK6, cyclin D1, cyclin D3, and PARP were purchased from Cell Signaling Technology (Beverly, MA). The IRS-2, total ERα, IGF-IRα, InRβ antibodies, and protein agarose A were purchased from Santa Cruz Biotechnology (Santa Cruz, CA). Horseradish peroxidase-conjugated anti-phosphotyrosine (PY-20) was purchased from BD Biosciences (San Jose, CA). Anti-rabbit and anti-mouse horseradish peroxidase-conjugated secondary antibodies were purchased from Pierce (Rockford, IL).

Cell lines and culture MCF-7, T47D, MDA-MB-231, and MDA-MB-468 cells were purchased from the ATCC (Manassas, VA) and cultured following ATCC's instruction. Cell line authenticity is verified by STR analysis on an annual basis (Genetics Resources Core Facility, Johns Hopkins School of Medicine, Institute of Genetic Medicine). MCF-7L cells were kindly provided by C. Kent Osborne (Baylor College of Medicine) and maintained in improved MEM Richter's modification medium (zinc option) supplemented with 5% FBS and 11.25 nmol/L insulin. MCF-7L were evaluated by comparative genomic hybridization and found to be nearly identical to the MCF-7 cells distributed by the ATCC. MCF-7L TamR and T47D TamR cells were generated as described[40]. All cells were grown at 37 °C in a humidified atmosphere containing 5% CO_2.

Immunoblot Cells were plated at a density of 3 x 10^5 in 60-mm-diameter. Upon reaching 80% confluency estimated by microscopy, cells were switched to serum-free medium (SFM) for 24 hour to synchronize cell status, after which treatments were added. Treated cells were washed twice with ice-cold phosphate buffered saline (PBS) on ice and lysed with TNESV lysis buffer of 50 mM Tris-Cl (pH 7.4), 1% Nonidet P-40, 2 mM EDTA

(pH 8.0), 100 mM NaCl, 10 mM sodium orthovanadate, 1 mM phenylmethysulforny fluoride, and with proteases inhibitor cocktails. Lysates were centrifuged at 21,000 rpm for 30 minutes at 4 °C. Protein concentrations were measured using the bicinchoninic acid protein assay reagent kit (Pierce). Cellular protein (80 μg) was resuspended in 5x Laemmli loading buffer with 60 mg/ml DTT and was resolved by SDS-PAGE, transferred to nitrocellulose membrane, and immunoblotted according to manufacturer guidelines.

Immunoprecipitation

Total cellular lysates (500 μg) were incubated overnight with IGF-IRα or InRβ antibody at 4 °C followed by incubation with protein agarose A for 4h at 4 °C. Samples were washed three times with TNESV buffer. 5X Laemmli loading buffer was added per immunoprecipitated sample and run on an 8% SDS-PAGE gel.

siRNA transfection and cell stimulation Cells were cultured in growth medium to reach confluency of 80% then were transfected with 25 nmol/L siRNA (siRNAs SMARTpool were purchased from Santa Cruz Biotechnology) using the TransIT-siQUEST transfection reagent (Mirus, Madison, WI) according to the manufacturer's protocol. 48 hours later, cells were washed twice with PBS and serum starved for another 24 hours in SFM followed by treatments as indicated in the figure legends.

Reverse transcription-quantitative real-time polymerase chain reaction Cells were plated at a density of 2 x 10^5 in 6-well-plates in growth media to reach 80% confluency then synchronized in SFM for 24 hours followed by treatments indicated in the figure legends. Cellular RNA was isolated using TriPure Reagent according to the manufacturer (Roche, Belgium). For quality control and to determine concentration, a 260:280 ratio assay was conducted on a spectrophotometer. Forward and reverse primers were designed to target the following transcripts: *IRS-1* 5'-TCACAGCAGAATGAAGACC-3' and 5'-CTACTGATGAGGAAGATATGAGG-3'; *IRS-2* 5'-TCGTGAAAGAGTGAAGATCTG-3' and 5'-TCCAAACACAGTCATTGCT-

3'; *ESR1* 5'-CCCAGGGAAGCTACTGTTTG-3' and 5'-CTCCACCATGCCCTCTACAC-3'; *CCND1* 5'-AAACAGATCATCCGCAAACAC-3' and 5'-GGTTCAGGCCTTGCACTG-3'; *P21* 5'-CAGGGGAGCAGGCTGAAG-3' and 5'-GGATTAGGGCTTCCTCTTGG-3'; and *RPLPO* 5'-TGCTGATGGGCAAGAACAC-3' and 5'-GAACACAAAGCCCACATTCC-3'. A total of 1 μg of RNA was reverse transcribed using the Transcriptor Reverse Transcriptase Kit, and quantitative PCR was conducted using the Universal SYBR Green Kit according to the manufacturer's protocol (Roche) on an Eppendorf (Hamburg, Germany) Mastercycler Realplex^4 machine. The relative concentration of mRNA was calculated using cycle threshold values that were derived from a standard curve and normalized to ribosomal protein, large, P_O (*RPLPO*) as an internal control.

Monolayer growth assay Cells were plated in 24-well-plates at a density of 15,000 cells per well, allowed to attach overnight and starved in SFM for 24 hours to synchronize cells. After 5 days of treatments, growth was assessed via the 3-(4,5-dimethylthiazol-2-yl)-2,5-diphenyltetrazolium bromide (MTT) assay. 50 μl of 5 mg/ml MTT solution in SFM were added to each well and incubated for 4 hours at 37 °C. Media were aspirated and formazan crystals were lysed with 500 μl of solubilization solution (95% dimethylsulfoxide + 5% improved minimal essential media). Absorbance was measured with a plate reader at 570 nm using a 650 nm differential filter to assess growth.

Anchorage-independent growth A 1 ml layer of 1% Seaplaque-agarose (BioWhittaker, Rockland, ME) in 1.5% FBS-containing growth media was solidified into each well of a 6-well plate. The bottom layer was overlaid with 1 ml of a 1% top agar mixture for 12,000 cells per well with indicated treatments. All plates were incubated at 37 °C for 14 days. Colonies was counted on a light microscope with an ocular grid. Five random fields were counted per well and only colonies exceeding half of a grid square were scored.

Cell cycle analysis Cells were typsinized, washed twice in ice-cold PBS, and fixed in 70% ice-cold ethanol -20 °C over night. Cell cycle analyses were performed on

propidium iodide-stained nuclei by using an Accuri™ C6 flow cytometer (BD Biosciences, San Jose, CA). Single cells were gated, 10,000 events were collected and analyzed by FlowJo (Tree Star Inc., Ashland, OR) software.

Boyden chamber migration assay Cell motility and invasion were measured by a modified boyden chamber assay as described previously[99]. Cells were briefly detached by trypsin, washed twice with SFM, and then resuspended in SFM with or without NT157 compound. Cells (150,000) were placed in the upper chamber of a 10-well Boyden chamber apparatus. Upper and lower chambers were separated by a polycarbonate polyvinylpyrrolidone–free filter with 8-µm pores. SFM (0.4 mL) with or without IGF (5 nmol/L) was placed in the bottom wells of the chamber. After 5 h of incubation at 37°C in a humidified atmosphere containing 5% CO2, cells remaining on the topside of the filter were removed with cotton swabs. The filter was then removed from the chamber and the cells that had migrated to the underside of the filter were fixed and stained in HEMA3. The filter was then mounted onto a glass microscope slide and cells were counted (in triplicate) in five different areas using a light microscope.

Clinical data set analysis The relative mRNA expression of *IRS-1 and IRS-2* in human breast tumor samples was determined by searching the Oncomine database (version 4.4.3, September 2012 data release[122]. *IRS-1* and *IRS-2* mRNA expression was queried in TCGA breast dataset using reporter A_32_P165472. For prognostic analyses, overall survival and distant metastasis-free survival, stratified by expression (all percentiles between the lower and upper quartiles were computed, and the best performing threshold was used as a cutoff) of the gene of interest (*IRS-1*: 204686_s_at; *IRS-2*: 209184_s_at), were presented as Kaplan–Meier plots and tested for significance using log-rank tests[123]. TCGA BRCA RNASeqV2 and clinical patient data was downloaded on 7/1/2014. *IRS-1*, *IRS-2* and *ESR1* expression values were normalized by the expression of the housekeeping gene GAPDH. Pearson correlations and linear regression was perfumed using R function cor and lm.

Statistical analysis All data except clinical data sets were analyzed with the unpaired Student's t test with the use of Excel 2008 (Microsoft, Redmond, WA). A p value of <0.05 was considered statistically significant (* $p<0.5$, ** $p<0.01$, *** $p<0.001$).

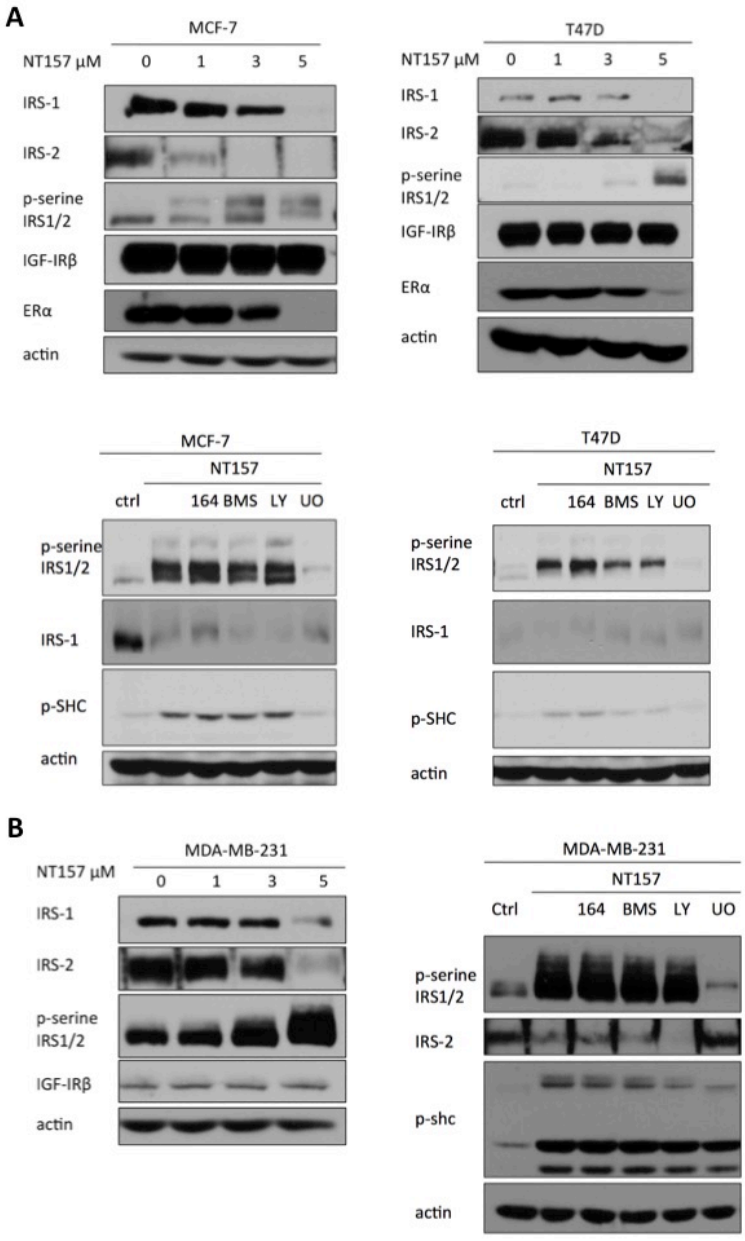

Figure 2.1 NT157 compound induced IRS protein degradation through serine phosphorylation of IRS-1/2 in multiple breast cancer cell lines.

A. Top panels: MCF-7 and T47D cells were serum starved overnight then treated with increasing concentrations of NT157 drug for 4 hours. Cellular lysates were separated by SDS-PAGE and indicated protein levels were assessed by immunoblotting. Bottom panels: MCF-7 and T47D cells were serum starved overnight then pretreated with huEM164 (164, 20 μg/ml, 24 hr), BMS-754807 (BMS, 1 nM, 1hr), LY294002 (LY, 10 μM, 1hr), or UO126 (UO, 10 μM, 1hr). Protein levels of phospho-serine IRS1/2, phospho-SHC, and actin were determined by immunoblotting. **B.** Left: MDA-MB-231 cells were serum starved overnight then treated with increasing concentrations of NT157 drug for 4 hours. Protein levels were assessed by immunoblotting. Right: MDA-MB-231 cells were serum starved overnight then pretreated with huEM164 (164, 20 μg/ml, 24 hr), BMS-754807 (BMS, 1 nM, 1hr), LY294002 (LY, 10 μM, 1hr), or UO126 (UO, 10 μM, 1hr). Protein levels were determined by immunoblotting.

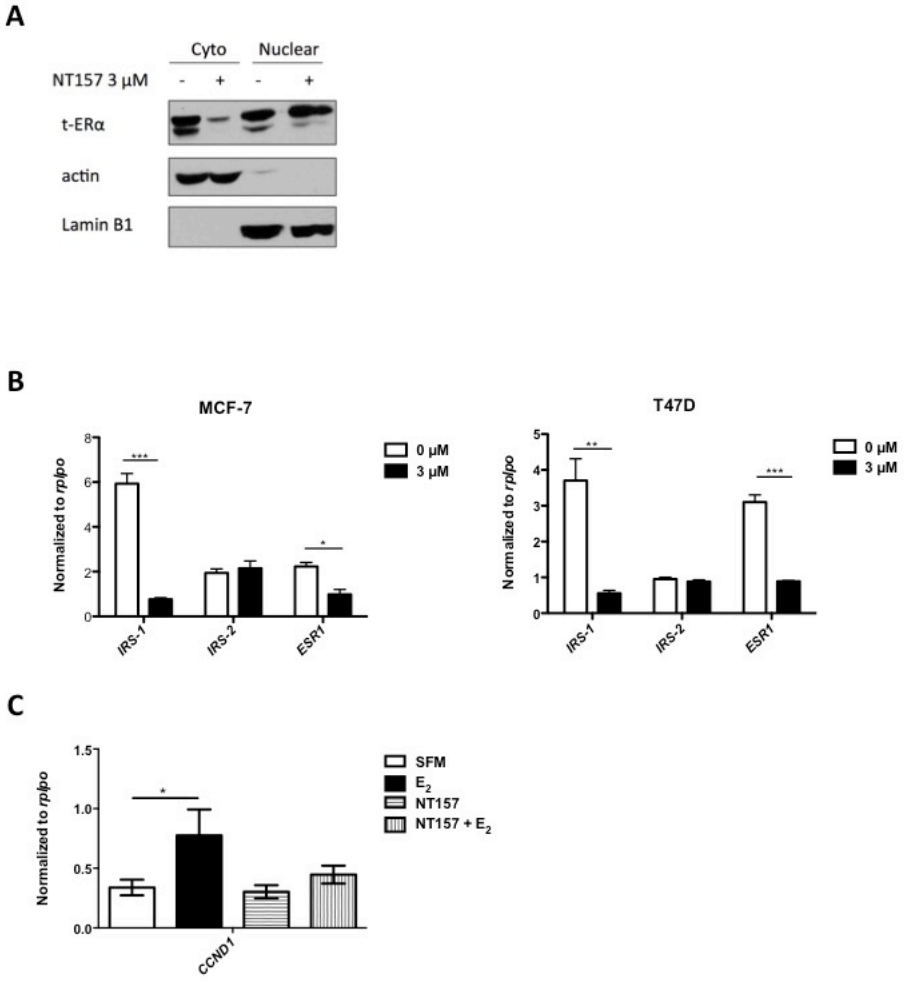

Figure 2.2 NT157-induced ERα expression and function suppression.
A. T47D cells were serum starved overnight then treated with or without NT157 (3 µM) for 4 hours. Cytoplasmic and nuclear ERα were extracted and assessed by immunoblotting. **B.** MCF-7 and T47D cells were serum starved overnight then treated with or without 3 µM of NT157 drug for 4 hours. Total RNA was isolated and reverse transcribed. *IRS-1*, *IRS-2*, and *ESR1* levels were analyzed using qRT-PCR. Data were normalized to *RPLP0* housekeeper gene. **C.** MCF-7 cells were cultured in estrogen depleted growth media for 2 days then serum starved overnight. Cells were pretreated with NT157 (3µM) for 4 hours followed by 4 hours of E_2 (1 nM) stimulation. Total RNA was isolated and reverse transcribed. *IRS-1* and *CCND1* levels were analyzed by qRT-PCR. Data were normalized to *RPLP0* housekeeper gene. Data are mean ± SEM; results are representative of at least three independent triplicates experiments.

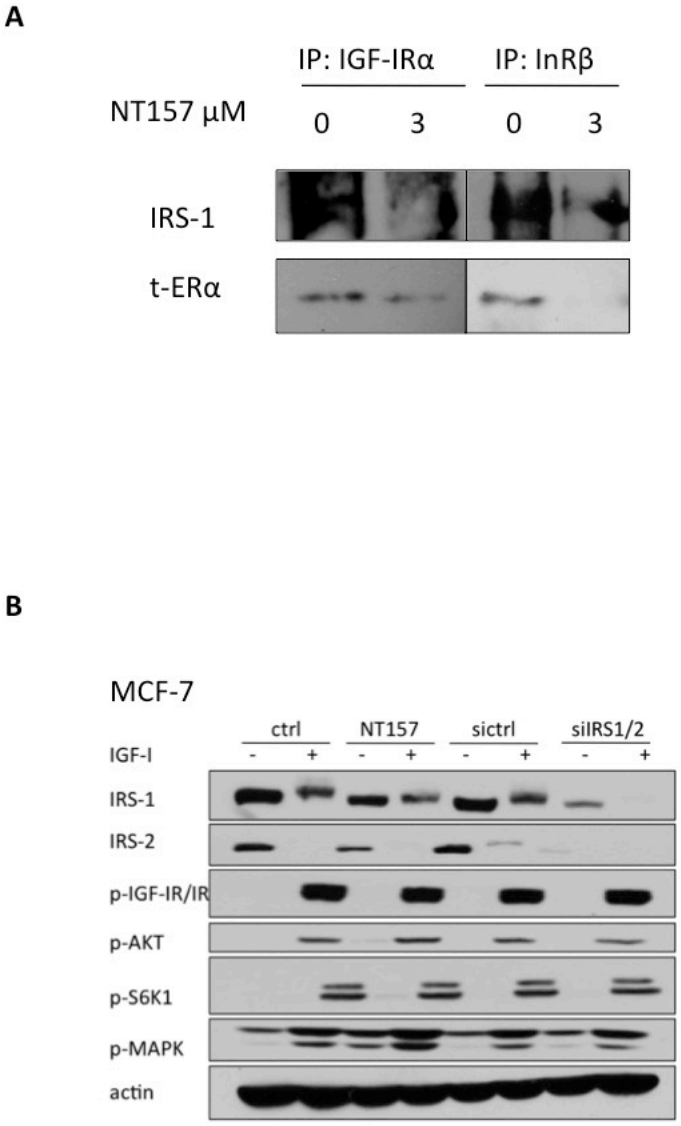

Figure 2.3 NT157 induced dissociation of IGF-IR/IR and IRS-1-ERα complex while not affecting major intracellular signaling cascades induced by short term IGF-I treatment.
A. MCF-7 cells were serum starved overnight then treated with indicated concentrations of NT157 drug for 1 hour. 500 μg cellular protein was immunoprecipitated with IGF-IRα or IRβ. Protein levels of IRS-1 and ERα were determined by immunoblotting. **B.** MCF-7 cells were 1) serum starved overnight, pretreated with 3 μM of NT157, then induced with or without 5nM IGF-I for 10 minutes; 2) transfected by control or IRS1/2 siRNA for 48 hr, starved overnight, then stimulated with or without 5 nM IGF-I. Protein levels of IRS-1, IRS-2, phospho-IGF-IR/IR, phospho-AKT, phospho-S6K1, phospho-MAPK, and actin were assessed by immunoblotting.

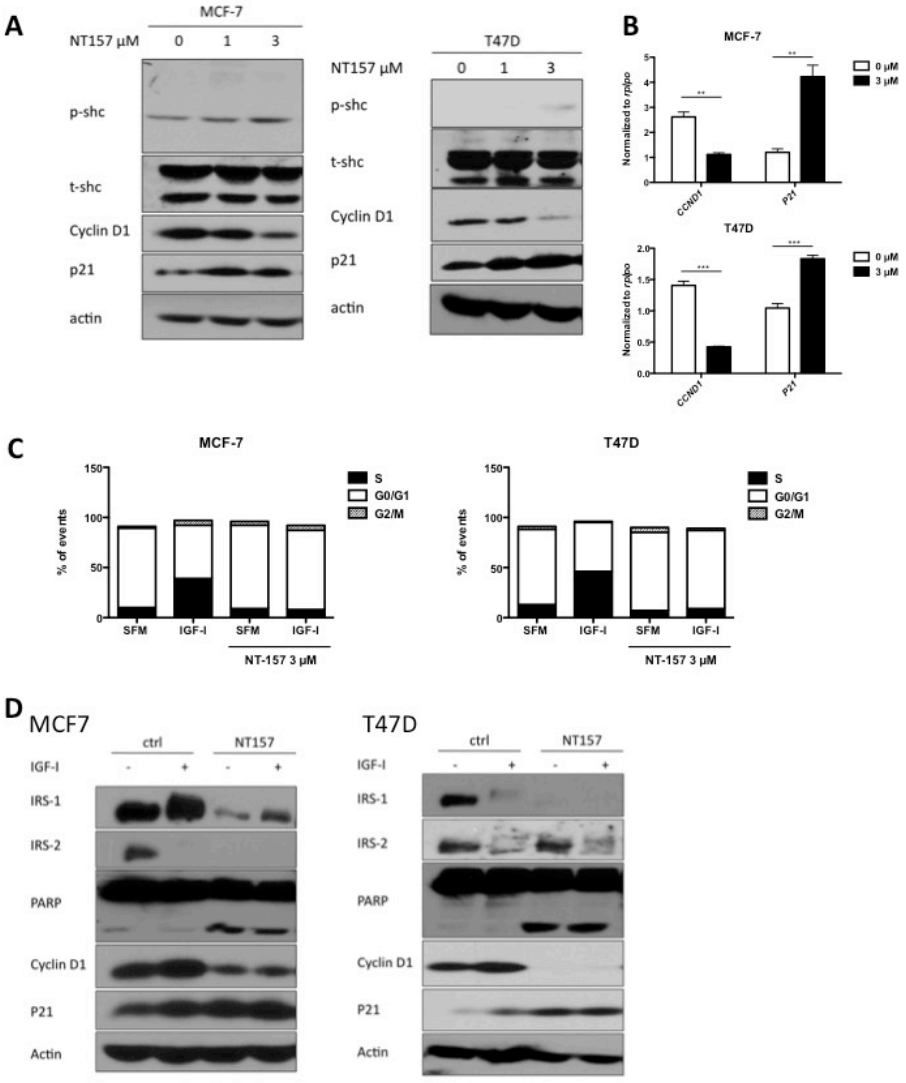

Figure 2.4 NT157 inhibited cell cycle regulatory machinery.
MCF-7 and T47D cells were serum starved overnight then treated with indicated concentrations of NT157 for 4 hours. **A.** Protein levels of phospho-SHC, total-SHC, cyclin D1, p21, and actin were determined by immunoblotting. **B.** Total RNA was isolated and reverse transcribed. *CCND1* and *p21* levels were analyzed using qRT-PCR. Data were normalized to *RPLP0* housekeeper gene. **C.** MCF-7 and T47D cells were serum starved overnight, pretreated with or without 3 µM NT157, then induced with or without 5 nM IGF-I for 24 hours. Cells were fixed then stained with propidum iodide. Cell cycle frequencies were determined by flow cytometry. **D.** MCF-7 and T47D cells were serum starved overnight, pretreated with or without 3 µM NT157 for 4 hours, then stimulated with or without 5 nM IGF-I for 6 hours. Indicated protein levels were determined by immunoblotting. Data are mean ± SEM; results are representative of at least three independent triplicates experiments.

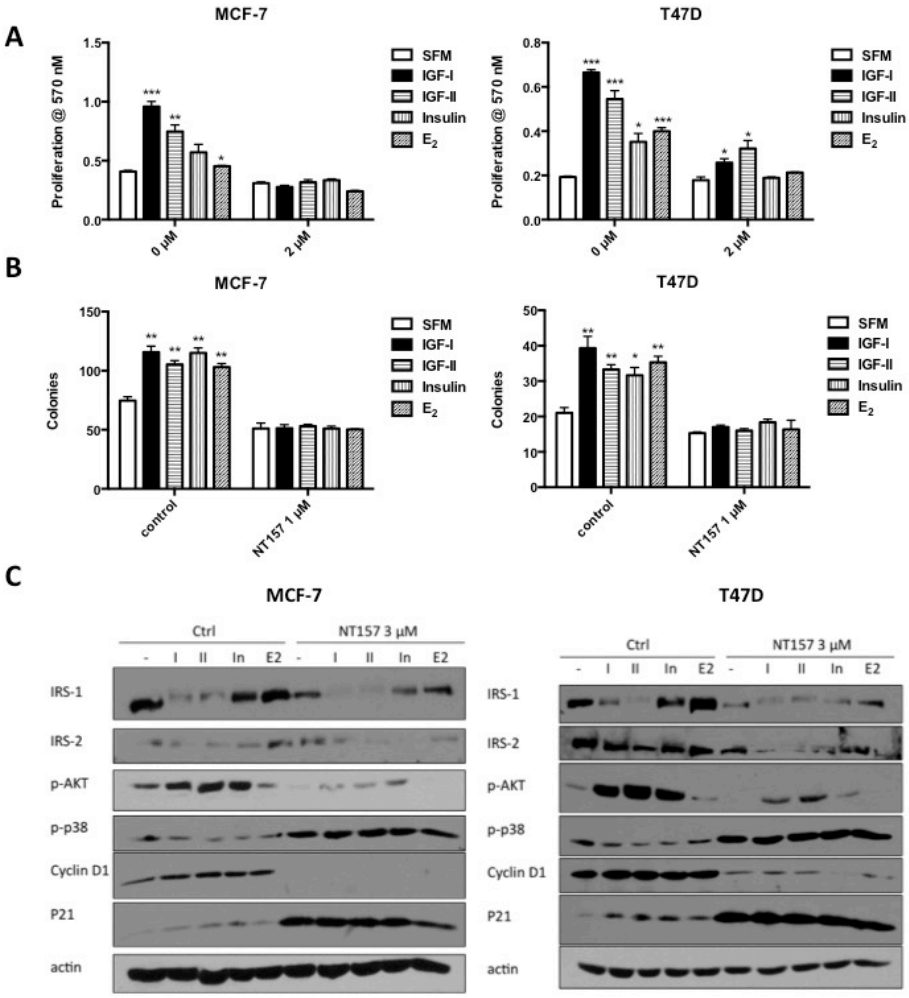

Figure 2.5 NT157 inhibited IGF/insulin system ligand and E_2 induced monolayer and anchorage independent growth in ERα+ breast cancer cells.

A. MCF-7 and T47D were plated in 24-well plates, serum starved overnight then treated with indicated treatments (IGF-I 5nM, IGF-II 10 nM, insulin 10 nM, and E_2 1 nM). Monolayer proliferation was evaluated using MTT assay, with results displayed as absorbance at 570 nm. **B.** MCF-7 and T47D cells were serum starved and treated with or without NT157 and ligands in 1% FBS in 0.45% agar and overlaid on 0.8% bottom agar. Colony growth in agarose was assessed after 14 days. Colonies formed were counted and averaged from 5 individual microscopic fields. Results displayed are the average number of colonies in 5 fields of 3 wells. **C.** MCF-7 and T47D cells were serum starved overnight, treated with or without NT157 and ligands for 24 hours. Indicated protein levels were determined by immunoblotting. Data are mean ± SEM; results are representative of at least three independent triplicates experiments.

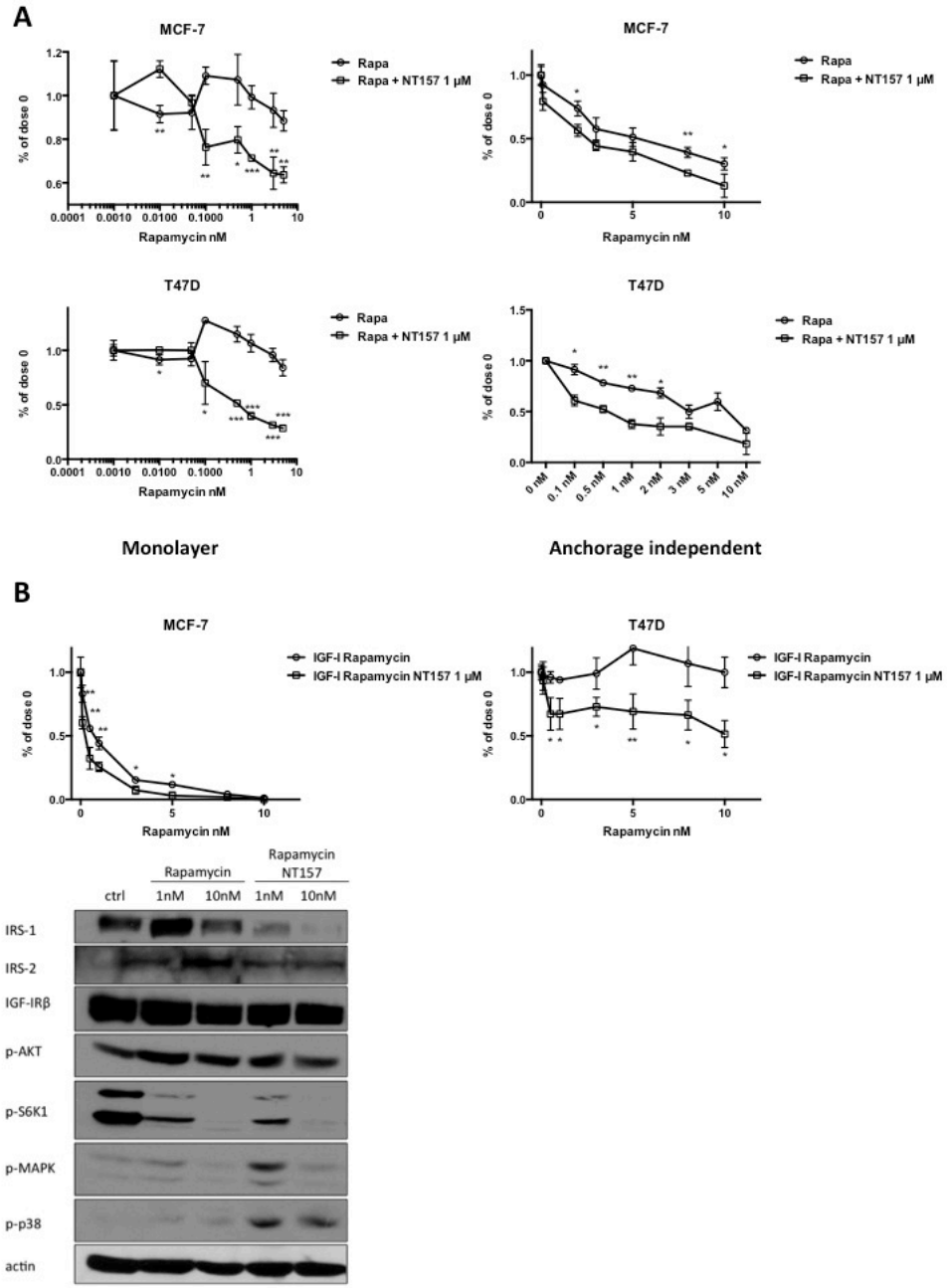

Figure 2.6 NT157 treatment sensitized ERα+ breast cancer cells to rapamycin.
A. Left panels: MCF-7 and T47D cells were plated then treated with indicated combinations for 5 days. Monolayer proliferation was evaluated by MTT assay. Right panels: MCF-7 and T47D cells were plated in 6-well plates treated with indicated combinations. Anchorage independent growth was determined by colony formation in agarose after 14 days. **B.** Top panels: MCF-7 and T47D cells were serum starved overnight, treated with indicated combinations. Formed colonies were counted and analyzed after 14 days. Bottom panel: MCF-7 cells were treated with indicated combinations. Protein levels of IRS-1, IRS-2, IGF-IRβ, phospho-AKT, phospho-S6K1, phospho-$p38^{MAPK}$, and actin were determined by immunoblotting. Data are mean ± SEM; results are representative of at least three independent triplicates experiments.

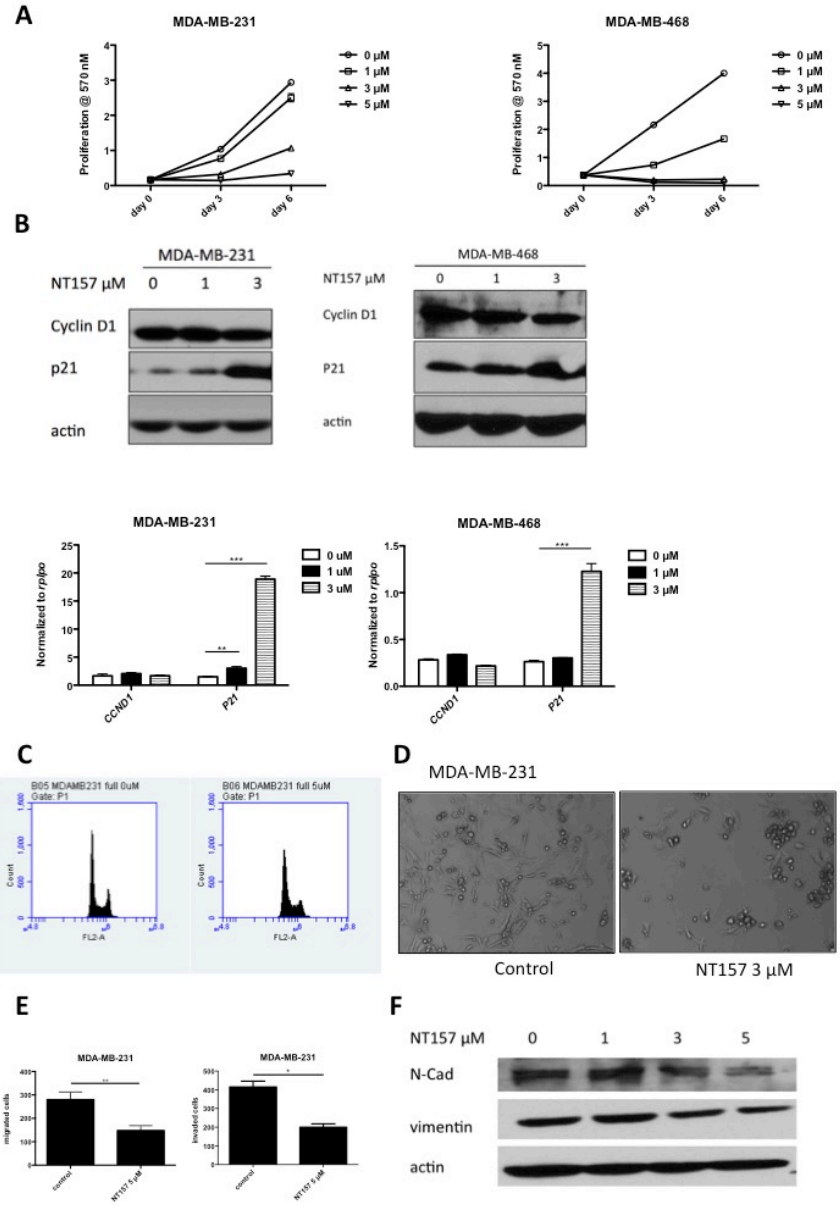

Figure 2.7 NT157 inhibited proliferation and migration in basal like breast cancer cells.
A. MDA-MB-231 and MDA-MB-468 cells were plated and treated with or without NT157 in full growth media. Proliferation was evaluated after 3 and 5 days by MTT assay. **B.** MDA-MB-231 and MDA-MB-468 cells were plated and treated with indicated dosages of NT157. Top panels: indicated protein levels were determined by immunoblotting. Bottom panels: total RNA was isolated and reverse transcribed. Indicated mRNA levels were assessed by qRT-PCR. **C.** MDA-MB-231 cells were treated with or without 5 µM NT157. Cells were fixed then stained with propidum iodide. Cell cycle frequencies were determined by flow cytometry. **D.** MDA-MB-231 cells were plated in 6-well plate and treated with with or without 3 µM NT157 for 24 hours. Phase-contrast images for cell morphology were captured by Leica microscopy. **E.** MDA-MB-231 cells were treated with or without 5 µM NT157 and 5 nM IGF-I. Cell migration potential was evaluated by boyden chamber assay. **F.** MDA-MB-231 cells were treated with indicated dosages of NT157 for 4 hours. Lysates were separated by SDS-PAGE and indicated protein levels were determined by immunoblotting. Data are mean ± SEM; results are representative of at least three independent triplicates experiments.

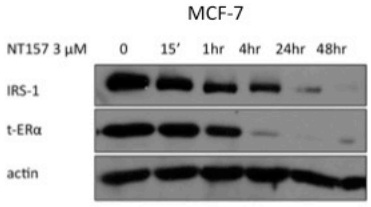

Figure 2.8 NT157-induced IRS protein degradation was specific.
A. MCF-7 cells were serum starved overnight then treated with 3 μM NT157 for indicated time period. Protein levels of IRS-1, total ERα, and actin were determined by immunoblotting.

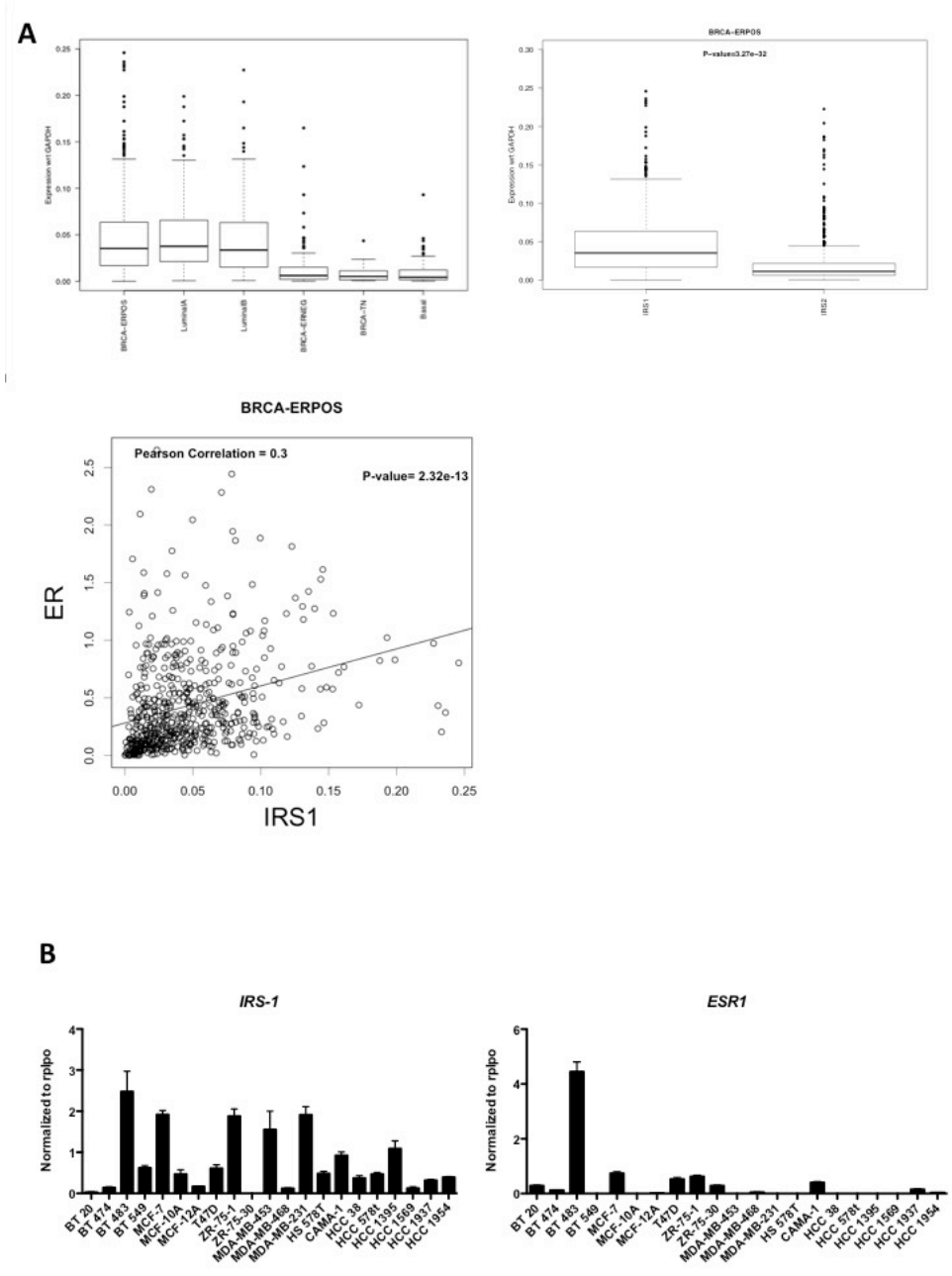

Figure 2.9 *ESR1* and *IRS-1* expression were positively correlated in primary breast cancers and cell lines.
A. Top panels: expression analysis of *IRS-1* and *IRS-2* genes in TCGA Breast Cancer subtypes. Left: Box-whisker plot of IRS1 expression normalized to the housekeep gene *GAPDH* in different breast cancer subtypes. Right: Box-whisker plots of normalized *IRS-1* and *IRS-2* expression in ER positive breast cancers. Bottom panel: scatter plot of *ESR1* vs *IRS-1* in ER positive breast cancers. Straight line shows the best fit with a Pearson correlation factor of 0.3. **B.** mRNA expression of *IRS-1* (left) and *ESR1* (right) in a panel of breast cancer cell lines were determined by qRT-PCR. Data are mean ± SEM; all qRT-PCR results are representative of at least three independent triplicates experiments.

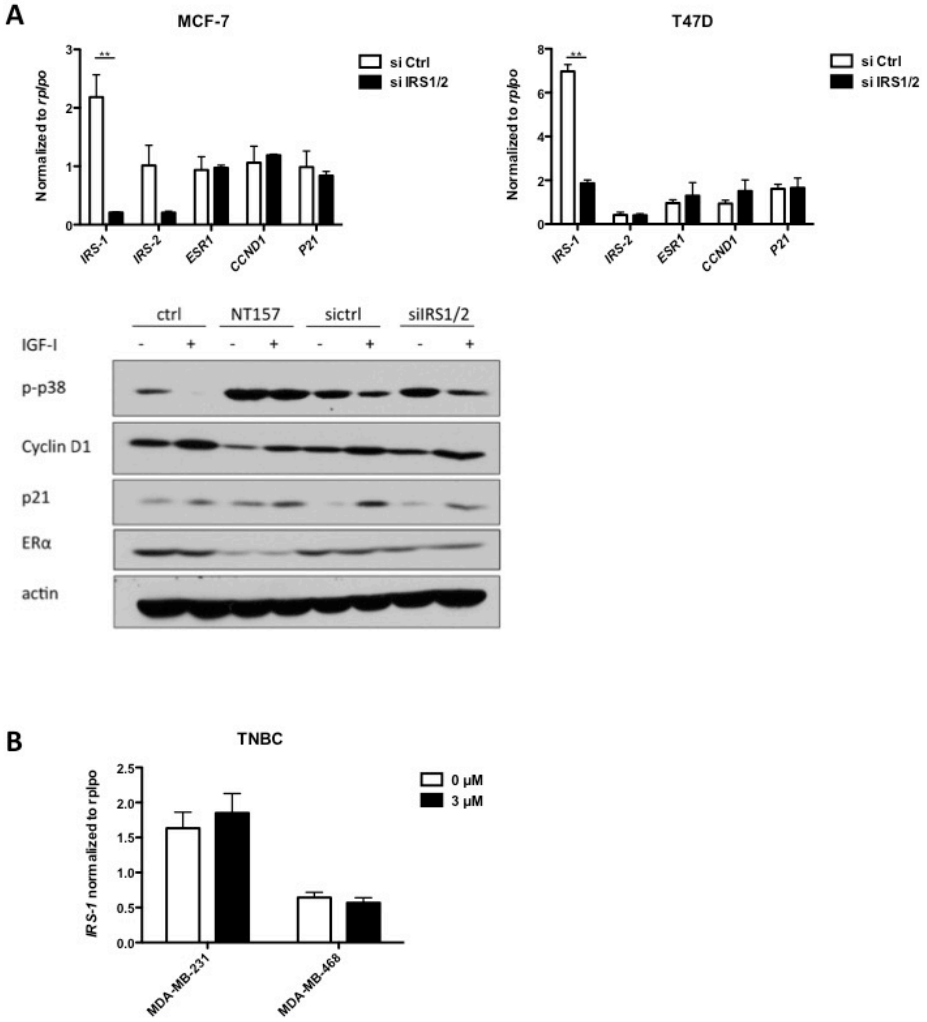

Figure 2.10 The suppressive effects of NT157 on cell cycle regulation was through ER degradation.
A. Top panels: MCF-7 and T47D cells were transfected with 25nM siRNA control or 25 nM siRNA IRS1/2 for 48 hours. Total RNA was isolated and reverse transcribed. mRNA expressions of *IRS-1*, *IRS-2*, *ESR1*, *CCND1*, and *p21* were determined by qRT-PCR. Bottom panel: MCF-7 cells were 1) serum starved overnight, pretreated with 3 μM of NT157 for 4 hours, then induced with or without 5nM IGF-I for 6 hours; 2) transfected by control or IRS1/2 siRNA for 48 hr, starved overnight, then stimulated with or without 5 nM IGF-I for 4 hours. Protein levels of phospho-p38^{MAPK}, cyclin D1, p21, ERα, and actin were assessed by immunoblotting. **B.** MDA-MB-231 and MDA-MB-468 cells were treated with 3μM NT157 drug for 4 hours. Total RNA was isolated and reverse transcribed. mRNA level of *IRS-1* was determined by qRT-PCR. Data are mean ± SEM; results are representative of at least three independent triplicates experiments.

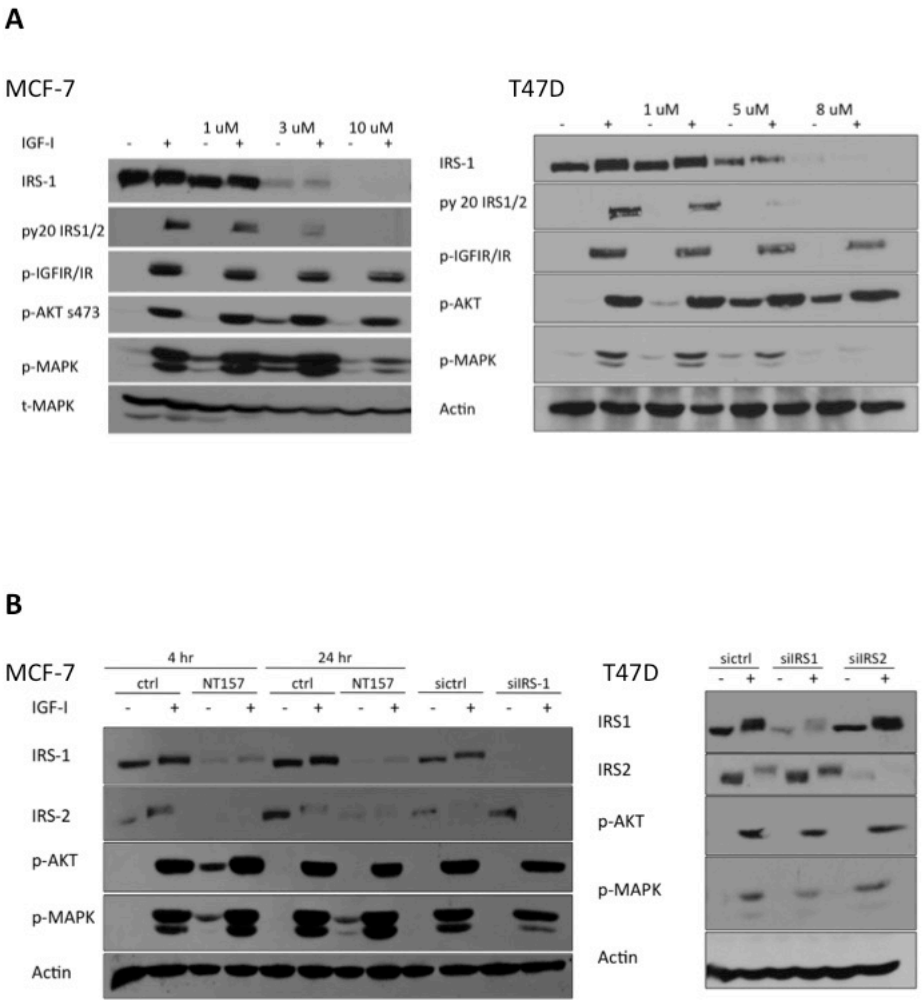

Figure 2.11 Neither NT157 treatment nor genetic down-regulation of IRS1 or IRS2 affected short term IGF-I stimulation induced PI3K and MAPK signaling.
A. MCF-7 and T47D cells were starved overnight, pretreated with indicated dosages of NT157 drug for 4 hours, and stimulated with or without 5 nM IGF-I for 10 minutes. Protein levels of IRS-1, py20, phospho-IGF-IR/IR, phospho-AKT, phospho-MAPK, total MAPK, and actin were determined by immunoblotting. **B.** MCF-7 and T47D cells were transfected with 25 nM siRNA control, siRNA IRS-1, or siRNA IRS-2 for 48 hours. Cells were then serum starved overnight and treated with 5 nM IGF-I for 10 minutes. Protein levels of IRS-1, IRS-2, phospho-AKT, phospho-MAPK, and actin were determined by immunoblotting.

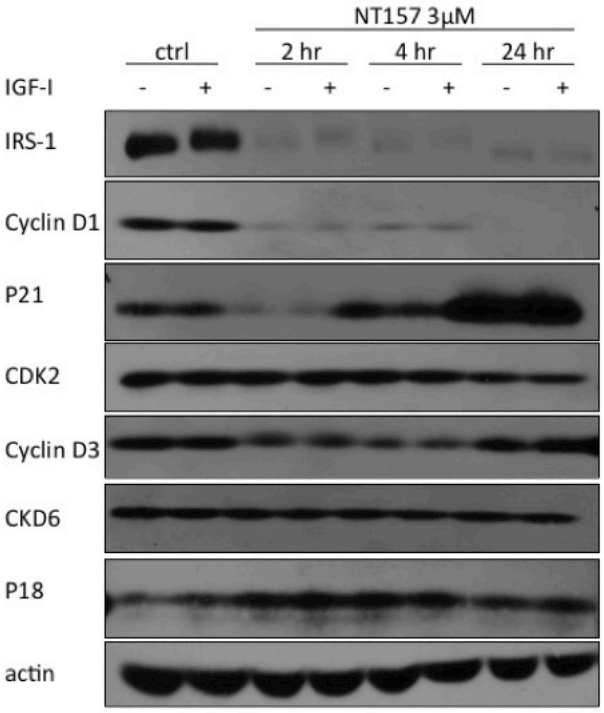

Figure 2.12 NT157 specifically suppressed cyclin D1 and induced p21 in MCF-7 cells.
MCF-7 cells were starved overnight, pretreated with or without 3μM NT157 drug for 4 hours, then stimulated with or without 5 nM IGF-I for 6 hours. Protein levels of IRS-1 cyclin D1, p21 CDK2, cyclin D3, CKD6, p18, and actin were determined by immunoblotting.

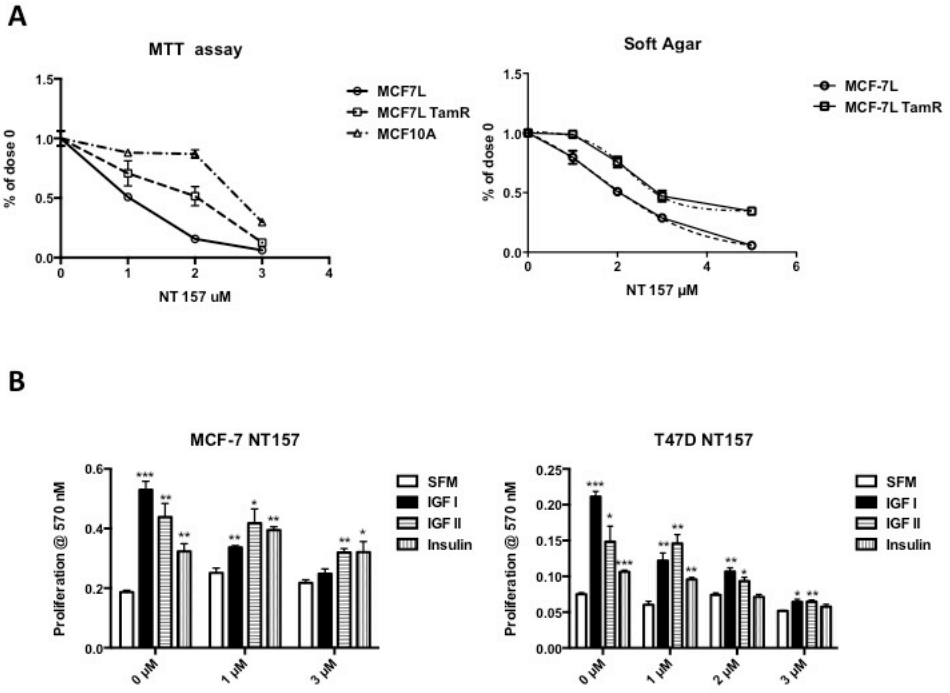

Figure 2.13 NT157 inhibited proliferation in ERα+ breast cancer cells in a dose dependent manner.
A. Left: MCF-7L and MCF-7L TamR cells were plated in 24 well plates and treated with indicated dosages of NT157 drug for 5 days. Monolayer proliferation was determined by MTT assay. Right: MCF-7L and MCF-7L TamR cells were plated in 6-well plates and treated with indicated dosages of NT157. Anchorage independent growth was determined by colonies formation in agarose after 14 days. **B.** MCF-7 and T47D cells were serum starved overnight then treated with indicated treatment combination for 5 days. Monolayer proliferation was measured by MTT assay. Data are mean ± SEM; results are representative of at least three independent triplicates experiments.

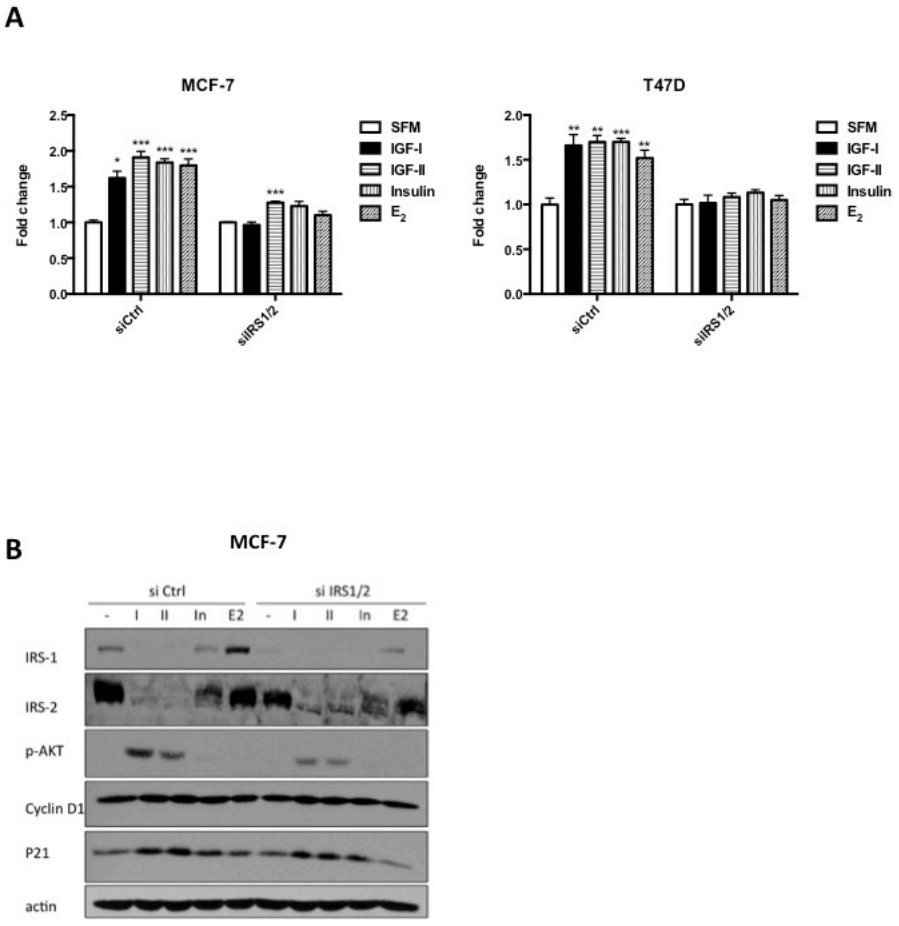

Figure 2.14 Genetic downregulation of IRS1/2 partially suppressed proliferation and prolonged IGF-I induced PI3K activation in ER*α*+ breast cancer cells.
A. MCF-7 and T47D cells were transfected with 25 nM siRNA control or 25 nM siRNA IRS1/2 for 48 hours. Cells were serum starved overnight then plated in 6-well plates and treated with IGF-I (5 nM), IGF-II (10 nM), insulin (10 nM), and E_2 (1 nM). Anchorage independent growth was determined by colonies formation in agarose after 14 days. **B.** MCF-7 cells were transfected with 25 nM siRNA control or 25 nM siRNA IRS1/2 for 48 hours. Cells were starved overnight then plated in 6-well plates and treated with IGF-I (5 nM), IGF-II (10 nM), insulin (10 nM), and E_2 (1 nM) for 24 hours. Protein levels of IRS-1, IRS-2, phospho-AKT, cyclin D1, p21, and actin were determined by immunoblotting. Data are mean ± SEM; results are representative of at least three independent triplicates experiments.

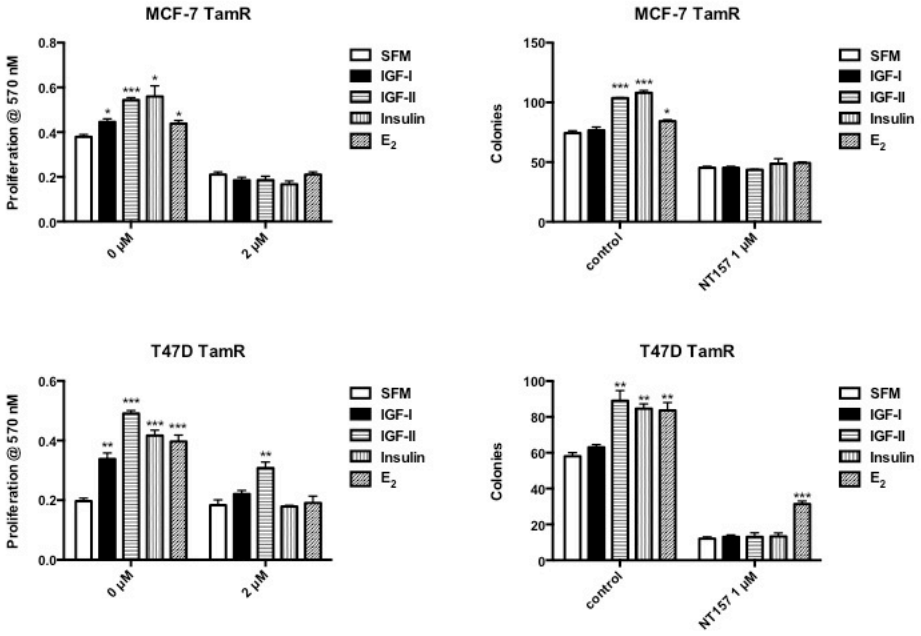

Figure 2.15 NT157 inhibited ligand induced proliferation in tamoxifen resistant ERα+ breast cancer cells.
MCF-7 TamR and T47D TamR cells were 1) serum starved overnight then treated with indicated combinations. Monolayer proliferation was assessed by MTT assay after 5 days (left panels). 2) Starved overnight then treated with indicated combinations. Anchorage independent growth was determined by colonies formation in agarose after 14 days (right panels). Data are mean ± SEM; results are representative of at least three independent triplicates experiments.

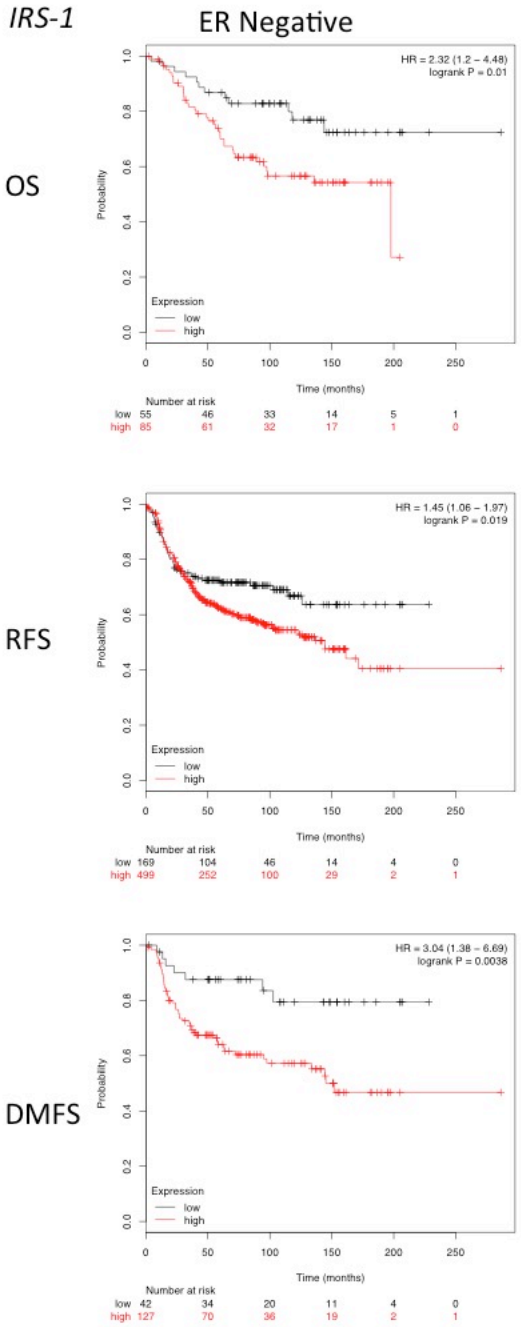

Figure 2.16 *IRS-1* expression had prognostic value in ER negative breast cancers.
Kaplan–Meier plots of overall survival (OS, top panel), refractory free survival (RFS, middle panel), and distant metastatic free survival (DMFS, bottom panel) of patients with ER negative breast cancer with high or low expression of *IRS-1*. Data obtained from the Kaplan–Meier plotter database[123].

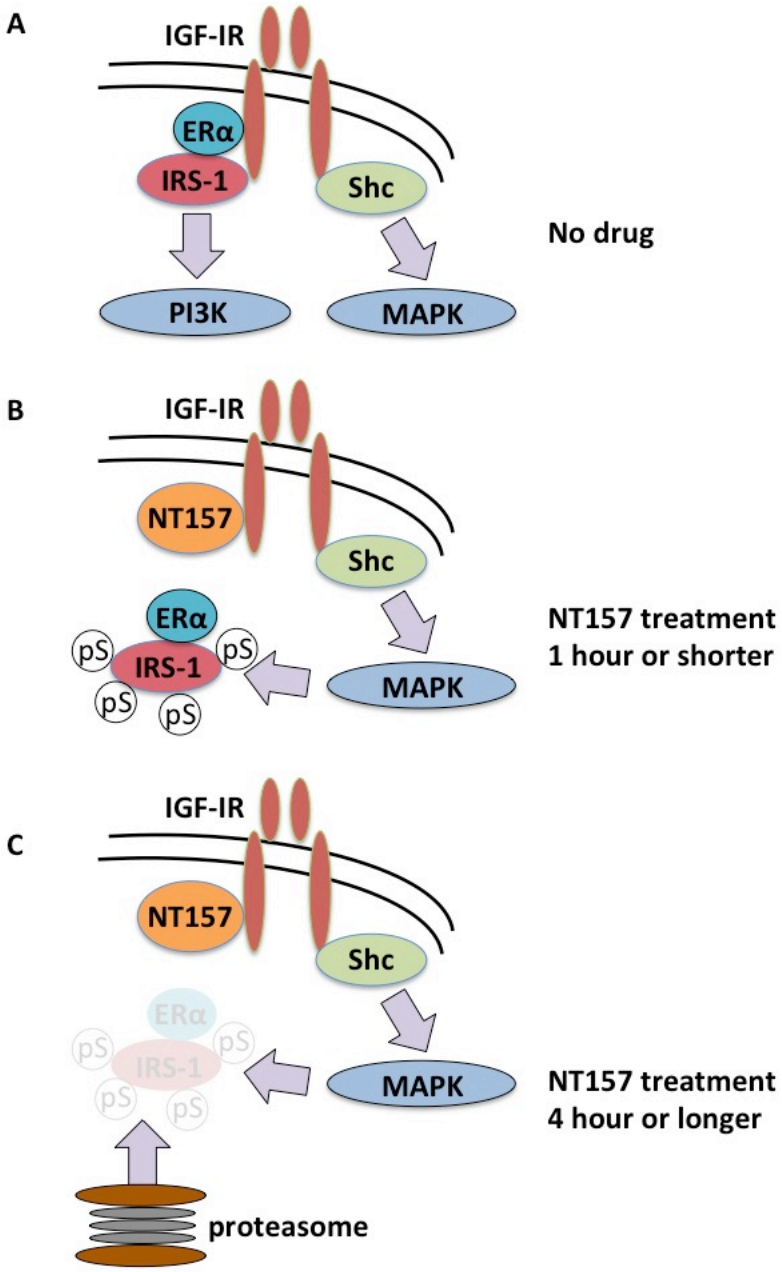

Figure 2.17 Model for the inhibitory effects of NT157 on IRS-1 and ERα in ER+ human breast cancer cells. **A.** Under normal condition, IGF-IR signals through the IRS-1/2-PI3K axis, inducing cellular proliferation. **B.** NT157 initially binds to an allosteric site on IGF-IRβ subunit and induces a conformational change, leading to the dissociation of IRS-1/ERα complex from the receptor. Compensational hyper-activated MAPK mediates cytoplasmic extensive serine-phosphorylation of IRS-1 protein. **C.** Serine-phosphorylated IRS-1/ERα complex is targeted for degradation by the proteasome and IGF ligand induced PI3K signaling becomes severely impaired.

Chapter 3

Targeting IGF/Insulin system downstream effector xC^- transporter in estrogen receptor positive breast cancer cells.

Yuzhe Yang and Douglas Yee

IGF-I regulates redox status in breast cancer cells by activating the amino acid transport molecule xc^-.

Cancer Res. 2014; 74**:** 2295-2305.

Introduction

The insulin like growth factor [61] signaling pathway stimulates growth and metastasis in many types of cancer [6, 124]. Ligand dependent activation of the type I IGF receptor (IGF-IR) results in recruitment of the insulin receptor substrate (IRS) adaptor molecules to transduce signals to downstream signaling cascades and ultimately regulate cell behavior. In breast cancer cells, IRS-1 and IRS-2 are the two primary adaptor proteins that regulate IGF-IR signaling [125]. In model systems, IRS-1 mainly promotes cell proliferation [100, 101], while IRS-2 stimulates cell motility [99, 101].

The clinical results of anti-IGF-IR monoclonal antibody trials in breast cancer have been disappointing [126]. Given that breast cancer is highly heterogeneous, there is an urgent need to identify predictive biomarkers [119, 127] that correlate with IGF-IR driven tumors and to characterize additional molecular targets that may synergize with anti-IGF-IR therapy. To identify potential biomarkers, our laboratory characterized the gene expression profiles of T47D variant cell lines with differential IRS protein expression [101] upon IGF-I stimulation (Becker *et al*, submitted). *SLC7A11* mRNA expression was upregulated by IGF-I in an IRS-1 specific manner.

SLC7A11 (or xCT) encodes the functional subunit of cystine-glutamate exchange transporter: xC^-. xC^- transporter mediates the uptake of extracellular L-cystine in exchange for L-glutamate. The cell membrane expression of xC^- transporter is essential for uptake of extracellular cystine to generate intracellular cysteine to maintain intracellular glutathione (GSH) levels [128]. GSH controls the intracellular redox state [128, 129] protecting cells from multiple sources of damage including chemical, radiological, and direct reactive oxygen species (ROS) [130] mediated damage. The roles of ROS in cancer are complex due to the heterogeneity of downstream signaling cascades activated in response to their generation [131, 132]. Continuous exposure to endogenous or exogenous ROS stress results in some cancer cells undergoing apoptosis or growth arrest [133]. Other cells can develop redox adaptive mechanisms [134] to prevent apoptosis and also increase genomic instability [135], promote malignant transformation,

metastasis [136], and contribute to drug resistance [137]. Recent studies reported that xCT deficiency sensitizes malignant cells' response to oxidative stress [133, 138] and inhibits cancer cell growth [128] and metastasis [139]. The expression level of xCT predicts chemosensitivity to multiple drugs [140], and combining the xCT chemical inhibitor sulfasalazine (SASP) with a HSP90 inhibitor celastrol shows synergistic anti-cancer effects [141].

This study determined the role for IGF-I stimulation of breast cancer cells in the generation of intracellular ROS through the regulation of xCT expression and function. Co-targeting xC^- transporter with anti-IGF-IR therapy was explored as a way to increase the efficacy of targeting both pathways. We found that IGF-I stimulated xC^- expression in an IRS-1 dependent manner. IGF-I also regulated cellular redox status partially through xC^- transporter and thereby enhancing cancer cell proliferation.

Results

IGF-I stimulated SCL7A11 (xCT) mRNA expression in an IRS-1 dependent manner in estrogen receptor positive luminal but not in basal-like breast cancer cells

T47D-YA cells express neither IRS-1 nor IRS-2 [130]. We created T47D-YA cells that stably expressed either IRS-1 or IRS-2 cDNA [101]. T47D-YA, T47D-YA IRS-1 expressing cells (T47D-YA-IRS-1), and T47D-YA IRS-2 expressing cells (T47D-YA-IRS-2) were used to generate IRS isoform specific gene profiling upon IGF-I stimulation (Becker *et al*, submitted). *SLC7A11* (xCT) was one of the genes regulated by IGF-I only in T47D-YA-IRS-1 cells. To confirm the gene array result, quantitative reverse transcript PCR was performed using primers specific to xCT. The result was consistent with gene array data, after 4 hours of IGF-I exposure, xCT mRNA expression was significantly induced only in the T47D-YA-IRS-1 cells (Figure 3.1 A).

We next examined the mRNA expression of xCT upon IGF-I stimulation in two classes of human breast cancer cells: three estrogen receptor (ER) positive breast cancer

cell lines: MCF-7, T47D, and ZR-75-1, where IRS-1 mRNA expression was higher than in the three ER-negative breast cancer cell lines: MDA-MB-231, BT549, and HS578T, where IRS-2 was the predominant isoform expressed (Figure 3.1 B left panel). IRS-1 and -2 protein expression was examined in four of the cell lines (Figure 3.1 C) to confirm the mRNA expression levels. In the three ER positive cell lines, xCT mRNA expression was significantly upregulated by IGF-I, while no regulation was observed in the ER-negative cells (Figure 3.1 B right panel) although the basal expression of xCT mRNA was significantly higher. Since ER regulates IRS-1 expression [75], we further investigated regulation of xCT in MCF-7L cells and MCF-7L selected for resistance to tamoxifen (TamR) cells as previously described [40]. TamR cells expressed lower levels of IRS-1 (Figure 3.1 D left panels) and IGF-IR while maintaining insulin receptor levels [40]. IGF-I treatment stimulated xCT mRNA and protein expression in MCF-7L parental cells but not in the MCF-7L TamR cells. In parental cells, IGF-II and insulin induced xCT mRNA and protein expression while in TamR cells none of the ligands stimulated expression of xCT (Figure 3.1 D right panels) above their higher basal levels. This suggested that without sufficient IRS-1 expression there is little effect on xCT expression despite functional insulin receptor signaling.

To evaluate the relevance of xCT expression in human primary breast cancers, we evaluated its expression in The Cancer Genome Atlas (TCGA) database. We found that the xCT relative mRNA expression in invasive ductal breast cancer (IDBC) samples was significantly higher than that in normal breast tissue. ER positive IDBC expressed lower levels of xCT gene compared to ER negative or triple negative IDBC (Figure 3.2 A). We next utilized a large public microarray database to evaluate the prognostic relevance of xCT in breast cancer patients [123]. We found that high xCT expression significantly correlated with poor overall survival (OS) and distant metastasis free survival (DMFS) in estrogen receptor positive patients (Figure 3.2 B). These findings from primary breast cancer specimens were consistent with our laboratory observations. The results implied that xCT expression and function might link to outcome and expression levels varied among the intrinsic subtypes of breast cancer.

To further confirm the role of IRS-1 in IGF-I regulation of xCT expression, either control or IRS-1 specific siRNAs (Figure 3.7) were transfected into ER positive cells (Figure 3.3 A upper panels, 3.8 A). xCT mRNA expression and protein expression in MCF-7, T47D, and ZR-75-1 were induced by IGF-I only when IRS-1 was expressed at normal levels (Figure 3.3 A lower panels, 3.8 B). Expression of xCT protein was seen after 24 hour of IGF-I stimulation likely due to a requirement for protein synthesis. These results suggested that IGF-I stimulated xCT expression in an IRS-1 dependent manner in ER positive breast cancer cells.

We next evaluated potential downstream signaling pathway required for IGF-I regulated xCT expression. MCF-7 cells were treated with anti-IGF-IR monoclonal antibody, huEM164, IGF-IR/insulin receptor tyrosine kinase inhibitor AEW-541, PI3K pathway inhibitor LY294002, or MEK inhibitor U01026 (Figure 3.3 B, 3.9). IGF-I regulated xCT mRNA expression via IGF-IR was dependent on PI3K pathway signaling but not MAPK.

IGF-I stimulated xC^- transporter function

To investigate whether xC^- function was affected by IGF-I stimulation, two direct functional assays were performed to measure the intracellular level of reduced GSH and the extracellular level of glutamic acid in three ER positive breast cancer cell lines and MDA-MB-231 cells. After 24 hours of IGF-I exposure, significant induction of both extracellular glutamic acid levels and intracellular reduced GSH concentrations in MCF-7 and T47D cells was observed but not in MDA-MB-231 (Figure 3.4 A, B, C).

To demonstrate that these effects were mediated by xCT, we used sulfasalzasine (SASP) an inhibitor of xC^- function. Cells treated with 0.1 mM SASP (Figure 3.10 A, B) [128, 133, 141], showed depletion of intracellular GSH and diminished IGF-I regulated GSH levels (Figure 4B). GSH production requires gamma-glutamylcysteine synthetase function to ligate cysteine with glutamate. Buthionine sulfoximine (BSO) [142] inhibits this ligation and Figure 3.4 B shows BSO had similar effects to SASP. Taken together,

these data show that IGF-I regulation of xC^- transporter function results in the import of cystine to increase the intracellular reduced GSH levels via an IRS-1 dependent manner in ER positive breast cancer cells. In the ER-negative breast cancer cell line, MDA-MB-231, high basal extracellular levels of glutamic acid were consistent with the expression of xCT in ER-negative primary breast cancers (Figure 3.2 A).

IGF-I regulated cellular redox status via xC^- transporter

Reduced GSH is a major cellular antioxidant molecule controlling cellular redox balance. We next examined whether IGF-I induced intracellular GSH level might further regulate cellular ROS level in cancer cells. We either irradiated [143] or treated cells with mitomycin C to induce intracellular ROS production. A ROS-sensitive fluorescent probe 2',7'-dichlorofluorescein diacetate (DCFH-DA) was used to detect cellular ROS.10 gray irradiation (Figure S5 A) or 0.1 μg/ml mitomycin C (Figure 3.11 B) significantly increased the intracellular ROS levels. The irradiation induced ROS was reduced by treating cells with ROS scavenger N-acetyl cysteine (NAC) [144] (Figure 3.5 C right panel, 3.10 E right panel). A ROS insensitive probe 5-(and-6)-carboxy-2',7'-dichlorofluorescein diacetate (carboxy-DCFDA) was used as assay control (Figure 3.5 C right panel). IGF-I treatment blunted the response to ROS production in MCF-7 and T47D (Figure 3.5 A, 3.11 A, B) but not in the basal-like MDA-MB-231 cells (Figure 3.11 A). The IGF-I-mediated reduction of ROS was diminished (Figure 3.5A, 3.11 A) or partially attenuated (Figure 3.4 A right panel, 3.11 B) when cells had been pretreated with 0.1 mM SASP. Since xCT expression and function were higher in basal like breast cancer cells (Figure 3.1 B right panel, 3.2 A, 3.4 A) than in ER positive MCF-7 cells, the basal ROS levels in MDA-MB-231 cells were lower than in MCF-7 (Figure 3.11 A).

IGF-I treatment markedly reduced the phosphorylated form of $p38^{MAPK}$, a major effecter of ROS [131, 145], in MCF-7 and T47D cells. Consistent with the results obtained from direct ROS measurement experiments, pretreatment of ER positive cells with SASP, attenuated phosphorylation of $p38^{MAPK}$ after IGF-I treatment (Figure 3.5 B, 3.11 B).

Thus, our results suggested that IGF-I reduced cellular redox level specifically, but not completely, by stimulating the expression and function of xC^- transporter in ER positive breast cancer cells. We also found that IGF-I-induced ROS reduction was mediated by the IGF-IR/PI3K signaling axis as pathway inhibitors (huEM164, LY 294002, and AEW-541) decreased IGF-I's ability to reduce ROS generation (Figure 3.5 C left panel).

In addition to the findings above, anchorage independent growth assays showed that SASP significantly sensitized MCF-7 cells response to both irradiation and mitomycin C treatments in serum depleting condition, which was reversed by treating cells with NAC (Figure 3.5 D). We further verified that BSO had similar effects as SASP did (Figure 3.14 A), which was partially over-tuned by adding NAC. Our data implied that SASP could enhance response to ROS inducing therapies by lowering intracellular GSH level.

Disruption xC^- transporter function suppressed IGF-I-induced monolayer and anchorage independent growth

Increased ROS levels have been reported to arrest growth or even cause apoptosis in cancer cells which lack oxidative adaptive mechanisms [131]. MCF-7 cells have relatively high basal levels of ROS under serum depleting condition (Figure 3.11 A), which resulted in partial growth arrest (Figure 3.6 A, B, Table 3.1). IGF-I induced MCF-7 cell proliferation might be mediated by stimulating xC^- transporter function to increase cellular GSH level to protect cells from ROS. To test this hypothesis, we either pretreated MCF-7 cells with SASP to disrupt xC^- transporter function or stably infected xCT-specific shRNA (Figure 3.12) to downregulate its expression level and performed monolayer growth assays. We found that 0.1 mM SASP inhibited the function of xC^- transporter without significant cytotoxicity in MCF-7 (Figure 3.10 A). Both chemical inhibition and genetic downregulation of xCT expression significantly suppressed IGF-I-induced monolayer growth (Figure 3.6 A, B). SASP effects were reversed by adding

NAC (Figure 3.6 A). Cell cycle flow cytometry analysis showed that IGF-I stimulated cell S phase frequency was partially repressed when xC^- transport was disrupted, which could be rescued by NAC (Table 3.1). Anchorage independent growth assays in MCF-7 cells showed similar results (Figure 3.6 C). Parallel sets of experiments were done by treating cells with BSO instead of SASP to directly investigate the involvement of cellular GSH in these observations (Figure 3.14 B, C) with similar results. These data indicated that IGF-I stimulates MCF-7 cell growth partially by regulation of xC^- transporters to control cellular GSH and redox levels.

Disruption of xC^- transporter sensitized ER positive breast cancer cells to anti-IGF-IR therapy.

SASP treated MCF-7 cells showed significant intracellular GSH depletion resulting in elevated ROS and phospho-$p38^{MAPK}$ (Figure 3.5 A-C). Anti-IGF-IR therapy such as huEM164 and AEW-541 both diminished IGF-I regulation of cellular ROS (Figure 3.5 C) and $p38^{MAPK}$ activation (Figure 3.9) while increasing the basal $p38^{MAPK}$ activity in MCF-7 cells (Figure 3.9). Thus, anti-IGF-IR drugs with xCT inhibition to improve growth suppression.

In anchorage independent growth assays, MCF-7 cells were treated with 1 μg/ml huEM164 or 0.1 μM AEW-541. These lower drug doses were unable to suppress IGF-I stimulated anchorage independent growth. However, when the IGF-IR targeted therapies were combined with SASP, IGF-I stimulated colony formation was completely (huEM164) or partially (AEW-541) inhibited in the MCF-7 cells, which was reversed by treating cells with NAC (Figure 3.6 C). Notably, SASP enhanced the growth inhibition of anti-IGF-IR drugs at lower concentrations of these anti-IGF drugs than normally required (normally 20 μg/ml huEM164, 0.3 μM AEW-541) for maximal inhibition of signaling and growth [40]. Similar results were observed by using BSO instead of SASP (Figure 3.14 C). Thus, the biological effects of IGF-IR inhibition could be enhanced by disrupting xCT effects while using lower doses of the anti-IGF-IR drugs.

Discussion

It is well known that cellular ROS causes genome instability and mutation to stimulate tumorigenesis and increase resistance to therapy. Our data revealed that IGF-I signaling increases xC^- transporter expression and function in IRS-1 activated ER positive to affect cellular redox status and promote proliferation. We also further found that stimulation MCF-7 cells with IGF-II or insulin both induced xCT mRNA expression (Figure 3.13) implying a similar role for insulin receptor acting through IRS-1. These data imply that ER positive breast cancer cells require activated IRS-1 signaling to overcome oxidative stress. In contrast, the high basal levels of xCT in ER-independent breast cancer cells might have mobilized a set of ROS adaptive mechanisms independent of the growth factor/IRS-1 signaling.

It has been recently reported that CD44 variant stabilizes cell surface xCT expression [133]. Given that MDA-MB-231 cells are CD44 positive and MCF-7 cells are CD44 negative [146], we confirmed that the basal expression and function of xCT was significantly higher in MDA-MB-231 cells than in MCF-7 cells (Figure 3.1 B right panel, 3.4 A). MCF-7 cells expressed little amount of CD44 variant, and none of the IGF ligands (IGF-I, IGF-II, insulin) regulated CD44v mRNA expression (Figure 3.13) indicating that the xCT regulation of IGF-I might be independent of CD44 variant.

Although in our study the expression and function of xC^- is not regulated by IGF-I in MDA-MB-231 cells, we still found that low concentration of SASP (0.1 mM) treatment depleted the cellular GSH level; genetically downregulation of xCT or SASP treatment also decreased the basal proliferation and migration in MDA-MB-231 cells (Figure 3.15 A, B). A recent study showed that xC^- transporters are commonly expressed in triple negative breast cancer cells. Targeting xC^- transporters might yield another therapeutic opportunity for the triple negative breast cancers as well [147]. Our data also suggested that xC^- targeting could have a role in ER-positive breast cancer cells.

We observed that down-regulation of IRS-1 by siRNA resulted in a significant increase of basal xCT protein expression (Figure 3.3 A lower right panel). Consistently, in our experiments, we also observed that the basal xCT expression in MCF-7L TamR was higher than that in MCF-7L parental cells (Figure 3.1 D lower right panel). We further examined the xCT protein expression in T47D-YA and T47D-YA-IRS-1 cells and found that T47D-YA cells expressed significantly more xCT protein than T47D-YA-IRS-1 cells did (Figure 3.15 C). In patient specimens, ER expression tended to negatively correlated with xCT expression while positively correlated with IRS-1 expression in TCGA breast cancer database. Given the development of new anti-IRS-1 targeted therapies [148], our data suggest that IRS-1 targeting might have adverse effects on ROS status. Further investigation is needed to understand the potential role of IRS-1 protein expression in regulating xCT expression levels.

In this study, we inhibited xCT function with SASP and also used the potent glutathione inhibitor BSO to examine the effects of GSH levels on breast cancer growth. (Figure 3.14). Both compounds were effective inhibitors highlighting the important role of glutathione in breast cancer cells.

Identification of predictive biomarkers to identify patient populations appropriate for treatment with targeted therapies would improve patient benefit. In addition, identification of key targets in a pathway could result in rational combination therapies. While anti-IGF-IR therapy has not yet proven to be of benefit in unselected patients, it is possible that biomarkers, such as IRS-1, might be used to identify IGF-IR driven tumors. Inhibition of xC^- transporter has been reported to have tumor growth inhibitory effects in several tumor models including triple negative breast cancers, where xCT expression levels are high [128, 133, 141, 147]. Our findings further suggested that xC^- transporter could be a promising predictive biomarker (Figure 3.2 B) and therapeutic target to benefit a much larger population – ER positive breast cancer patients. Both clinic breast cancer patients' data (Figure 3.2 A) and cell culture qPCR data (Figure 3.1 B left panel) showed that the basal expression of xCT mRNA is lower than basal like breast cancers. However,

our study suggests that IGF-I, IGF-II, and insulin could stimulate xCT expression in the ER positive breast cancers through IRS-1 to promote growth. ER positive patients with higher circulating IGF-I, IGF-II, or hyperinsulinemia may have higher expression of xCT and more aggressive tumors. Our laboratory previously accomplished several studies confirmed that anti-IGF-IR monoclonal antibody suppressed ER positive breast cancer growth in mouse model [40, 149]. Targeting IGF-IR together with inhibiting xC^- transporter function might have better therapeutic outcome with lower dosage and less side effects than mono-therapy in ER positive breast cancer patients with high circulating IGFs or hyperinsulinemia. These hypotheses require further investigations in patients' data set or animal models.

Besides directly inhibition of xC^- transporter, recently a promising novel positron emission tomography tracer, (4S)-4-(3-[18F]fluoropropyl)-L-glutamate, specifically for imaging xC^- transporter activity has been proved to have high cancer detection rate in rodents [150] and in clinic trial of patients with non-small cell lung cancer and metastasis or invasive breast cancer [151]. This imaging technique also would offer clinicians a convenient way to monitor malignant cells' adaptation to oxidative stress *in vivo*. Besides, our findings also implied that co-targeting IGF-IR with xC^- transporter might reduce the dosage of anti-IGF-IR agents and attenuate potential side effects. Coupling chemotherapy or radiotherapy with xC^- inhibitor might also achieve synergic therapeutic effect.

In conclusion, our study reveals that IGF-I regulates oxidative stress and thereby promotes proliferation by stimulating xC^- transporter function in an IRS-1 dependent mechanism. xC^- transporter expression level could be a promising biomarker to indicate tumor metabolic status to oxidative stress. xC^- transporter could be also be a target to enhance anti-IGF-IR therapy, chemotherapy, and radiotherapy in multiple subtypes of breast cancer.

Materials and Methods

Reagents and antibodies Growth media and supplements were purchased from Invitrogen (Grand Island, NY). IGF-I was purchased from GroPep (Adelaide, Australia). IGF-II was purchased from Gemini (Woodland, CA). Sulfasalazine (≥98%), L-Buthionine-sulfoximine (≥97%), N-Acetyl-L-cysteine, LY294002, U0126, and actin antibody were purchased from Sigma-Aldrich (St. Louis, MO). Humanized anti-IGF-IR monoclonal antibody huEM164 was generously provided by Immunogen Inc. (Norwood, MA). Antibodies for phosphorylated AKT serine 473, total and phospho-IGF-IR, total and phospho-phosphorylated p44/42 (MAPK), phospho-p38 ^{MAPK}, and IRS-1 were purchased from Cell Signaling Technology (Beverly, MA). The IRS-2 antibody was purchased from Santa Cruz Biotechnology (Santa Cruz, CA). The xCT antibody for Western blot analysis was purchased from Novus Biologicals (Littleton, CO). Horseradish peroxidase-conjugated anti-phosphotyrosine (PY-20) was purchased from BD Biosciences (San Jose, CA). Anti-rabbit and anti-mouse horseradish peroxidase-conjugated secondary antibodies were purchased from Pierce (Rockford, IL). 5-(and-6)-carboxy-2',7'-dichlorofluorescein diacetate was purchased from Invitrogen (Carlsbad, CA).

Cell lines and culture MCF-7, ZR-75-1, T47D, MDA-MB-231, BT549, and HS578T cells were purchased from the ATCC (Manassas, VA) and cultured following ATCC's instruction. MCF-7L cells were kindly provided by C. Kent Osborne (Baylor College of Medicine) and maintained in improved MEM Richter's modification medium (zinc option) supplemented with 5% FBS and 11.25 nmol/L insulin. MCF-7L were evaluated by comparative genomic hybridization and found to be nearly identical to the MCF-7 cells distributed by the ATCC. MCF-7 TamR cells were generated as described [40]. T47D-YA-IRS-1 and T47D-YA-IRS-2 were maintained in Eagle's Minimal Essential Medium supplemented with 5% fetal bovine serum, 11.25 nmol/L insulin, 10 ml/L 100X non-essential amino acids, 200 μg/ml of G418, and 200 μg/ml of hygromycin. All cells were grown at 37 °C in a humidified atmosphere containing 5% CO_2.

Immunoblot Cells were plated at a density of 3 x 10^5 in 60-mm-diameter. Upon reaching 80% confluency, cells were switched to serum-free medium (SFM) for 24 hour to synchronize cell status, after which treatments were added. Treated cells were washed twice with ice-cold phosphate buffered saline (PBS) on ice and lysed with lysis buffer of 50 mM Tris-Cl (pH 7.4), 1% Nonidet P-40, 2 mM EDTA (pH 8.0), 100 mM NaCl, 10 mM sodium orthovanadate, 1 mM phenylmethysulforny fluoride, and with proteases inhibitor cocktails. Lysates were centrifuged at 21,000 rpm for 15 minutes at 4 °C. Protein concentrations were measured using the bicinchoninic acid protein assay reagent kit (Pierce). Cellular protein (80 μg) was resuspended in 5x Laemmli loading buffer with 60 mg/ml DTT and was resolved by SDS-PAGE, transferred to nitrocellulose membrane, and immunoblotted according to manufacturer guidelines.

siRNA transfection and cell stimulation Cells were cultured in growth medium to reach confluency of 80% then were transfected with 30 nmol/L siRNA (siRNAs SMARTpool were purchased from Santa Cruz Biotechnology) using the TransIT-siQUEST transfection reagent (Mirus, Madison, WI) according to the manufacturer's protocol. 48 hours later, cells were washed twice with PBS and serum starved for another 24 hours in SFM followed by treatments as indicated in the figure legends.

Stable xCT down-regulation with shRNA

Lentiviral pKLO.1 vectors encoding a xCT mRNA specific shRNA sequence (CCGGGCTGATTTATCTTCGATACAACTCGAGTTGTATCGAAGATAAATCAGC TTTTTG) or a scrambled shRNA were purchased from BioMedical Genomics Center (University of Minnesota) and were introduced to MCF-7 cells. 8 mg/ml polybrene was added to increase infection efficiency. MCF-7 cells infected with shRNA were maintained by 1 μg/ml puromycin selection pressure.

Reverse transcription-quantitative real-time polymerase chain reaction Cells were plated at a density of 2 x 10^5 in 6-well-plates in growth media to reach 80% confluency

then synchronized in SFM for 24 hours followed by treatments indicated in the figure legends. Cellular RNA was isolated using TriPure Reagent according to the manufacturer (Roche, Belgium). For quality control and to determine concentration, a 260:280 ratio assay was conducted on a spectrophotometer. Forward and reverse primers were designed to target the following transcripts: *SLC7A11* (xCT) 5'-GGCAACCGCGTAATACTTG-3' and 5'-TTGCAAGCTCACAGCAATTC-3'; *IRS-1* 5'-TCACAGCAGAATGAAGACC-3' and 5'-CTACTGATGAGGAAGATATGAGG-3'; *IRS-2* 5'-TCGTGAAAGAGTGAAGATCTG-3' and 5'-TCCAAACACAGTCATTGCT-3'; *CD44v* 5'-AGAAGGTGTGGGCAGAAGAA-3' and 5'-AAATGCACCATTTCCTGAGA-3'; and *RPLPO* 5'-TGCTGATGGGCAAGAACAC-3' and 5'-GAACACAAAGCCCACATTCC-3'. A total of 1 μg of RNA was reverse transcribed using the Transcriptor Reverse Transcriptase Kit, and quantitative PCR was conducted using the Universal SYBR Green Kit according to the manufacturer's protocol (Roche) on an Eppendorf (Hamburg, Germany) Mastercycler Realplex^4 machine. The relative concentration of mRNA was calculated using cycle threshold values that were derived from a standard curve and normalized to ribosomal protein, large, P_O (RPLPO) as an internal control.

Monolayer growth assay Cells were plated in 24-well-plates at a density of 15,000 cells per well, allowed to attach overnight and starved in SFM for 24 hours to synchronize cells. After 5 days of treatments, growth was assessed via the 3-(4,5-dimethylthiazol-2-yl)-2,5-diphenyltetrazolium bromide (MTT) assay. 50 μl of 5 mg/ml MTT solution in SFM were added to each well and incubated for 4 hours at 37 °C. Media were aspirated and formazan crystals were lysed with 500 μl of solubilization solution (95% dimethylsulfoxide + 5% improved minimal essential media). Absorbance was measured with a plate reader at 570 nm using a 650 nm differential filter to assess growth.

Anchorage-independent growth A 1 ml layer of 1% Seaplaque-agarose (BioWhittaker, Rockland, ME) in 1.5% FBS-containing growth media was solidified into each well of a 6-well plate. The bottom layer was overlaid with 1 ml of a 1% top agar mixture for

12,000 cells per well with indicated treatments. All plates were incubated at 37 °C for 14 days. Colonies was counted on a light microscope with an ocular grid. Five random fields were counted per well and only colonies exceeding half of a grid square were scored.

Radiation delivery A dosage from 1~10 Gray was delivered to cell cultures by X-RAD 320 Biological Irradiator (Precision X-ray, North Branford, CT). Beam hardening filter= 2mm Al, dose rate: 3 Gy/min at 320 kV, 12.5 mA, 50 cm SSD.

Glutathione measurement Cells were plated at a density of 10,000 in 96-well clear bottom white plates, allowed to equilibrate overnight, and starved in SFM for 24 hours followed by treatments. Intracellular reduced glutathione concentrations were measured by using GSH/GSSG-Glo™ Assay following manufacturer's instruction (Promega, Madison, WI). Readings were further normalized to CellTiter-Glo® Luminescent Cell Viability Assay following the manufacturer's guideline (Promega).

Glutamic acid assay Cells were plated at a density of 20,000 in 24-well plates, allowed to equilibrate overnight, and starved in SFM for 24 hours followed by treatments. Glutamic acid level in extracellular media was determined by Amplex® Red Glutamic Acid/Glutamate Oxidase Assay Kit according to manufacturer's protocol (Invitrogen, Carlsbad, CA). The glutamic acid readings were further normalized to CellTiter-Glo® Luminescent Cell Viability Assay following the manufacturer's guideline (Promega).

Reactive oxygen species assay Cells were seeded at a density of 10,000 in 96-well clear bottom black plates, allowed to equilibrate overnight, and starved in SFM for 24 hours followed by treatments. Intracelluar ROS levels were determined by using OxiSelect™ Intracellular ROS Assay Kit according to manufacturer's guideline (Cell Biolabs, Inc., San Diego, CA)

Cell cycle analysis Cells were typsinized, washed twice in ice-cold PBS, and fixed in 70% ice-cold ethanol -20 °C over night. Cell cycle analyses were performed on propidium

iodide-stained nuclei by using a FACSCalibur flow cytometer (Becton-Dickinson Biosciences, Heidelberg, Germany). Single cells were gated, 10,000 events were collected and analyzed by FlowJo (Tree Star Inc., Ashland, OR) software.

Clinical data set analysis The relative mRNA expression of *xCT* in human breast tumor samples was determined by searching the Oncomine database (version 4.4.3, September 2012 data release [122]. *xCT* mRNA expression was queried in TCGA breast dataset using reporter A_32_P165472. For prognostic analyses, overall survival and distant metastasis-free survival, stratified by expression (all percentiles between the lower and upper quartiles were computed, and the best performing threshold was used as a cutoff) of the gene of interest (*xCT*: 207528_s_at), were presented as Kaplan–Meier plots and tested for significance using log-rank tests.

Statistical analysis All data except clinical data sets were analyzed with the unpaired Student's t test with the use of Excel 2008 (Microsoft, Redmond, WA). A p value of <0.05 was considered statistically significant (* $p<0.5$, ** $p<0.01$, *** $p<0.001$).

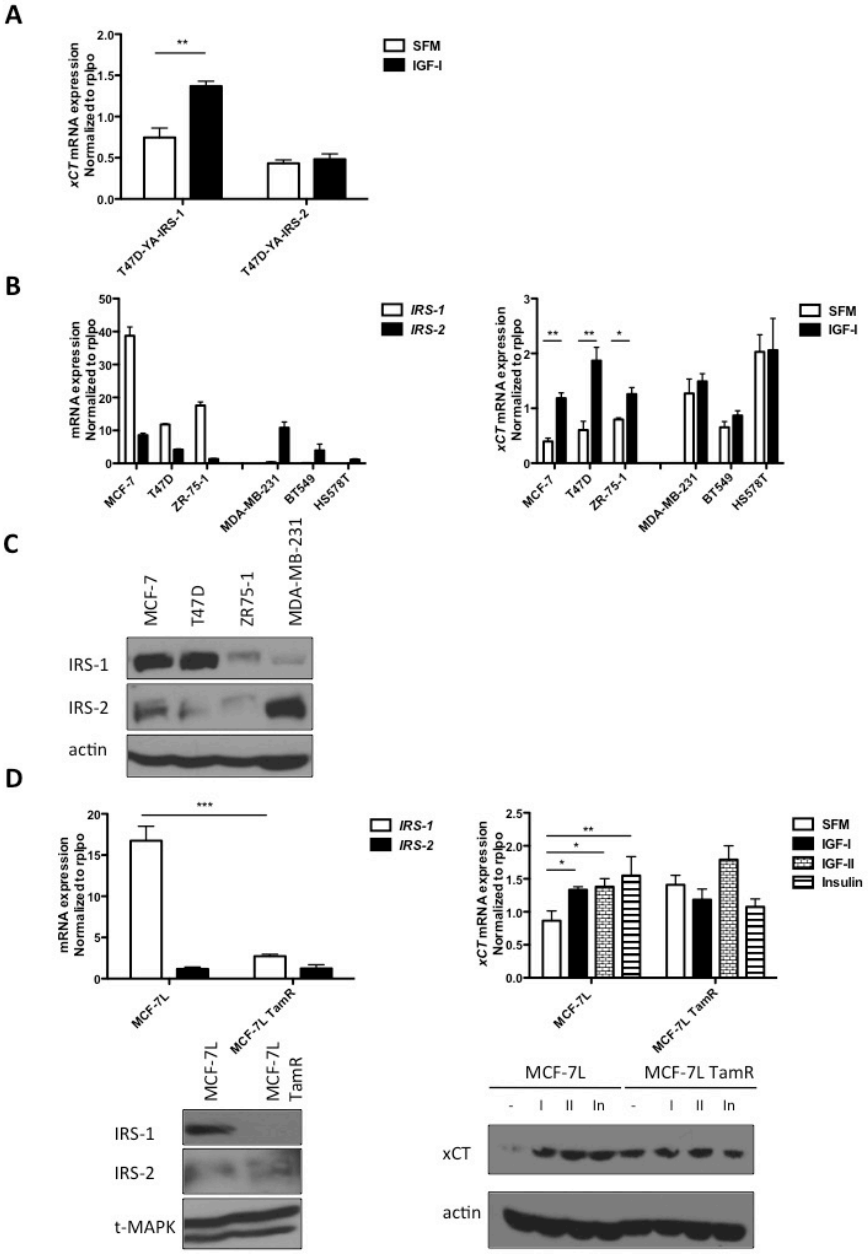

Figure 3.1 IGF-I induced *xCT* mRNA expression in an IRS-1 dependent manner in breast cancer cell lines.
A. T47D-YA-IRS-1 and Y47D-YA-IRS-2 cells were grown in SFM for 24 h. After 4 h of IGF-I (5 nM) exposure, mRNA was isolated and analyzed by qRT-PCR. mRNA expression of *xCT* was normalized to the *RPLPO* housekeeper gene. **B.** Left: mRNA expression of IRS-1 and IRS-2 in ER positive cell lines: MCF-7, T47D, and ZR-75-1; ER negative breast cancer cell lines: MDA-MB-231, BT549, and HS578T were analyzed by qRT-PCR. Right: mRNA expression of *xCT* in SFM or 4 hours after IGF-I exposure was analyzed by qRT-PCR. **C.** Immunoblot analysis of the expression levels of IRS-1 and IRS-2 in indicated breast cancer cell lines. **D.** mRNA expression of IRS-1 and IRS-2 in full growth media were analyzed in MCF-7L and MCF-7L TamR cells (upper panels left). Right: mRNA expression of *xCT* in MCF-7L and MCF-7L TamR cells after 4 h of IGF-I (5 nM), IGF-II (10 nM), or insulin (10 nM) exposure. Lower panels right: IRS-1 and IRS-2 protein expression in MCF-7L and MCF-7L TamR cells in full growth media condition. xCT expression in MCF-7L and MCF-7L TamR after 24 h of ligand stimulation was analyzed by immunoblot (right panel). Data are presented as mean ± standard error of the mean (SEM); all results are representative of three independent replicates.

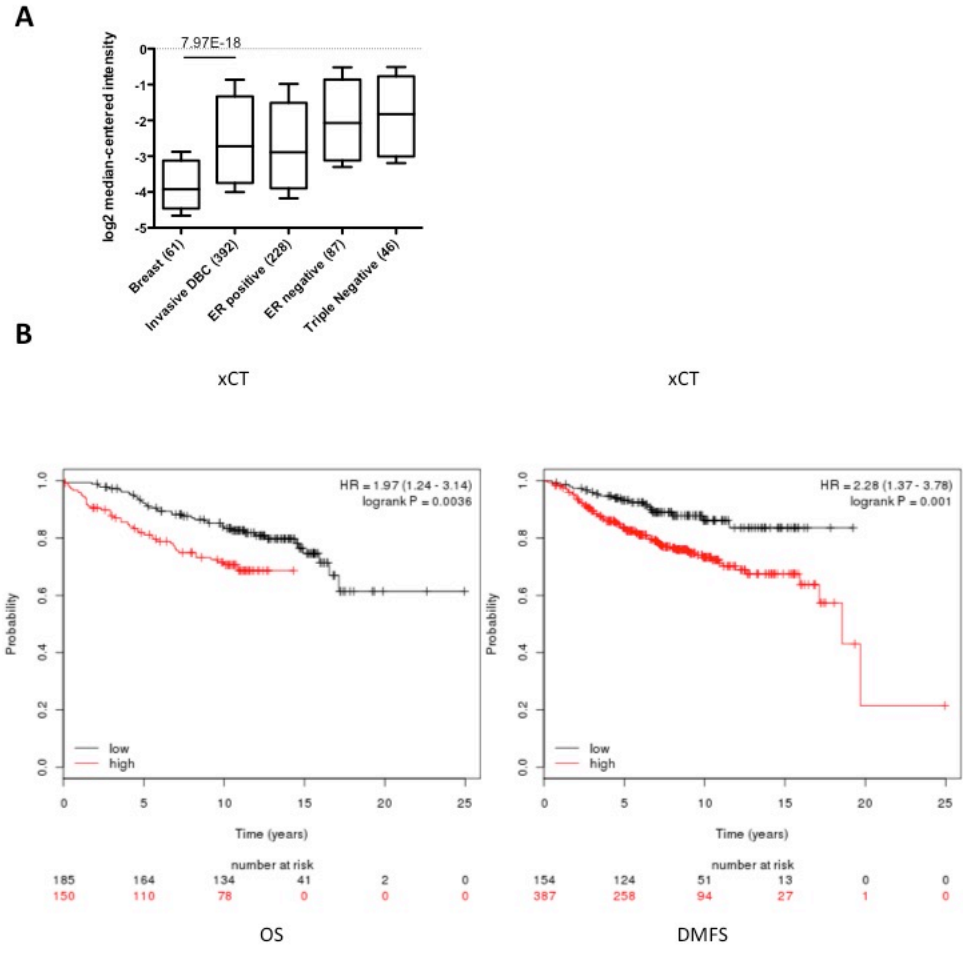

Figure 3.2 xCT is overexpressed breast tumor and associated with poor prognosis in ER positive breast cancer. **A.** Oncomine output data was sorted to isolate specified associations as indicated and reported as the mRNA copy number unit expression values for normal breast, invasive ductal breast carcinoma, ER positive breast carcinoma, ER negative breast carcinoma, and triple negative breast carcinoma samples using box-and-whiskers plots (whiskers: 90/10 percentiles, box: 75/25 percentiles, line: median of all samples). **B.** Kaplan-Meier plots of OS (left) and DMFS (right) of ER positive breast cancer patients with high or low expression of xCT. Data obtained from the Kaplan-Meier plotter database.

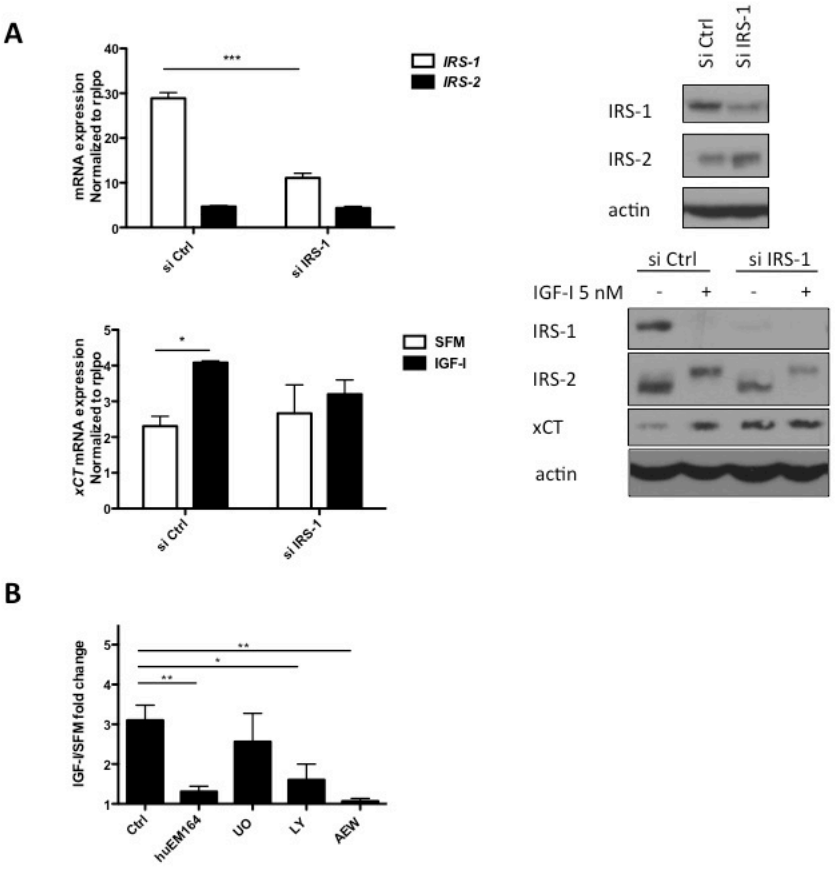

Figure 3.3 IGF-I induced xCT mRNA and protein expression specifically through IRS-1 and via PI3K dependent pathway in MCF-7 cells.

A. MCF-7 cells were transfected with either 30 nM of control or IRS-1 siRNA for 48h. siRNA knockdown efficiency was determined by both qRT-PCR (upper left) and immunoblot analysis (upper right). Cells then were grown in SFM for 24 h followed by IGF-I (5 nM) stimulation for 4 h for mRNA measurement (lower left) and 24 h for protein detection (lower right). **B.** MCF-7 cells were grown in SFM for 24 h and pretreated with huEM164 (20 μg/ml) for 24 h; pretreated with 10 UO126 (UO; 10 μM), LY294002 (LY; 10 μM), or NVP AEW-541 (AEW; 0.5 μM) for 30 min. Cells were then treated with IGF-I for 4 h for qRT-PCR. Data are mean ± SEM; all qRT-PCR results are representative of at least three independent triplicates-experiments.

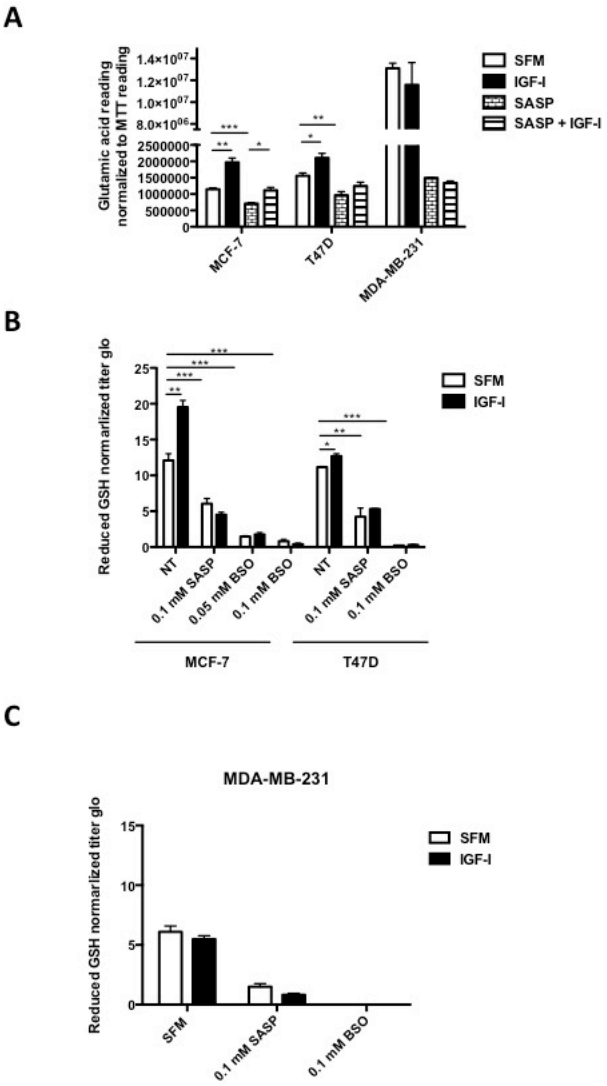

Figure 3.4 IGF-I stimulated xC- transporter function in ER positive breast cancer cells.
Cells were pretreated with SASP (0.1 mM) for 48 h, BSO (0.05 or 0.1 mM) for 24 h. **A.** MCF-7, T47D, and MDA-MB-231 cells were grown in SFM for 24 h then treated with indicated treatments with or without IGF-I (5nM) for another 24 h. Culture media glutamic acid levels were analyzed and readings were normalized to MTT reading. MCF-7, T47D (**B**), or MDA-MB-231 (**C**) cells were grown in SFM for 24 h then treated with indicated treatments with or without IGF-I (5nM) for another 24 h. Intracellular reduced GSH concentration was determined as described. Data are mean ± SEM; all results are representative of three independent replicates.

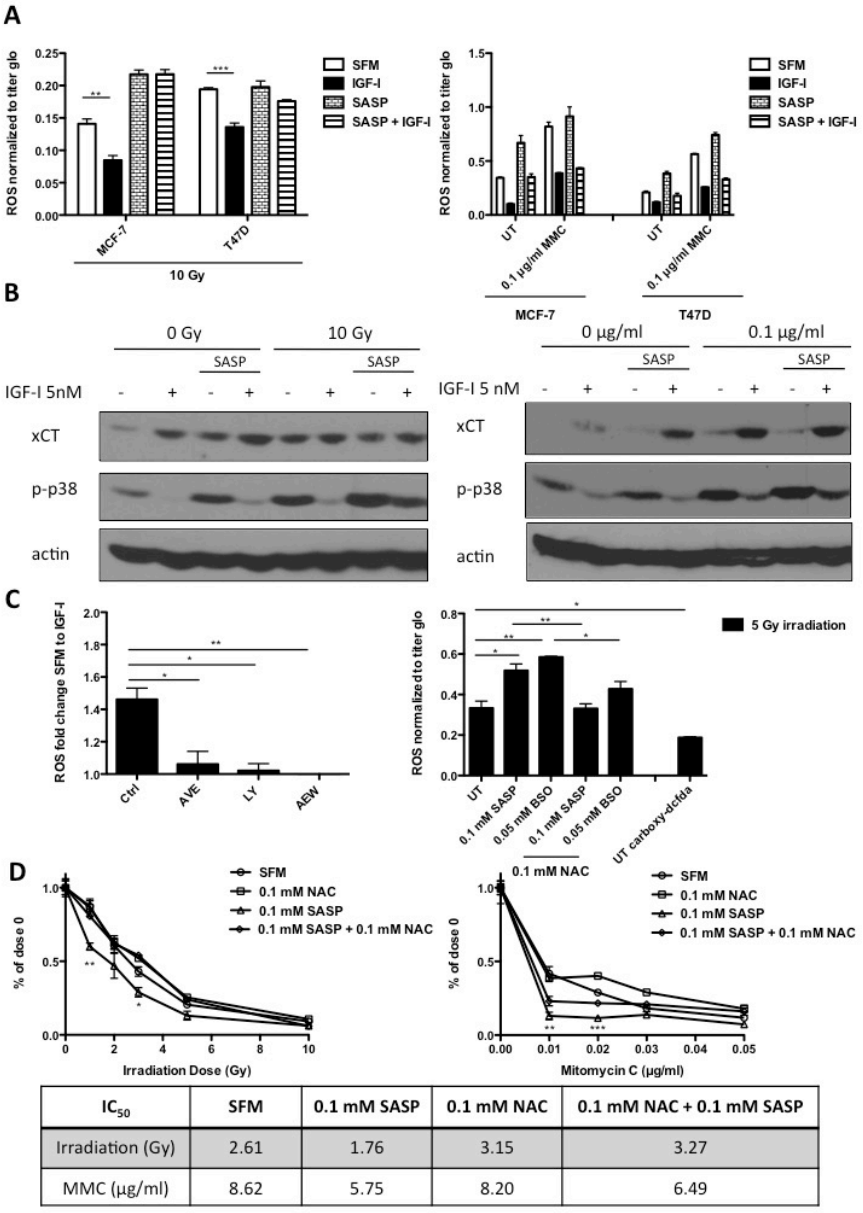

IC_{50}	SFM	0.1 mM SASP	0.1 mM NAC	0.1 mM NAC + 0.1 mM SASP
Irradiation (Gy)	2.61	1.76	3.15	3.27
MMC (µg/ml)	8.62	5.75	8.20	6.49

Figure 3.5 IGF-I regulated intracellular ROS level via xC^- transporter and through PI3K dependent pathway in ER positive breast cancer cells.

A. MCF-7 and T47D cells were pretreated with or without SASP (0.1 mM) for 48 h, grown in SFM for 24h, treated with IGF-I (5 nM) for another 24h, and then irradiated (10 Gy, left panel) or treated with mitomycin C treatment (1 µg/ml for ROS assay; 0.1 µg/ml for immunoblot) for 3 days (right panel). Intracellular ROS levels were measured as described. **B.** Cellular phospho-$p38^{MAPK}$ level was determined by immunoblot. **C.** MCF-7 cells were grown in SFM, pretreated huEM164 (20 µg/ml), LY294002 (10 µM), or NVP AEW-541 (0.5 µM) (Left panel). MCF-7 cells were pretreated with indicated dosage of SASP, BSO, or NAC. Acute ROS were induced by 5 gy irradiation. MCF-7 cells incubated with ROS insensitive probe carboxy-DCFDA (0.1 mM) was presented as assay control (Right panel). Cellular ROS levels were determined as described. **D.** MCF-7 cells were treated with indicated treatments in soft agar. After 24h of synchronization in SFM condition, cells were either irradiated or treated with mitomycin C. Colony formation was assessed after 14 days. Survival rate curve was made by normalizing colony number of each treatment to its own no treatment control. IC_{50} values were shown in the table. Data are mean ± SEM; all results are representative of three independent replicates.

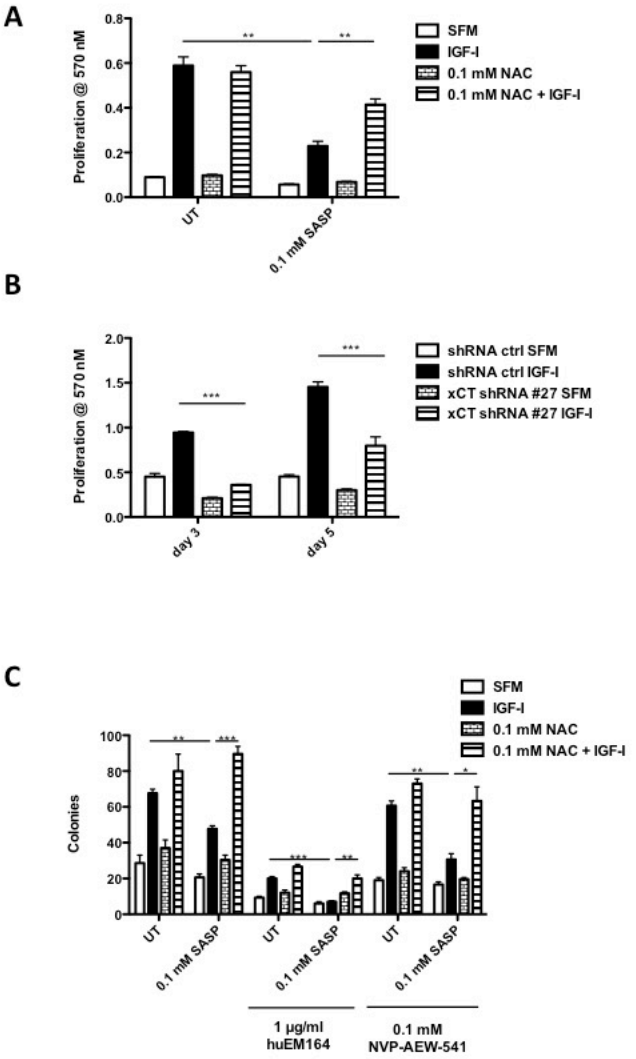

Figure 3.6 Disruption of xC⁻ transporter function resulted in partial suppression in IGF-I-induced cell proliferation and sensitized cells to IGF-IR inhibitors.
A. MCF-7 cells were first pretreated with SASP (0.1 mM) for 48 h or NAC (0.1 mM) for 24 h in SFM and then treated with IGF-I (5 nM) for 5 days. Cell viability was determined by performing MTT assay. **B.** MCF-7 cells were infected by either scrambled shRNA or xCT specific shRNA to generate stable xCT down-regulation clone. Cells were grown in SFM for 24h then treated with IGF-I (5 nM) for 3 days or 5 days. Cell monolayer growth was measured by MTT assay. **C.** MCF-7 cells were treated with indicated treatment combinations. Anchorage independent growth was determined after 14 days. Data are mean ± SEM; all results are representative of three independent replicates.

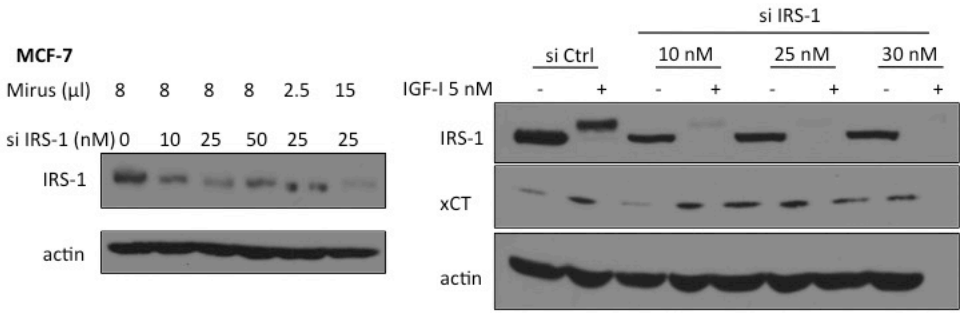

Figure 3.7 siRNA titration in MCF-7 cells.
MCF-7 cells were treated with indicated concentrations of IRS-1 specific siRNA and Mirus *Trans*IT- siQUEST transfection reagent. Cellular IRS-1 protein expression was determined by immunoblot analysis (left). xCT protein expression levels upon 24h of IGF-I (5 nM) stimulation in IRS-1 siRNA down- regulated MCF-7 cells were analyzed by immunoblot (right).

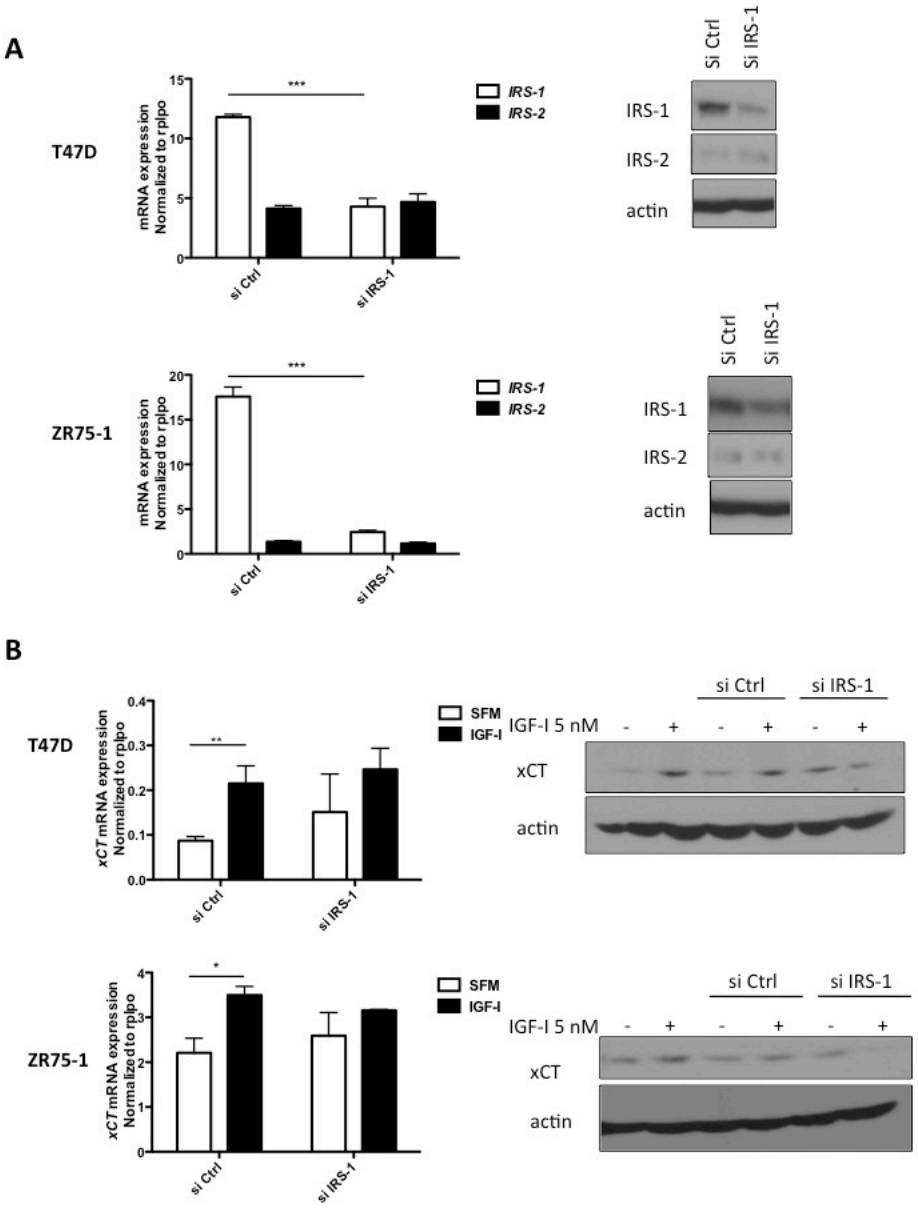

Figure 3.8 IGF-I induced xCT mRNA and protein expression specifically through IRS-1 in T47D and ZR-75-1 cells.

A. T47D and ZR-75-1 cells were transfected with either 30 nM of control or IRS-1 siRNA for 48h. siRNA knockdown efficiency was determined by both qRT-PCR (left panels) and immunoblot analysis (right panels). **B.** T47D and ZR-75-1 cells were grown in SFM for 24 h followed by IGF-I (5 nM) stimulation for 4 h for mRNA measurement (left panels) and 24 h for protein detection (right panels). Data are mean ± SEM; all results are representative of three independent replicates.

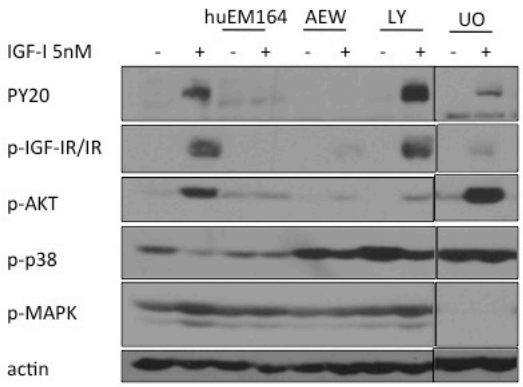

Figure 3.9 Inhibition of IGF-I signaling.
MCF-7 cells were grown in SFM, pretreated huEM164 (20 μg/ml), NVP AEW-541 (AEW, 0.5 μM), LY294002 (LY, 10 μM), or UO126 (UO, 10 μM). Phosphorylated tyrosine (PY20), IGF-1R/IR, AKT, $p38^{MAPK}$, and MAPK were analyzed by immunoblot.

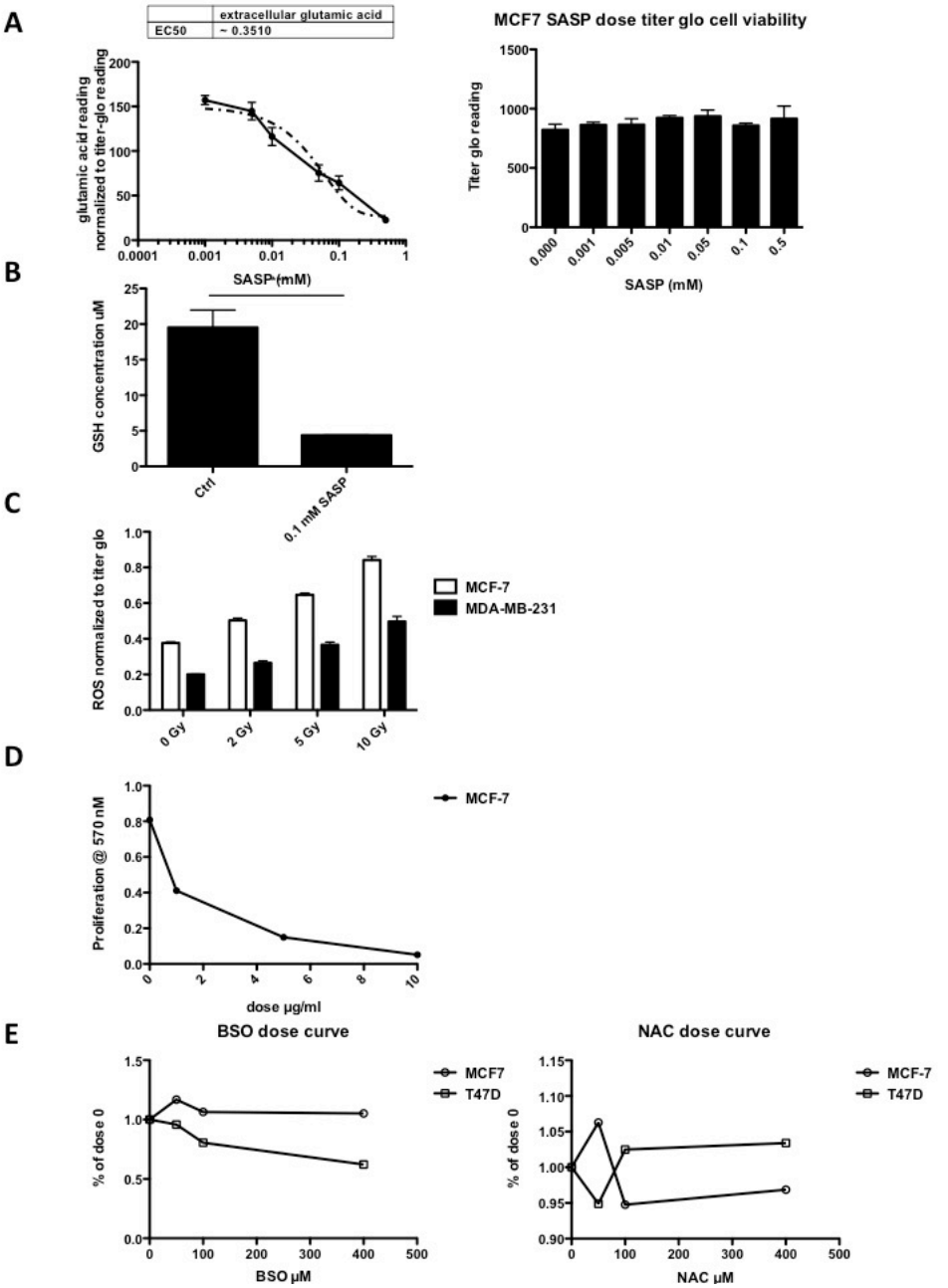

Figure 3.10 Effect of SASP, BSO, and NAC concentration on growth.

A. MCF-7 cells were pretreated with various dosages of SASP for 48 h. Culture media glutamic acid levels were analyzed and readings were normalized to titer glo cell viability reading (right). **B.** MCF-7 cells were pretreated in the presence or absence of SASP (0.1 mM). Intracellular GSH concentration was determined as described. **C.** MCF-7 and MDA-MB-231 cells were grown in SFM overnight and treated with various dosages of irradiation. Intracellular ROS levels were measured as described. **D.** MCF-7 or T47D cells were grown in SFM overnight and treated with various dosages of mitomycin C (upper panel), BSO (lower left panel), or NAC (lower right panel). Cell viability was measured by MTT assay after 3 days of treatment. Data are mean ± SEM; all results are representative of three independent replicates.

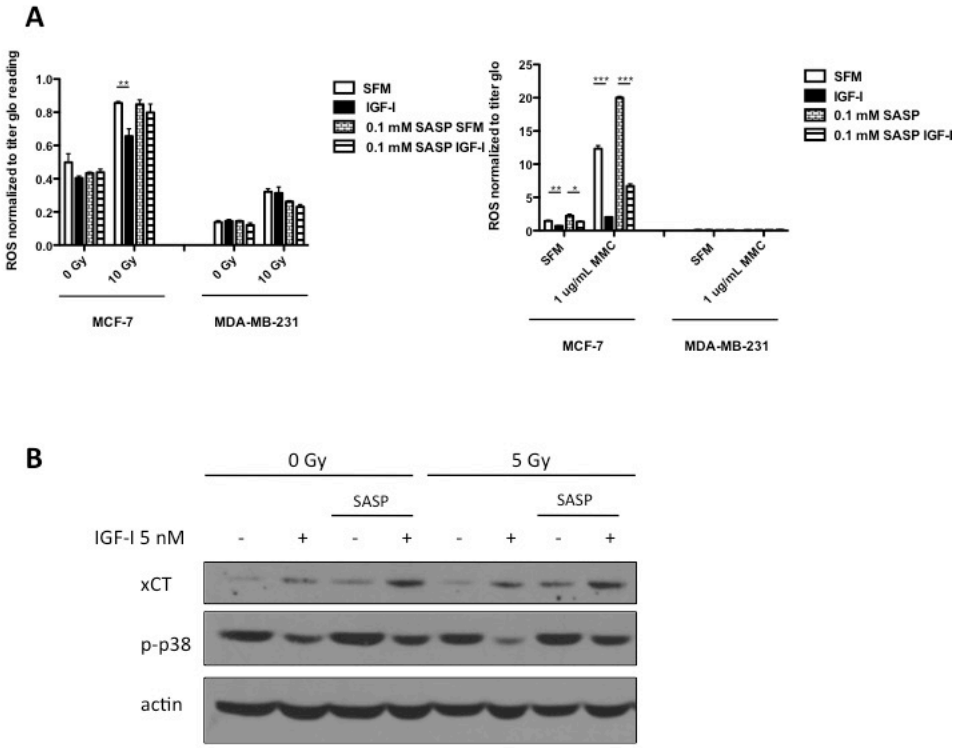

Figure 3.11 IGF-I regulated intracellular ROS level via xC^- transporter in MCF-7 and T47D cells but not in MDA-MB-231 cells.

A. MCF-7 and MDA-MB-231 cells were pretreated with or without SASP (0.1 mM) for 48 h, grown in SFM for 24h, then treated with IGF-I (5 nM) for another 24h, and then processed for irradiation (10 Gy, left panel) or mitomycin C treatment (1 μg/ml) for 3 days (right panel). Intracellular ROS levels were measured as described. **B.** T47D were pretreated with or without SASP (0.1 mM) for 48 h, grown in SFM for 24h, treated with IGF-I for another 24h, and then treated with mitomycin C (0.1 μg/ml) cellular phospho-$p38^{MAPK}$ level was determined by immunoblot. Data are mean ± SEM; all results are representative of three independent replicates.

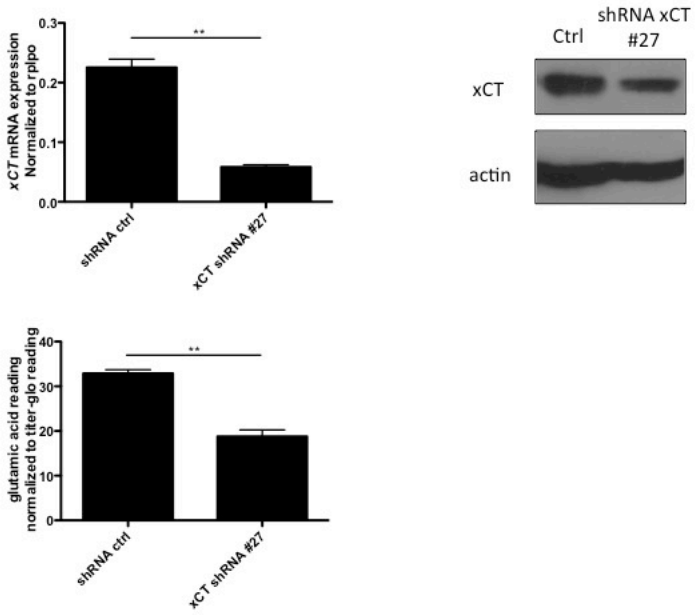

Figure 3.12 xCT shRNA downregulation in MCF-7 cells.
MCF-7 cells were infected by either scrambled shRNA or xCT specific shRNA to generate stable xCT downregulation clone. shRNA downregulation efficiency was determined by qRT-PCR (upper left panel), immunoblot (upper right panel), and xC^- transporter functional assay (Lower panel). Data are mean±SEM; all results are representative of three independent replicates.

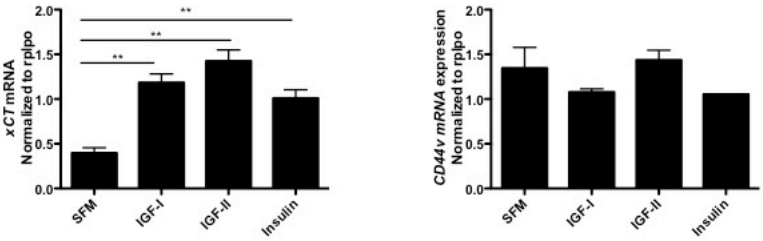

Figure 3.13 Ligands of the insulin/IGF system stimulated xCT mRNA expression but not CD44v mRNA expression in MCF-7 cells.
mRNA expression of *xCT* (left) and *CD44v* (right) in MCF-7 cells after 4 h of IGF-I (5 nM), IGF-II (10 nM), or insulin (10 nM) exposure were analyzed by qRT-PCR. Data are mean±SEM; all results are representative of three independent replicates.

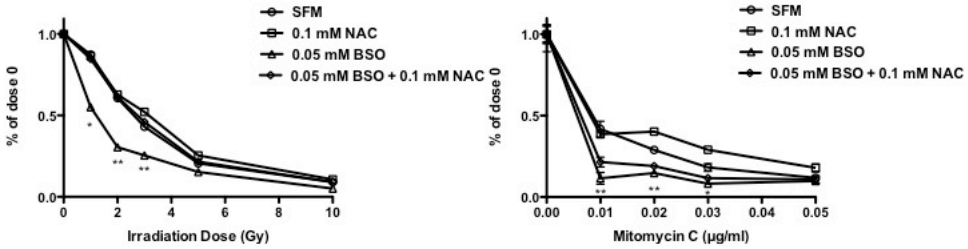

IC_{50}	SFM	0.05 mM BSO	0.1 mM NAC	0.1 mM NAC + 0.05 mM BSO
Irradiation (Gy)	2.61	1.21	3.15	2.73
MMC (ng/ml)	8.62	5.61	8.20	6.33

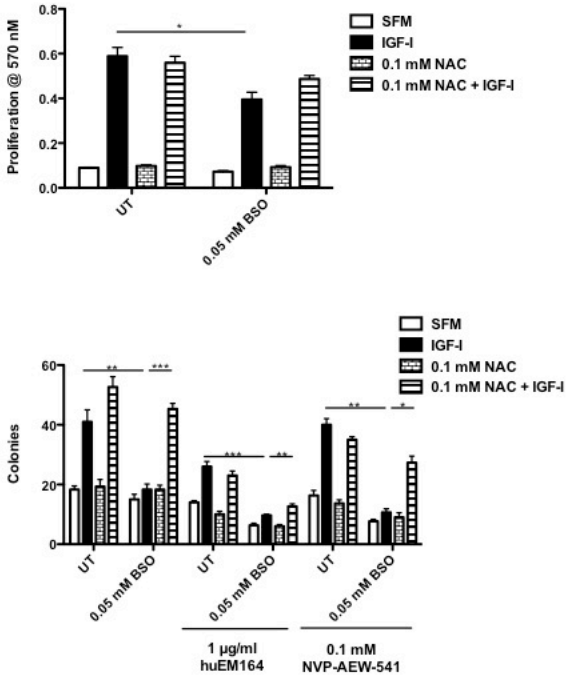

Figure 3.14 BSO mediated cellular behaviors assays in MCF-7 cells.
A. MCF-7 cells were treated with indicated treatments in soft agar. After 24h of synchronization in SFM condition, cells were either irradiated or treated with mitomycin C. Colony formation was assessed after 14 days. Survival rate curve was determined by normalizing colony number of each treatment to its own no treatment control. Statistically significant differences are noted (* or # $p<0.5$, ** or ## $p<0.01$, *** or ### $p<0.001$). The table shows IC_{50} values. **B.** MCF-7 cells were first pretreated with BSO (0.05 mM) or NAC (0.1 mM) for 24 h, grown in SFM for 24h and then treated with IGF-I (5 nM) for 5 days. Cell viability was determined by performing MTT assay. **C.** MCF-7 cells were treated with indicated treatment combinations. Anchorage independent growth was determined after 14 days. Data are mean ± SEM; all results are representative of three independent replicates.

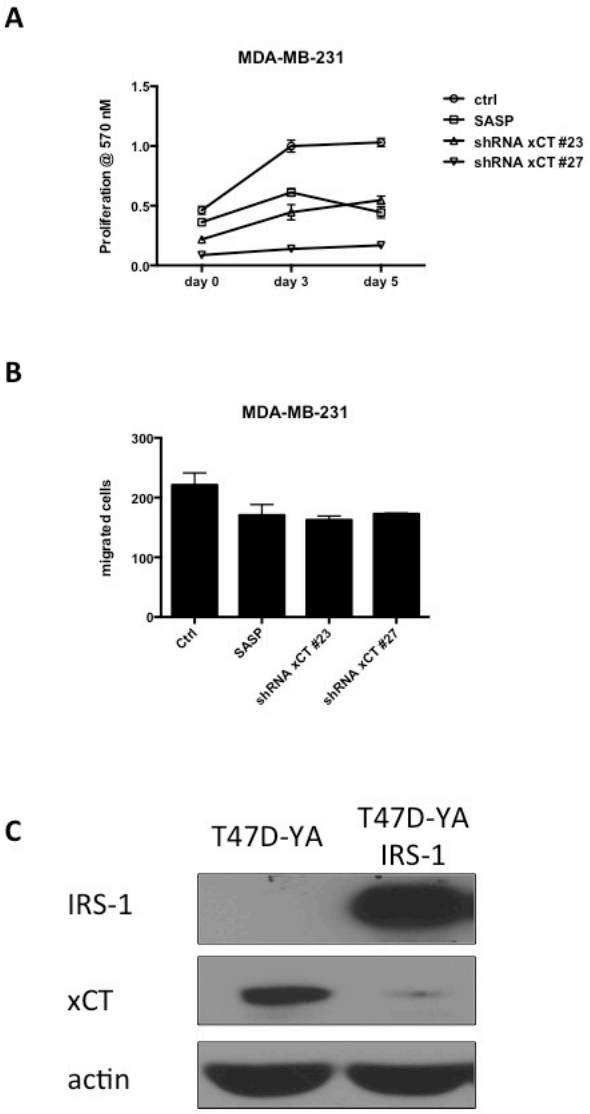

Figure 3.15 Inhibition of xCT suppressed basal proliferation and migration in MDA-MB-231 cells.
MDA-MB-231 cells were treated with SASP (0.1 mM) or transfected with shRNAs specific targeting xCT. Cells proliferation and migration were measured by MTT monolayer growth assay (**A**) and boyndern chamber migration assay (**B**) respectively. **C.** Basal expression of xCT in T47D-YA and T47D-YA-IRS-1 cells were assessed by western blotting. Data are mean ± SEM; all results are representative of three independent replicates.

Table 1. Cell-cycle phase percentages were determined by flow cytometry

Cell-cycle phase (%)	SFM	IGF-I	SASP	SASP + IGFI	NAC+ SASP	NAC + SASP + IGFI
G_0–G_1	74.84	45.16	72.64	62.81	74.77	47.06
S	8.42	46.88	8.81	23.26	8.65	41.94
G_2–M	15.99	7.28	17.62	13.21	14.95	10.64

Table 3.1 Cell-cycle phase percentages were determined by flow cytometry

Chapter 4

Targeting Nrf2 in breast cancer cells

Yuzhe Yang and Douglas Yee
Targeting Nrf2 in breast cancer.
Manuscript under revision. 2015

Introduction

Nuclear factor-erythroid 2-related factor 2 (Nrf2) is a master transcriptional activator that specifically binds to the antioxidant response element (ARE) to initiate expression of various anti-oxidative and anti-inflammatory genes to protect cells from oxidative stress. One of Nrf2's canonical transcriptional targets is xCT. Normally, cytosolic Nrf2 is constantly bound to Keap1 to be ubiquitinated and degraded by proteasome. Inactivation of Keap1 stabilizes Nrf2 and promotes its translocation into the nucleus where Nrf2 binds to ARE and initiates the transcription of cytoprotective genes. Constitutive stabilization of Nrf2 has been observed in many human cancers and confers chemo- and radio-resistance of cancer cells. Recently, Nrf2 has been shown to redirect glucose and glutamine into anabolic pathways to reduce cellular redox level and promote cell proliferation in lung carcinoma models [152].

Breast cancer is the second most diagnosed malignancy and second leading cause of cancer death among women in the United States (American Cancer Society). Molecular profiling has identified at least four subtypes of breast cancer: luminal A, luminal B, triple negative/basal-like, and human epidermal growth factor receptor 2 (Her2)-enriched breast cancer. Successes in developing hormonal therapy (estrogen receptor antagonists and aromatase inhibitors) [1, 153] and Her2-targeted therapy [154] have significantly decreased breast cancer mortality in the past few decades. However, the conquest of breast cancer still faces great challenge due to the extreme heterogeneous nature of this disease.

Estrogen receptor positive (ER+) breast cancer patients are treated with endocrine-targeted therapy, *de novo* or acquired resistances often happen years after the initial treatment, which makes ER+ breast cancer still an incurable disease and novel molecular targets or novel combination therapies are in need to be established.

The insulin-like growth factor (IGF) signaling system has been well documented to regulate ER+ breast cancer proliferation [6, 105]. However, type 1 IGF receptor (IGF-

IR)-targeted therapy concurs obstacles in processing to late phase clinical trials possibly due to lack of predictive biomarkers or inappropriate combination therapies [105, 119]. Previous studies indicated that estrogen regulates Nrf2 expression and function in hormone sensitive, insensitive, and BRCA mutant breast cancer cells via Phosphoinositide 3-kinase (PI3K) signaling pathway [155, 156]. Crosstalk between estrogen receptor and IGF signaling system has been extensively studied [157]. Crosstalk between IGF signaling system and Nrf2 has not yet been explored. Since estrogen and IGF signaling system both activate PI3K-AKT pathway and in the previous chapter we reported that IGF-I regulates Nrf2's canonical transcriptional target xCT, we proposed that IGF/insulin signaling pathway may regulate Nrf2 expression and function in ER+ breast cancer cells.

About 20% of breast cancer patients are diagnosed as triple negative/basal-like (estrogen receptor, progesterone receptor, and Her2 negative) breast cancer (TNBC). The lack of these molecular targets causes TNBC/basal-like cells unresponsive to hormonal therapy or Her2-targeted therapy, which makes it the most aggressive subtype and with poorest prognosis. To date, there is no established targeted therapy for TNBC/basal-like patients thus identifying novel therapeutic targets is eagerly needed. A recent study showed that TNBC/basal-like cell lines were extremely sensitive to glutamine restriction which decreased cystine import via xC^- transporter, which was critically required for synthesis of the reduced form of glutathione (GSH) [114, 128] and was upregulated in TNBC/basal-like cells [114, 158]. Inhibition of xC^- resulted in reduced GSH, increased reactive oxygen species (ROS), and inhibited growth of the TNBC cells [158]. TNBC/basal-like breast cancer cells are well known for their stem-like ($CD44^+/CD24^-$) properties. Cancer stem cells contain lower level of ROS and are often radioresistance [159]. xC^- has been reported to be directly regulated by Nrf2 [128, 160]. Taken together, we hypothesized that Nrf2 expression may also be highly expressed in TNBC/basal-like breast cancer cell lines and may contribute to clonogenicity, stemness maintenance, and radioresistance.

The aim of this study was to thoroughly investigate the IGF's regulation on Nrf2 in ER+ breast cancers and evaluate Nrf2 as a target in TNBC/basal-like breast cancers.

Results

Nrf2 expression and its prognostic value in breast cancer cell lines and patients

To address whether Nrf2 expression was upregulated in certain subtypes of breast cancer cells, mRNA levels of Nrf2 (*NFE2L2*) were quantified in a panel of breast cancer cell lines (Figure 4.1 A, B left panel). Protein expression of Nrf2 was further confirmed in selected cell lines by immunoblot (Figure 4.1 B right panel). Nrf2 expression was generally significantly higher in TNBC/basal-like breast cancer cells than immortalized or ER+ cell lines. Prognostic value of Nrf2 expression was also assessed by using an online survival analysis tool [123]. The result suggested that higher expression of Nrf2 was associated with poor prognosis in all breast cancer patients (TCGA database) (Figure 4.1 C).

IGF-I regulated Nrf2 protein expression and function in ER+ breast cancer cells

Nrf2 basal expression was relatively low in ER+ breast cancer cells. Nrf2 is detected as two bands corresponding to its phosphorylation status. IGF signaling system ligands (IGF-I, IGF-II, and insulin) stimulated Nrf2 protein expression while suppressing the expression of intracellular redox indicator phospho-p38^{MAPK} in MCF-7 and T47D cells (Figure 4.2 A). The insulin receptor substrates (IRS) are important regulators of IGF-IR and insulin receptor signaling [105, 119]. Control, IRS-1, or IRS-2 siRNAs was introduced to MCF-7 and T47D cells to examine the effect on Nrf2 induction. Only IRS-1 downregulation attenuated IGF-I-induced Nrf2 expression, which implied that the regulation was through IRS-1 protein (Figure 4.2 B top panels). Cells were further treated with anti-IGF-IR monoclonal antibody huEM164, IGF-IR/ insulin receptor kinase inhibitor BMS-754807, or PI3K inhibitor LY294002 prior to IGF-I stimulation. All three inhibitors suppressed IGF-I regulation of Nrf2 implicating the role for activation of IGF-IR and PI3K in Nrf2 expression (Figure 4.2 B bottom panel). IGF-I promoted the nuclear

translocation of phospho-Nrf2, which was eliminated by pretreating cells with IGF-IR/insulin receptor kinase inhibitor NVP-AEW541 (Figure 4.2 C).

Nrf2 suppression resulted in intracellular redox upregulation in MCF-7 cells

To assess Nrf2 as a target in ER+ breast cancer cells, siRNA or short hairpin RNAs to Nrf2 were introduced to MCF-7 and T47D cells (Figure 4.3 A, C right, D, 4.8 A). Nrf2 downregulation resulted in significantly suppression of its typical target genes: *GCLC*, *GCLM*, *xCT*, and *NQO-1*; as well as genes coding for the enzymes in the pentose phosphate pathway (PPP): *G6PD*, *PGD*, *ME-1*, *PPAT*, *TALDO1*, *TKT*, and *MTHFD2* (Figure 4.3 B, 4.8 B). The Nrf2 downregulation did not affect the expression of unrelated genes: *CD44* (Figure 4.3 B, 4.8 B). Nrf2 knockdown also resulted in increased intracellular reactive oxygen species (ROS) in MCF-7 cells (Figure 4.3 C). Suppression of Nrf2 led to lower levels of cytoprotective gene expression and should result in reduced nicotinamide adenine dinucleotide phosphate (NADPH) production in the PPP, which may have contributed to the elevation of intracellular ROS. While Nrf2 downregulation did not significantly suppress IGF-I-stimulated cell proliferation (Figure 4.3 D), however suppression of Nrf2 abrogated the IGF-I mediated protection from irradiation (Figure 4.3 E right panel).

Nrf2 suppression resulted in redox upregulation in MDA-MB-231 and MDA-MB-436 cells

MDA-MB-231 and MDA-MB-436 cells expressed high basal levels of Nrf2 (Figure 4.1A, B) and IGF-I did not further increase Nrf2 expression (Figure 4.9). Downregulation of Nrf2 (Figure 4.4 A, 4.9) resulted in activation of AMPKα, and $p38^{MAPK}$ (Figure 4.9, 4.10 A; 4.4 C left); suppression of PPP enzymes coding genes: *G6PD*, *PGD*, *ME-1*, *TALDO1*, and *TKT*; and suppression of typical Nrf2 regulated genes: *GCLC*, *GCLM*, *xCT*, and *NQO-1* (Figure 4.4 B, 4.11 A, B). Citric acid cycle metabolism analysis was further performed in control and Nrf2 downregulated MDA-MB-231 cells. Nrf2 down-regulated cells showed reduced NADPH production, reduced ATP production, decreased intermediates involved in PPP pathway, and increased intermediates in

glycolysis pathway, which were consistent with the gene expression change: cells were redirected to glycolytic pathway instead of PPP (Table 4.1). Direct measurement of intracellular ROS showed redox increase in Nrf2 downregulation clones (Figure 4.4 D, 4.11 C). In TNBC/basal-like cells, cysteine/glutamate antiporter xC^- (coded by *SLC7A11*) has been identified as a potential drug target [158]. Nrf2 directly regulated xCT expression (Figure 4.4 A, B right panel, 4.9, 4.11 A, B). xC^- together with GCLC and GCLM are necessary for intracellular cysteine transport and subsequent production of glutathione (GSH). Nrf2 downregulation caused depletion of GSH and increased cellular ROS, which were partially restored when overexpressing xCT in the Nrf2 knockdown clone (Figure 4.4 C, D, E).

It is known that mitochondrial membrane potential controls ATP synthesis. Activation of AMPKα in Nrf2 downregulated cells (Figure 4.4 C right, 4.9, 4.10 A) suggested an increased intracellular ADP/ATP ratio (Table 4.1) thus also implied mitochondrial function impairment. To confirm this, mitochondrial membrane potential assay detecting active mitochondria in living cells were performed in controlled and Nrf2 downregulated MDA-MB-231 cells. The results indicated that loss of Nrf2 impaired mitochondrial function (Figure 4.4 F). Overexpressing xCT did not rescue impaired mitochondrial function in Nrf2 downregulated cells as indicated by AMPKα status (Figure 4.4 C right) indicating xCT was not implicated in the regulation of the glycolysis/PPP metabolic pathway. ARE-GFP reporter assays showed that ARE binding activity was not detectable when Nrf2 was suppressed (Figure 4.4 G). Collectively, these data suggested that in TNBC/basal-like cells, Nrf2 regulated ROS and cellular GSH level partially through xC^- transporter function and partially through the regulation of PPP.

Nrf2 suppression resulted in growth inhibition in TNBC/basal-like cells

Loss of Nrf2 decreased mitochondrial potential as well as elevated cellular redox level. To assess the biological consequences of this regulation, monolayer growth assay, clonogenic assay, and three-dimensional culture in Matrigel were performed. All these assays showed significant growth inhibition in Nrf2 downregulated clones (Figure 4.5 A,

B, C, 4.11 D). Cell cycle analysis further demonstrated that loss of Nrf2 caused G0/G1 increase and S phase decrease (Figure 4.5 D).Overexpressing xCT in Nrf2 downregulated cells partially rescued the growth inhibitory phenotype (Figure 4.5 A right, B) All trans retinoic acid (ATRA) has been reported as an inhibitor function as competitively inhibits the binding of Nrf2 to the ARE enhancer [161]. In this study, ATRA reduced mitochondrial potential (Figure 4.4 F), while signaling analysis also showed that retinoic acid induced the activation of AMPKα (Figure 4.10 A). ATRA inhibited MDA-MB-231 cell proliferation in a dose dependent manner (Figure 4.10 B). Taken together, the data indicated that target Nrf2 by genetic knockdown or chemical inhibitor both resulted in growth inhibition in TNBC/basal-like cells.

Nrf2 suppression sensitized MDA-MB-231 response to irradiation

Nrf2 expression contributes to chemo- and radiation therapy resistance. Targeting Nrf2 by shRNA knockdown significantly sensitized MDA-MB-231 response to irradiation in both monolayer and anchorage independent growth conditions (Figure 4.6 A, B, C). MDA-MB-231 has stem cell-like properties as characterized by cell surface markers ($CD44^{+}/CD24^{-)}$. Cancer stem cells are considered to be resistant to multiple cancer therapies due to their slow self-renewal rate. xCT has been reported to stabilize cell surface CD44 expression in a colorectal cancer model [133]. As mentioned above, Nrf2 directly suppressed xCT mRNA and protein expression (Figure 4.4 A, B right panel, 4.11 A, B right panel). Cell surface CD makers were analyzed in MDA-MB-231 control and Nrf2 downregulated cells under normal and stressed conditions induced by hydrogen peroxide. Data suggested that loss of Nrf2 decreased the $CD44^{+}/CD24^{-}$ stem cell population (Figure 4.5 D top panels). This decrease was further enlarged when cells were under stressed condition induced by hydrogen peroxide (Figure 4.5 D bottom panels). Overexpression of xCT in Nrf2 downregulated clone rescued $CD44^{+}/CD24^{-}$ population (Figure 4.12).

Nrf2 suppression reduced migration potential in MDA-MB-231 cells

Besides growth arrest, Nrf2 downregulated cells also showed morphologic changes (Figure 4.7 A). IGF-I stimulated migration was abolished in Nrf2 downregulated MDA-MB-231 cells (Figure 4.7 B). To understand the mechanism, mesenchymal markers were further analyzed. Data suggested that the reduced migration potential might due to regulation of vimentin and snail (Figure 4.7 C, D).

Discussion

In the first half of this study, we have shown that IGF signaling regulated Nrf2 expression in a PI3K dependent pathway that involves IRS-1 adaptor protein in ER+ breast cancers. In our previous study, we found that IGF system also regulates xC^- transporter expression and function to promote cancer cell proliferation through IRS-1-PI3K regulated signaling pathway[114]. Given that xC^- is a direct transcriptional target of Nrf2, the data are consistent suggesting a therapy targeting both Nrf2/xC^- and IGF-IR in conjunction with conventional chemotherapy or radiotherapy may have synergistic effects in ER+ breast cancers.

ER+ breast cancers frequently acquire resistance to endocrine therapies. In the supplementary data, we found that tamoxifen resistant breast cancer cells expressed lower levels of Nrf2 than the parental counterparts (Figure 4.13 A, B). Further analysis also showed that the canonical targets of Nrf2 were downregulated (Figure 4.13 A), while intracellular ROS levels were increased as indicated by the activation of $p38^{MAPK}$ (Figure 4.13 B) in tamoxifen resistant breast cancer cells. Moreover, data also suggested that tamoxifen resistant cells were more sensitive to irradiation possibly due to the loss of Nrf2 (Figure 4.13 C).

The growth of TNBC/basal-like breast cancer cells was dependent on Nrf2 expression and IGF signaling did not affect Nrf2 expression or function. We confirmed the six genes involved in the PPP and NADPH production pathways in addition to *GCLC*, *GCLM*, *xCT*, and *NQO-1* were direct targets of Nrf2 in TNBC/basal-like cell lines. Nrf2 scavenged intracellular ROS in TNBC/basal-like breast cancer cells via two pathways:

PPP metabolic pathway and traditional cytoprotective pathway. By targeting Nrf2, cell metabolism switched to glycolysis, less NADPH was produced, and ROS increased, which resulted in impairment of mitochondrial function as indicated by hyper-activation of AMPKα and direct measurement of mitochondrial membrane potentials. Meanwhile, Nrf2 suppression also led to the decrease of cellular GSH synthesis due to the downregulation of cysteine importer xC^- and glutamate-cysteine ligase *GCLC* and *GCLM*. Moreover, the loss of xCT caused cell surface $CD44^+/CD24^-$ stem cell population elimination [133]. Nrf2 downregulation did not affect CD44 expression. Overexpression of xCT in Nrf2 downregulated cells restored $CD44^+/CD24^-$ population, intracellular reduced GSH level, and partially rescued cellular ROS level. As previous studies suggested, $CD44^+$ cancer stem cells manifest upregulation of antioxidant genes and possess an enhanced ROS defense system therefore are relatively radioresistant [159, 162]. All the above contributed to sensitization of MDA-MB-231 cells to irradiation.

In addition to the citric acid cycle metabolism analysis, we also performed amino acid metabolomics profiling in the scramble and Nrf2 shRNA infected MDA-MB-231 cells. Among 23 amino acids, the levels of hydroxyproline, histidine, and cystine were not detectable due to sample preparation or sensitivity limitation of the mass spectrometry. Alanine was downregulated while glycine and aspartic acid were significantly increased in the Nrf2 knockdown cells (Figure 4.14). In a recent report which compared metabolomics differences between ER+ and ER- breast cancer, alanine demonstrated the strongest differences between ER- and ER+ breast tumors [163]. These findings suggested that alanine metabolism might affect cancer cell phenotype. Additional research should be conducted to explore Nrf2's regulation on cellular amino acid metabolomics and its potential contribution to cancer malignancy and phenotypes.

Materials and Methods

Reagents and antibodies Growth media and supplements were purchased from Invitrogen (Grand Island, NY). IGF-I was purchased from GroPep (Adelaide, Australia).

IGF-II was purchased from Gemini (Woodland, CA). Sulfasalazine (≥98%), L-Buthionine-sulfoximine (≥97%), N-Acetyl-L-cysteine, LY294002, U0126, and actin antibody were purchased from Sigma-Aldrich (St. Louis, MO). Humanized anti-IGF-IR monoclonal antibody huEM164 was generously provided by Immunogen Inc. (Norwood, MA). BMS-754807 was provided by Bristol Myers Squibb (New Jersey, Marco Gottardis). Antibodies for phosphorylated AMPKα, phospho-$p38^{MAPK}$, xCT, and phsopho-PERK were purchased from Cell Signaling Technology (Beverly, MA). The keap1 antibody was purchased from Santa Cruz Biotechnology (Santa Cruz, CA). The total and phospho-Nrf2 antibody for Western blot analysis was purchased from Abcam (Cambridge, MA). Anti-rabbit and anti-mouse horseradish peroxidase-conjugated secondary antibodies were purchased from Pierce (Rockford, IL). 5-(and-6)-carboxy-2',7'-dichlorofluorescein diacetate was purchased from Invitrogen (Carlsbad, CA).

Cell lines and culture Breast cancer cell lines were purchased from the ATCC (Manassas, VA) and cultured following ATCC's instruction. MCF-7L cells were kindly provided by C. Kent Osborne (Baylor College of Medicine) and maintained in improved MEM Richter's modification medium (zinc option) supplemented with 5% FBS and 11.25 nmol/L insulin. MCF-7L were evaluated by comparative genomic hybridization (data not shown) and found to be nearly identical to the MCF-7 cells distributed by the ATCC. MCF-7 TamR cells were generated as described [40]. All cells were grown at 37 °C in a humidified atmosphere containing 5% CO_2.

Immunoblot Cells were plated at a density of 3×10^5 in 60-mm-diameter. Upon reaching 80% confluency, cells were switched to serum-free medium (SFM) for 24 hour to synchronize cell status, after which treatments were added. Treated cells were washed twice with ice-cold phosphate buffered saline (PBS) on ice and lysed with lysis buffer of 50 mM Tris-Cl (pH 7.4), 1% Nonidet P-40, 2 mM EDTA (pH 8.0), 100 mM NaCl, 10 mM sodium orthovanadate, 1 mM phenylmethysulforny fluoride, and with proteases inhibitor cocktails. Lysates were centrifuged at 21,000 rpm for 30 minutes at 4 °C. Protein concentrations were measured using the bicinchoninic acid protein assay reagent

kit (Pierce). Cellular protein (80 μg) was resuspended in 5x Laemmli loading buffer with 60 mg/ml DTT and was resolved by SDS-PAGE, transferred to nitrocellulose membrane, and immunoblotted according to manufacturer guidelines.

siRNA transfection and cell stimulation Cells were cultured in growth medium to reach confluency of 80% then were transfected with 30 nmol/L siRNA (siRNAs SMARTpool were purchased from Santa Cruz Biotechnology) using the TransIT-siQUEST transfection reagent (Mirus, Madison, WI) according to the manufacturer's protocol. 48 hours later, cells were processed to indicate experimental procedure.

Stable Nrf2 down-regulation with shRNA

Lentiviral pKLO.1 vectors encoding five Nrf2 mRNA specific shRNA sequences: #55 (5'-AAACCCAGGGCTGCCTTGGAAAAG-3'); #56 (5'-AAACCCAGGGCTGCCTTGGAAAAG-3'); #57 (5'-AAACCCAGGGCTGCCTTGGAAAAG-3'); #58 (5'-AAACCCAGGGCTGCCTTGGAAAAG-3'); #59 (5'-AAACCCAGGGCTGCCTTGGAAAAG-3') or a scrambled shRNA were purchased from BioMedical Genomics Center (University of Minnesota) and were introduced to MCF-7, T47D, MDA-MB-231, and MDA-MB-436 cells. 8 mg/ml polybrene was added to increase infection efficiency. MCF-7 and T47D cells infected with shRNA were maintained by 1 μg/ml puromycin selection pressure, while MDA-MB-231 cells and MDA-MB-436 cells were maintained by 1.5 μg/ml and 2 μg/ml puromycin selection pressure respectively.

Overexpression of xCT

Lentiviral pLOC vector encoding the open reading frame of SLC7A11 without stop codon (OHS5898-219582558) was purchased from Dharmacon (Lafayette, CO) and was introduced to MDA-MB-231 and MDA-MB-436 cells. 8 mg/ml polybrene was added to increase infection efficiency. Infected cells were maintained by 5 – 15 μg/ml blasticidin select pressure.

Reverse transcription-quantitative real-time polymerase chain reaction Cells were plated at a density of 2 x 10^5 in 6-well-plates in growth media to reach 80% confluency then synchronized in SFM for 24 hours followed by treatments indicated in the figure legends. Cellular RNA was isolated using TriPure Reagent according to the manufacturer (Roche, Belgium). For quality control and to determine concentration, a 260:280 ratio assay was conducted on a spectrophotometer. Forward and reverse primers were designed to target the following transcripts: *SLC7A11* (xCT) 5'-GGCAACCGCGTAATACTTG-3' and 5'-TTGCAAGCTCACAGCAATTC-3'; *NFE2L2 (Nrf2)* 5'-CAAGACTTGGGCCACTTAAAAGAC-3' and 5'-AGTAAGGCTTTCCATCCTCATCAC-3'; *G6PD* 5'-TGACCTGGCCAAGAAGAAGA-3' and 5'-CAAAGAAGTCCTCCAGCTTG-3'; *PGD* 5'- ATATAGGGACACCACAAGACGG-3' and 5'-GCATGAGCGATGGGCCATA-3'; *ME-1* 5'-GGAGCTCCAGGTCCTTAGAA-3' and 5'-TGAGCACGCTGTAGAAGAGC-3'; *PPAT* 5'-AATAGCTGTGGCCCATAACG-3' and 5'-ACGTGGAAAGCCCAATACC-3'; *TALDO1* 5'-GTCATCAACCTGGGAAGGAA-3' and 5'-CAACAAATGGGGAGATGAGG-3'; *TKT* 5'-GCTGAACCTGAGGAAGATCA-3' and 5'-TGTCGAAGTATTTGCCGGTG-3'; *MTHFD2* 5'-CCGCCAGTCACTCCTATGTT-3' and 5'-TCCTCTGAAACTGAGGCTGG-3'; *NQO-1* 5'-AGCTGGAAGCTGCAGACCTG-3' and 5'-CCTTTCAGAATGGCTGGCA-3'; *SLC3A2* 5'-ACCGGGGTGAGAACTCGTGGT-3' and 5'-TGGAACCCATCCACGCCAGC-3'; *SLC7A5* 5'-GGCAACCGCGTAATACTTG-3' and 5'-TTGCAAGCTCACAGCAATTC-3'; *GCLC* 5'-TGCGAAAACGCCGGAAGGAGG-3' and 5'-ACCTCGGGCAGTGTGAACCCA-3'; *GCLM* 5'-AAGTGCCCGTCCACGCACAG-3' and 5'-ACTCCCTGACCAAATCTGGGTTGA-3'; *CD44* 5'-AGAAGGTGTGGGCAGAAGAA-3' and 5'-AAATGCACCATTTCCTGAGA-3'; *CD44v* 5'-AGAAGGTGTGGGCAGAAGAA-3' and 5'-AAATGCACCATTTCCTGAGA-3'; *SNAIL* 5'-ACCACTATGCCGCGCTCTT-3' and 5'-GGTCGTAGGGCTGCTGGAA-3'; *SLUG* 5'-TGTTGCAGTGAGGGCAAGAA-3' and 5'-GACCCTGGTTGCTTCAAGGA-3'; *TWIST1* 5'-

CGACGACAGCCTGAGCAACA-3' and 5'-TGCAGCTCCTCGTACGACTG-3'; *ZEB1* 5'-GCACCTGAAGAGGACCAGAG-3' and 5'-TGCATCTGGTGTTCCATTTT-3'; *CDH1* 5'-ACGTTAGCCTCGTTCTCAGG-3' and 5'-TGAGGGGTTAAGCACAACAG-3'; and *RPLPO* 5'-TGCTGATGGGCAAGAACAC-3' and 5'-GAACACAAAGCCCACATTCC-3'. A total of 1 μg of RNA was reverse transcribed using the Transcriptor Reverse Transcriptase Kit, and quantitative PCR was conducted using the Universal SYBR Green Kit according to the manufacturer's protocol (Roche) on an Eppendorf (Hamburg, Germany) Mastercycler Realplex^4 machine. The relative concentration of mRNA was calculated using cycle threshold values that were derived from a standard curve and normalized to ribosomal protein, large, P_O (RPLPO) as an internal control.

Monolayer growth assay Cells were plated in 24-well-plates at a density of 15,000 cells per well, allowed to attach overnight and starved in SFM for 24 hours to synchronize cells. After 5 days of treatments, growth was assessed via the 3-(4,5-dimethylthiazol-2-yl)-2,5-diphenyltetrazolium bromide (MTT) assay. 50 μl of 5 mg/ml MTT solution in SFM were added to each well and incubated for 4 hours at 37 °C. Media were aspirated and formazan crystals were lysed with 500 μl of solubilization solution (95% dimethylsulfoxide + 5% improved minimal essential media). Absorbance was measured with a plate reader at 570 nm using a 650 nm differential filter to assess growth.

Anchorage-independent growth A 1 ml layer of 1% Seaplaque-agarose (BioWhittaker, Rockland, ME) in 1.5% FBS-containing growth media was solidified into each well of a 6-well plate. The bottom layer was overlaid with 1 ml of a 1% top agar mixture for 12,000 cells per well with indicated treatments. All plates were incubated at 37 °C for 14 days. Colonies was counted on a light microscope with an ocular grid. Five random fields were counted per well and only colonies exceeding half of a grid square were scored.

Radiation delivery A dosage from 1~10 Gray was delivered to cell cultures by X-RAD 320 Biological Irradiator (Precision X-ray, North Branford, CT). Beam hardening filter= 2mm Al, dose rate: 3 Gy/min at 320 kV, 12.5 mA, 50 cm SSD.

Glutathione measurement Cells were plated at a density of 10,000 in 96-well clear bottom white plates and allowed to equilibrate overnight followed by treatments. Intracellular reduced glutathione concentrations were measured by using GSH/GSSG-Glo™ Assay following manufacturer's instruction (Promega, Madison, WI). Readings were further normalized to CellTiter-Glo® Luminescent Cell Viability Assay following the manufacturer's guideline (Promega).

Reactive oxygen species assay Cells were seeded at a density of 10,000 in 96-well clear bottom black plates, allowed to equilibrate overnight, and starved in SFM for 24 hours followed by treatments. Intracelluar ROS levels were determined by using OxiSelect™ Intracellular ROS Assay Kit according to manufacturer's guideline (Cell Biolabs, Inc., San Diego, CA)

Mitochondrial potential measurement Cells were seeded and treated with indicated reagents then mitochondrial potential were measured by following the instruction of TMRE-Mitochondrial membrane potential assay kit (Abcam, Cambridge, MA).

Radiation delivery A dosage from 1~10 Gray was delivered to cell cultures by X-RAD 320 Biological Irradiator (Precision X-ray, North Branford, CT). Beam hardening filter= 2mm Al, dose rate: 3 Gy/min at 320 kV, 12.5 mA, 50 cm SSD.

Metabolic profiling Cells were seeded, equilibrated, and quenched following the instruction provided by University of Michigan Metabolomics Core.

Cell cycle analysis Cells were typsinized, washed twice in ice-cold PBS, and fixed in 70% ice-cold ethanol -20 °C over night. Cell cycle analyses were performed on propidium

iodide-stained nuclei by using an Accuri™ C6 flow cytometer (BD Biosciences, San Jose, CA). Single cells were gated, 10,000 events were collected and analyzed by FlowJo (Tree Star Inc., Ashland, OR) software.

Three-dimensional cell culture 0.8 x 10^5 MDA-MB-231 cells were seeded in 12-well plates on top of matrigel. Detailed protocol was extensively described previously [164].

Boyden chamber migration assay Cell motility and invasion were measured by a modified Boyden chamber assay as described previously[5]. Cells were briefly detached by trypsin, washed twice with SFM, and then resuspended in SFM with or without NT157 compound. Cells (150,000) were placed in the upper chamber of a 10-well Boyden chamber apparatus. Upper and lower chambers were separated by a polycarbonate polyvinylpyrrolidone–free filter with 8-µm pores. SFM (0.4 mL) with or without IGF (5 nmol/L) was placed in the bottom wells of the chamber. After 5 h of incubation at 37°C in a humidified atmosphere containing 5% CO2, cells remaining on the topside of the filter were removed with cotton swabs. The filter was then removed from the chamber and the cells that had migrated to the underside of the filter were fixed and stained in HEMA3. The filter was then mounted onto a glass microscope slide and cells were counted (in triplicate) in five different areas using a light microscope.

Clinical data set analysis The relative mRNA expression of *xCT* in human breast tumor samples was determined by searching the Oncomine database (version 4.4.3, September 2012 data release [122]. *xCT* mRNA expression was queried in TCGA breast dataset using reporter A_32_P165472. For prognostic analyses, overall survival and distant metastasis-free survival, stratified by expression (all percentiles between the lower and upper quartiles were computed, and the best performing threshold was used as a cutoff) of the gene of interest (*NFE2L2*, 201146_at), were presented as Kaplan–Meier plots and tested for significance using log-rank tests.

Statistical analysis All data except clinical data sets were analyzed with the unpaired Student's t test with the use of Excel 2008 (Microsoft, Redmond, WA). A p value of <0.05 was considered statistically significant (* $p<0.5$, ** $p<0.01$, *** $p<0.001$).

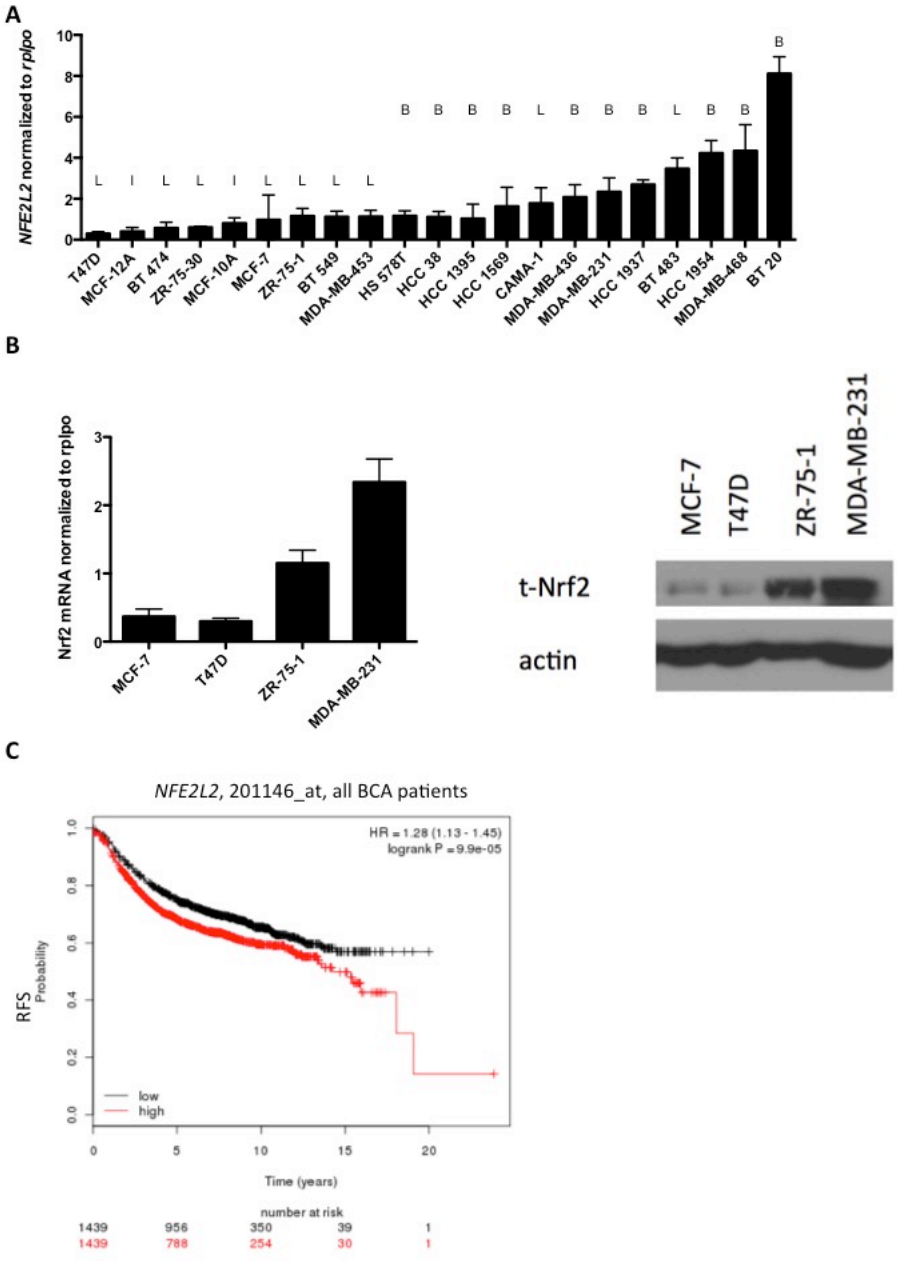

Figure 4.1 Upregulation of Nrf2 expression in TNBC/basal-like breast cancer cell lines and had prognostic value in patients' samples.

A. Total RNA was isolated from a panel of immortalized breast epithelial cell lines and breast cancer cell lines, and reverse transcribed to DNA. NFE2L2 gene expression was quantified by qRT-PCR. L indicates Luminal; B indicates Basal-like. **B.** mRNA (left) and protein (right) expressions of Nrf2 in indicated breast cancer cell lines. **C.** Kaplan-Meier plots of refractory free survival (RFS) of patients with breast cancer. Data was obtained from the Kaplan-Meier plotter database [16]. qRT-PCR data were normalized to RPLP0 housekeeper gene. Graphic data are mean ± SEM; results are representative of at least three independent triplicates experiments.

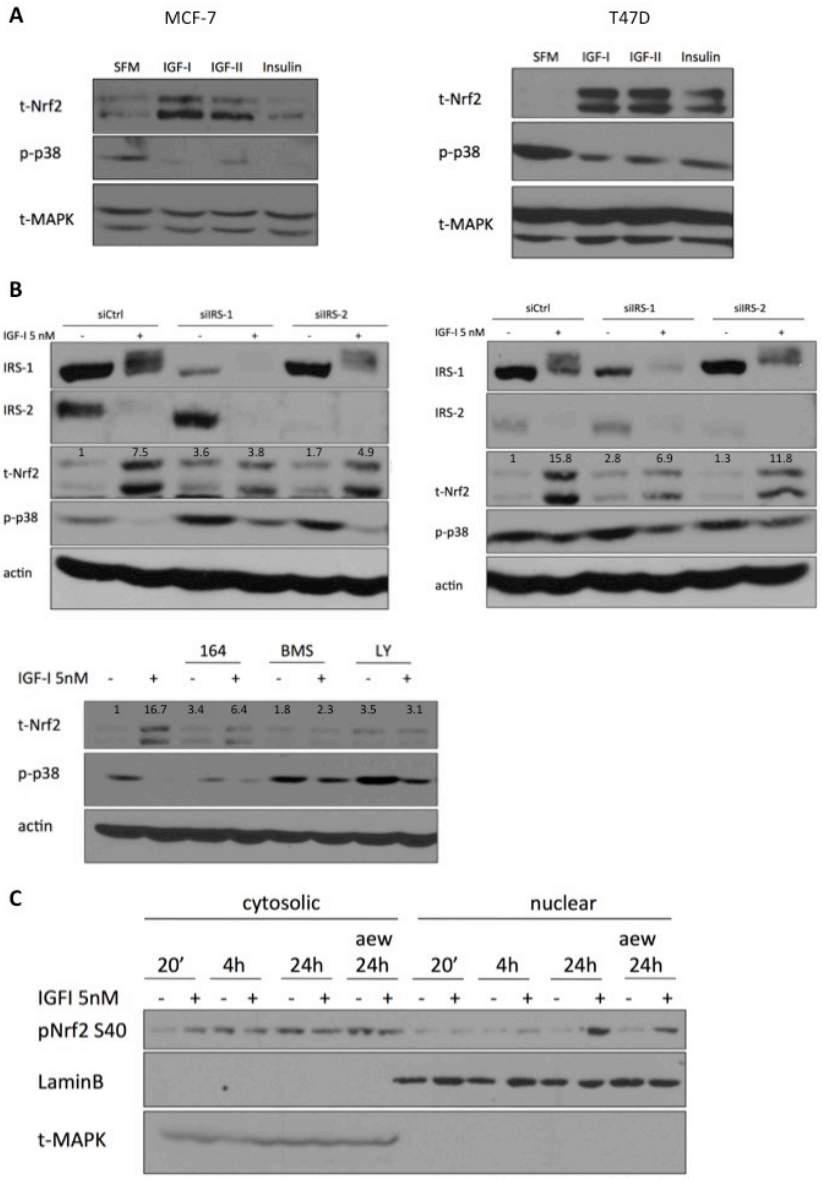

Figure 4.2 IGF signaling system regulated Nrf2 protein expression and function in ER+ breast cancer cells. **A.** MCF-7 (left) and T47D (right) cells were serum starved overnight then treated with or without IGF-I (5 nM), IGF-II (10 nM), or insulin (10 nM) for 24 hours. Cellular lysates were separated by SDS-PAGE and indicated protein levels were assessed by immunoblotting. **B.** Top panels: MCF-7 (left) or T47D (right) cells were transfected with control, IRS-1, or IRS-2 siRNAs (25 nM) for 48 hours. Cells were serum starved then treated with or without IGF-I (5 nM) for 24 hours. Indicated protein levels were analyzed by immunoblotting. Bottom panel: MCF-7 cells were serum starved overnight then pretreated with huEM164 (164, 20 μg/ml, 24 hr), BMS-754807 (BMS, 1 nM, 1hr), or LY294002 (LY, 10 μM, 1hr). Protein levels of total Nrf2, phospho-p38^{MAPK}, and actin were determined by immunoblotting. The intensity of Nrf2 bands were further digitized and quantified by ImageJ then normalized to the reading (as the denominator) of the first lane of each experiment. The numbers indicated the relative intensities of total Nrf2 bands. **C.** MCF-7 cells were pretreated with or without AEW-541 (AEW, 1 nM, 1 hr) and serum starved overnight then treated with or without IGF-I (5 nM) for indicated time period. Cytoplasmic and nucleus phosphor-serine 40 Nrf2 protein were extracted and assessed by immunoblotting.

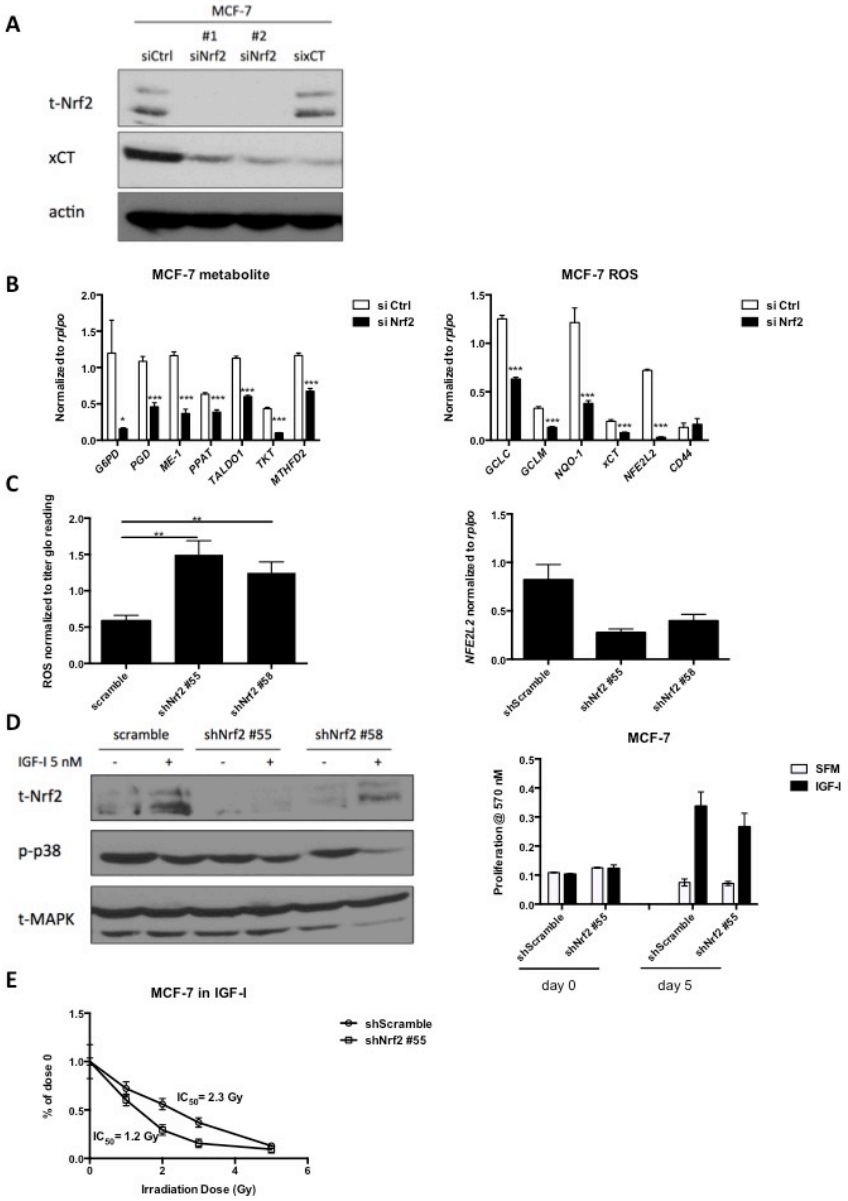

Figure 4.3 Nrf2 suppression resulted in intracellular redox upregulation in MCF-7 cells.
A. MCF-7 cells were transfected with control or Nrf2-targeted siRNAs (25 nM) for 48 hours. Protein expressions were assessed by immunoblotting. **B.** MCF-7 cells were transfected with control or Nrf2 siRNAs (25 nM) for 48 hours. mRNA expressions of PPP metabolic pathway related genes (left) and ROS pathway related genes (right) were quantified by qRT-PCR. **C.** Cellular ROS levels of indicated manipulated MCF-7 cells were measured and normalized to cell viability titer glo readings (left). Nrf2 shRNA downregulation efficiency was analyzed by qRT-PCR (right). **D.** Indicated shRNAs infected MCF-7 cells were serum starved overnight then treated with IGF-I (5 nM) for 24 hour (signaling, left) and 5 days (monolayer proliferation, right). **E.** MCF-7 cells infected with scrambled or Nrf2-targeted shRNAs were starved and treated with IGF-I (5 nM) for anchorage independent soft agar assay analysis. qRT-PCR data were normalized to *RPLP0* housekeeper gene. Graphic data are mean ± SEM; results are representative of at least three independent triplicates experiments.

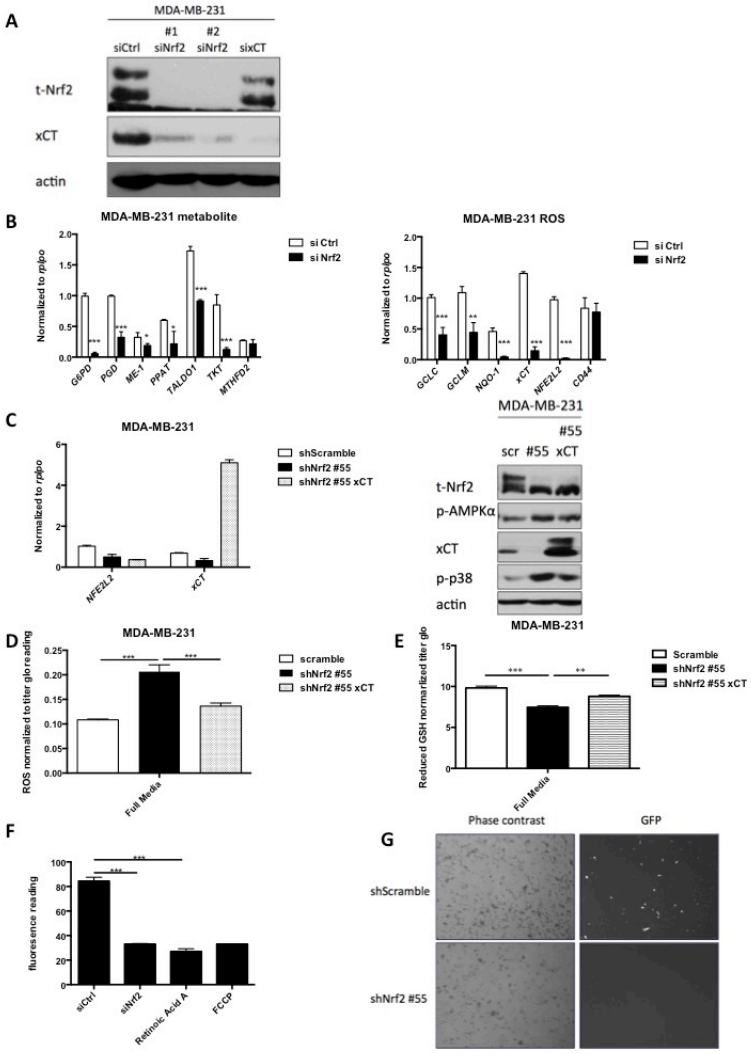

Figure 4.4 Nrf2 suppression resulted in redox upregulation, cellular reduced GSH downregulation, and mitochondrial function impairment in MDA-MB-231 cells.

A. MDA-MB-231 cells were transfected with control or Nrf2-targeted siRNAs (25 nM) for 48 hours. Protein expression level of Nrf2 were assessed by immunoblotting. **B.** MDA-MB-231 cells were transfected with control, or Nrf2 targeted siRNAs (25 nM) for 48 hours. mRNA expressions of PPP metabolic pathway related genes (left) and ROS pathway related genes (right) were quantified by qRT-PCR. **C.** MDA-MB-231 cells with indicated genetic manipulations were maintained in full growth media. Left: *NFE2L2* and *xCT* mRNA expressions were assessed by qRT-PCR. Right: Indicated protein expressions were assessed by western blotting. **D.** Cellular ROS levels of MDA-MB-231 cells with indicated genetic manipulations. Data were normalized by titer glo reading. **E.** Cellular reduced GSH levels of MDA-MB-231 cells with indicated genetic manipulations were measured and normalized to titer glo reading. **F.** Mitochondrial membrane potentials were measured by using microplate reader in MDA-MB-231 cells with indicated treatment. Carbonyl cyanide-4-(trifluoromethoxy)phenylhydrazone (FCCP) served as an assay control. **G.** MDA-MB-231 cells infected with scrambled or Nrf2-targeted shRNAs were transfected with an inducible ARE-responsive GFP reporter for 48 hours. Phase contrast and GFP images were captured by Leica microscopy. qRT-PCR data were normalized to *RPLP0* housekeeper gene. Graphic data are mean ± SEM; results are representative of at least three independent triplicates experiments.

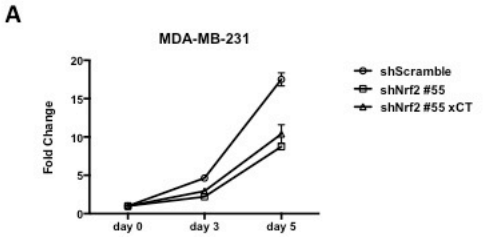

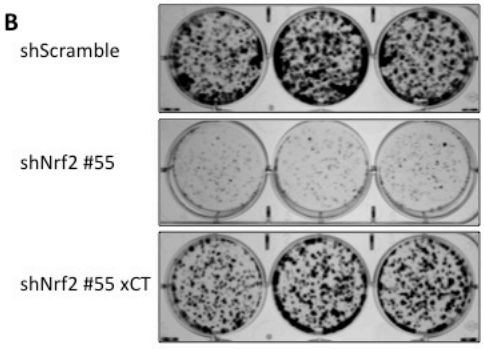

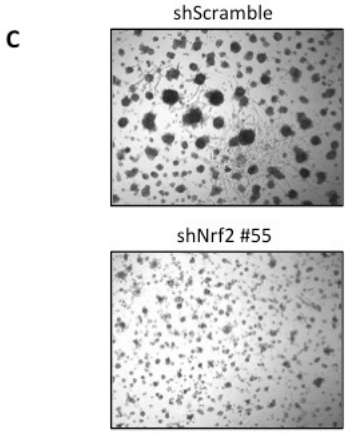

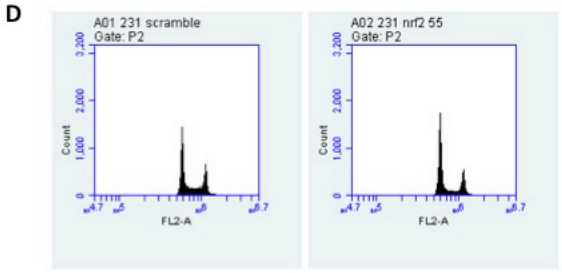

	Sub G1	G0/G1	S	G2/M	Super G2
shScramble	4.69	62.09	21.81	10.67	0.84
shNrf2 #55	3.57	68.53	15.57	13.11	0.47

Figure 4.5 Suppression of Nrf2 inhibited the proliferation of MDA-MB-231 cells.
A. MDA-MB-231 cells with indicated genetic manipulations were plated in 24-well plates. Monolayer cell growth were measured by MTT assay. **B.** Clonogenic assay of MDA-MB-231 with indicated genetic manipulations. **C.** MDA-MB-231 cells infected with scrambled or Nrf2-targeted shRNAs were plated on-top of matrigel for 3-dimentional culture. **D.** MDA-MB-231 cells were infected with scrambled or Nrf2-targeted shRNAs. Cells were fixed then stained with propidum iodide. Cell cycle frequencies were determined by flow cytometry. Graphic data are mean ± SEM; results are representative of at least three independent triplicates experiments.

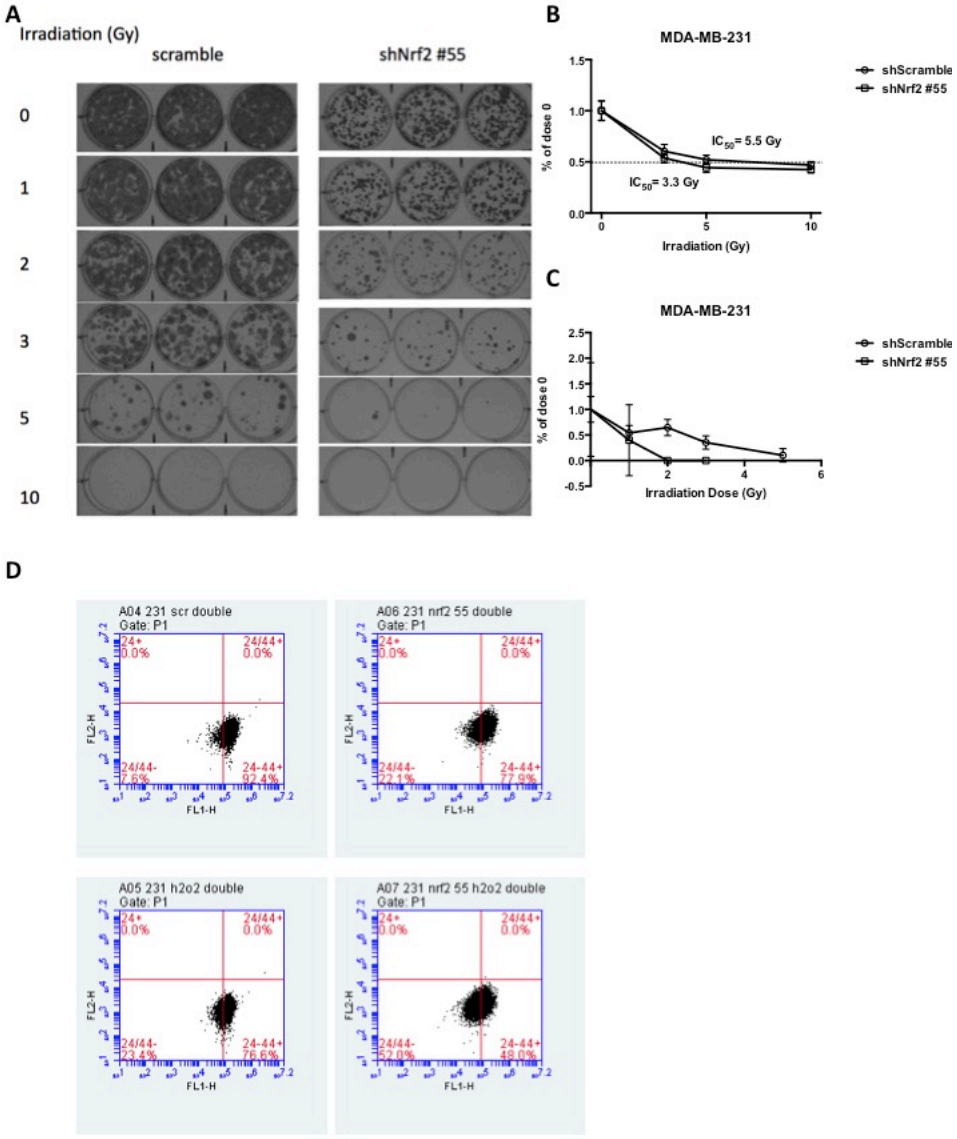

Figure 4.6 Loss of Nrf2 sensitized MDA-MB-231 cells' response to irradiation.
MDA-MB-231 cells infected with scrambled or Nrf2-targeted shRNAs were treated with increasing dosage of irradiation then cell proliferation was analyzed by clonogenic assay (**A**), MTT monolayer growth (**B**), and anchorage-independent growth (**C**). **D.** MDA-MB-231 cells with indicated genetic manipulations were treat with or without H_2O_2 (10 μM). Cell surface CD makers were analyzed by flow cytometry. Graphic data are mean ± SEM; results are representative of at least three independent triplicates experiments.

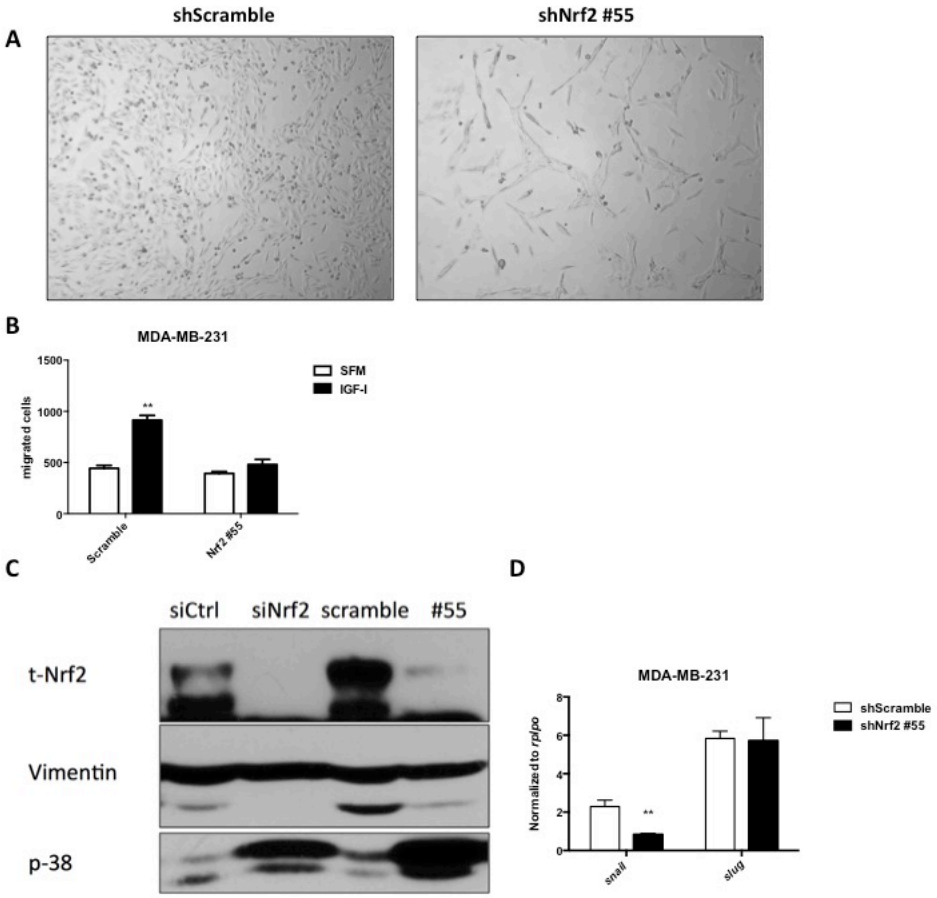

Figure 4.7 Loss of Nrf2 reduced EMT in MDA-MB-231 cells.
A. Phase-contrast images for cell morphology were captured by Leica microscopy. **B.** Indicated MDA-MB-231 cells were treated with or without IGF-I (5 nM). Cell migration potential was evaluated by boyden chamber assay. **C.** Indicated protein levels were assessed by immunoblotting in cells with indicated genetic manuniplations. **D.** mRNA expression levels of EMT makers were quantified by qRT-PCR in MDA-MB-231 cells with indicated genetic manipulations. qRT-PCR data were normalized to *RPLP0* housekeeper gene. Graphic data are mean ± SEM; results are representative of at least three independent triplicates experiments.

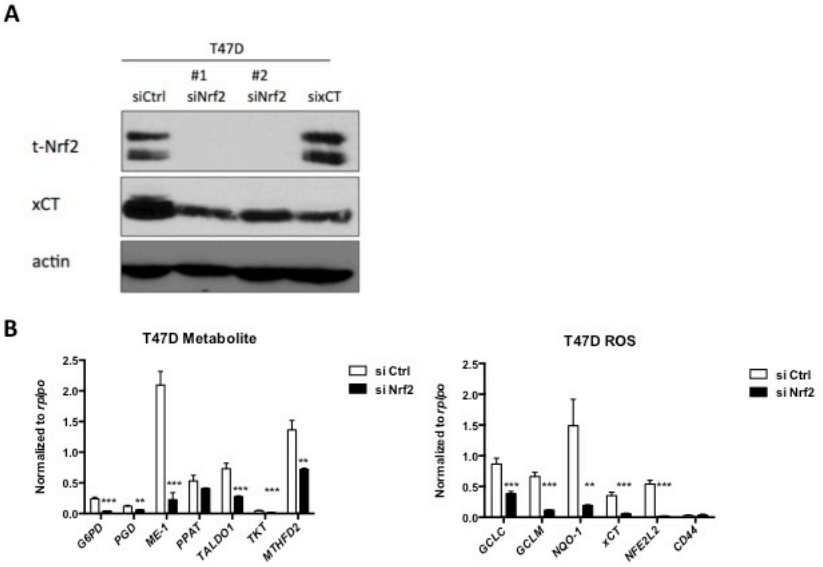

Figure 4.8 Effects of siRNA downregulation of Nrf2 in T47D cells.
A. T47D cells were transfected with or without control or Nrf2-targeted siRNAs (25 nM) for 48 hours. Protein expressions level of Nrf2 and xCT were quantified by immunoblotting. **B.** T47D cells were transfected with control or Nrf2 siRNAs (25 nM) for 48 hours. mRNA expressions of PPP metabolic pathway related genes (left) and ROS pathway related genes (right) were quantified by qRT-PCR. qRT-PCR data were normalized to *RPLP0* housekeeper gene. Graphic data are mean ± SEM; results are representative of at least three independent triplicates experiments.

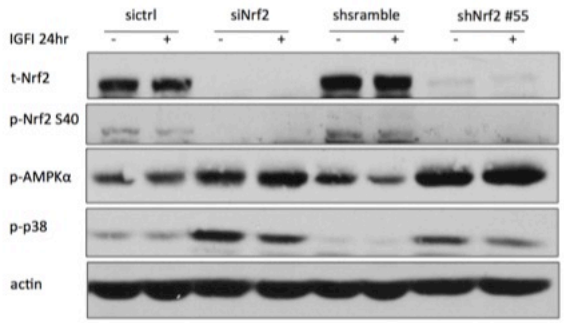

Figure 4.9 IGF-I did not stimulate Nrf2 expression in MDA-MB-231 cells.
A. MDA-MB-231 cells with indicated genetic manipulations were serum starved then treated with IGF-I (5 nM) for 24 hours. Protein levels of total Nrf2, phospho-Nrf2, phospho-AMPKα, phospho-p38MAPK, and actin were measured by immunoblotting.

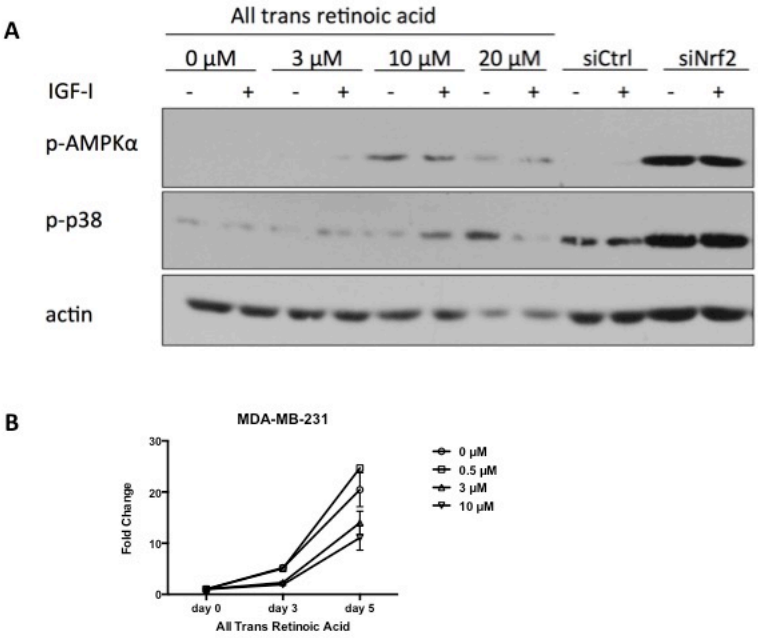

Figure 4.10 Chemical inhibition of Nrf2 using all trans retinoic acid A (ATRA) resulted in ROS upregulation, AMPK α activation, and growth inhibition in MDA-MB-231 cells.

A. MDA-MB-231 cells were treated with indicated dosage of all trans retinoic acid or Nrf2-targeted siRNA (25 nM) then serum starved followed by IGF-I (5 nM) stimulation. Indicated protein levels were assessed by immunoblot. **B.** MDA-MB-231 cells were treated with increasing concentrations of ATRA. Cell monolayer growth was measured by MTT assay. Graphic data are mean ± SEM; results are representative of at least three independent triplicates experiments.

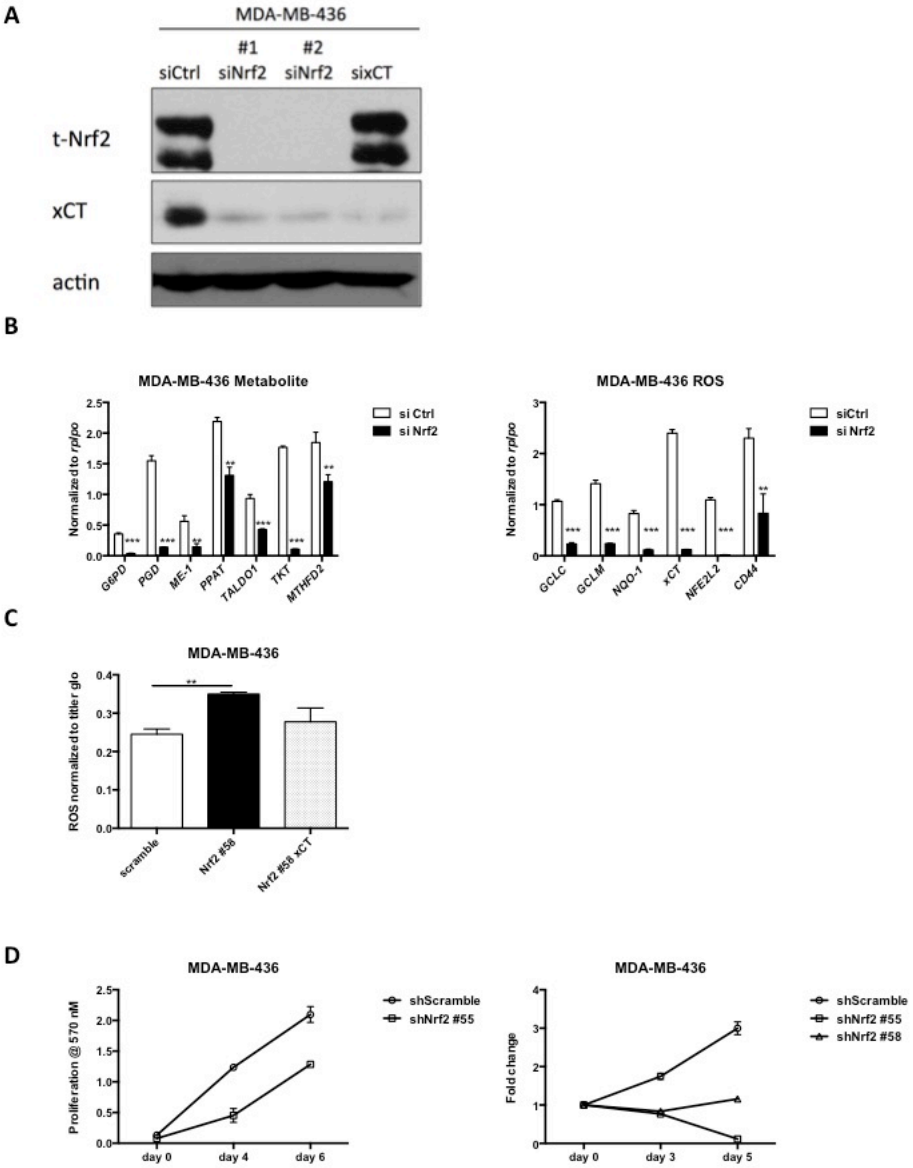

Figure 4.11 Nrf2 suppression resulted in ROS upregulation and growth inhibition in MDA-MB-436 cells.
MDA-MB-436 cells were transfected with control or Nrf2 siRNAs (25 nM) for 48 hours. **A.** Protein expression of Nrf2 and xCT were assessed by immunoblotting. **B.** mRNA expressions of PPP metabolic pathway related genes (left) and ROS pathway related genes (right) were quantified by qRT-PCR. **C.** Intracellular ROS levels were measured and normalized to titer glo reading in MDA-MB-436 cells with indicated genetic manipulations. **D.** Monolayer cell growth was analyzed in MDA-MB-436 cells infected with scrambled or Nrf2-targeted shRNAs. qRT-PCR data were normalized to *RPLP0* housekeeper gene. Graphic data are mean ± SEM; results are representative of at least three independent triplicates experiments.

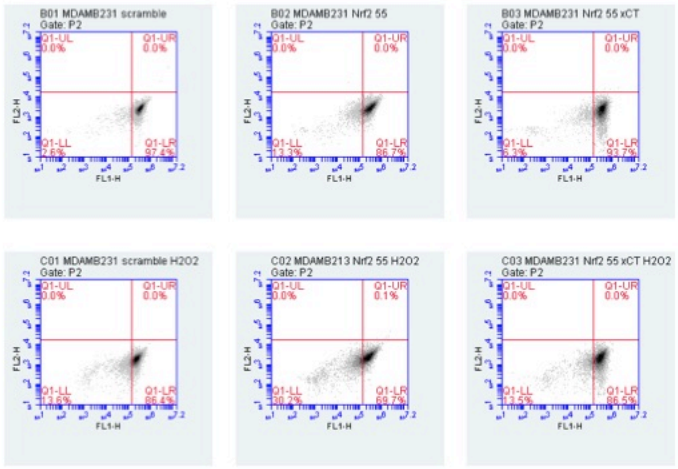

Figure 4.12 Overexpression of xCT rescued CD44+/24- population in Nrf2 downregulated cells.
MDA-MB-231 cells with indicated genetic manipulations were treat with or without H_2O_2 (10 μM). Cell surface CD makers were analyzed by flow cytometry.

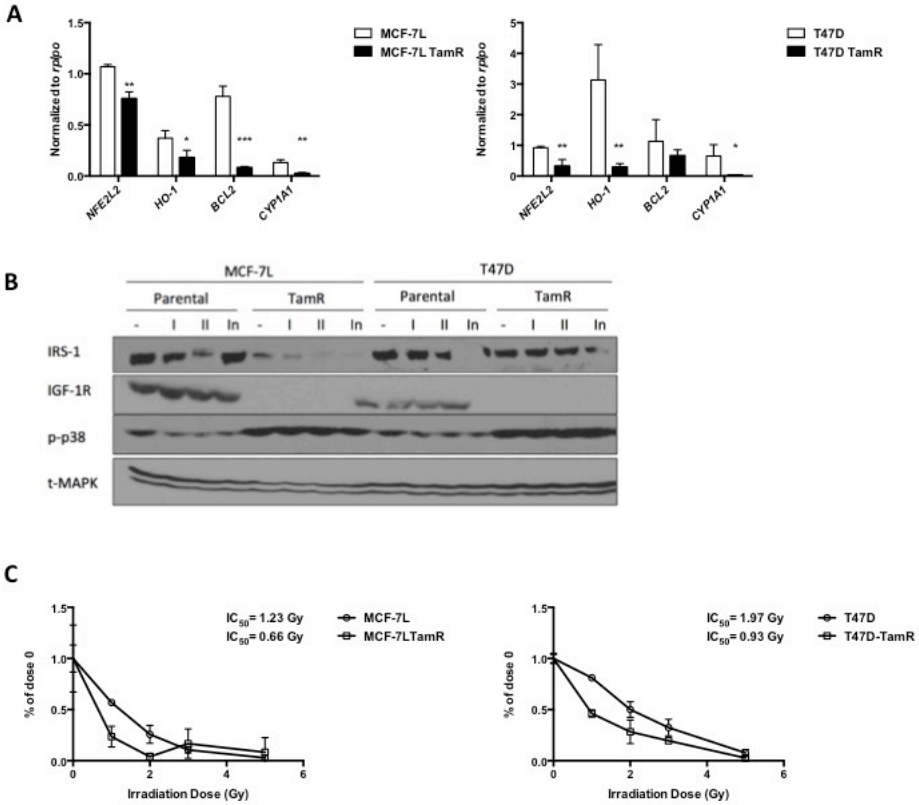

Figure 4.13 Tamoxifen resistant cells expressed less Nrf2, exhibited higher level of cellular ROS, and were more sensitive to irradiation.

A. mRNA expressions of *NFE2L2* mRNA and ROS related genes were analyzed by qRT-PCR. **B.** Indicated cellular protein expressions were assessed by immunoblotting. **C.** Indicated cell lines were irradiated at an increasing dosage. Anchorage independent growth was determined by colonies formation in agarose after 14 days. Data are mean ± SEM; results are representative of at least three independent triplicates experiments.

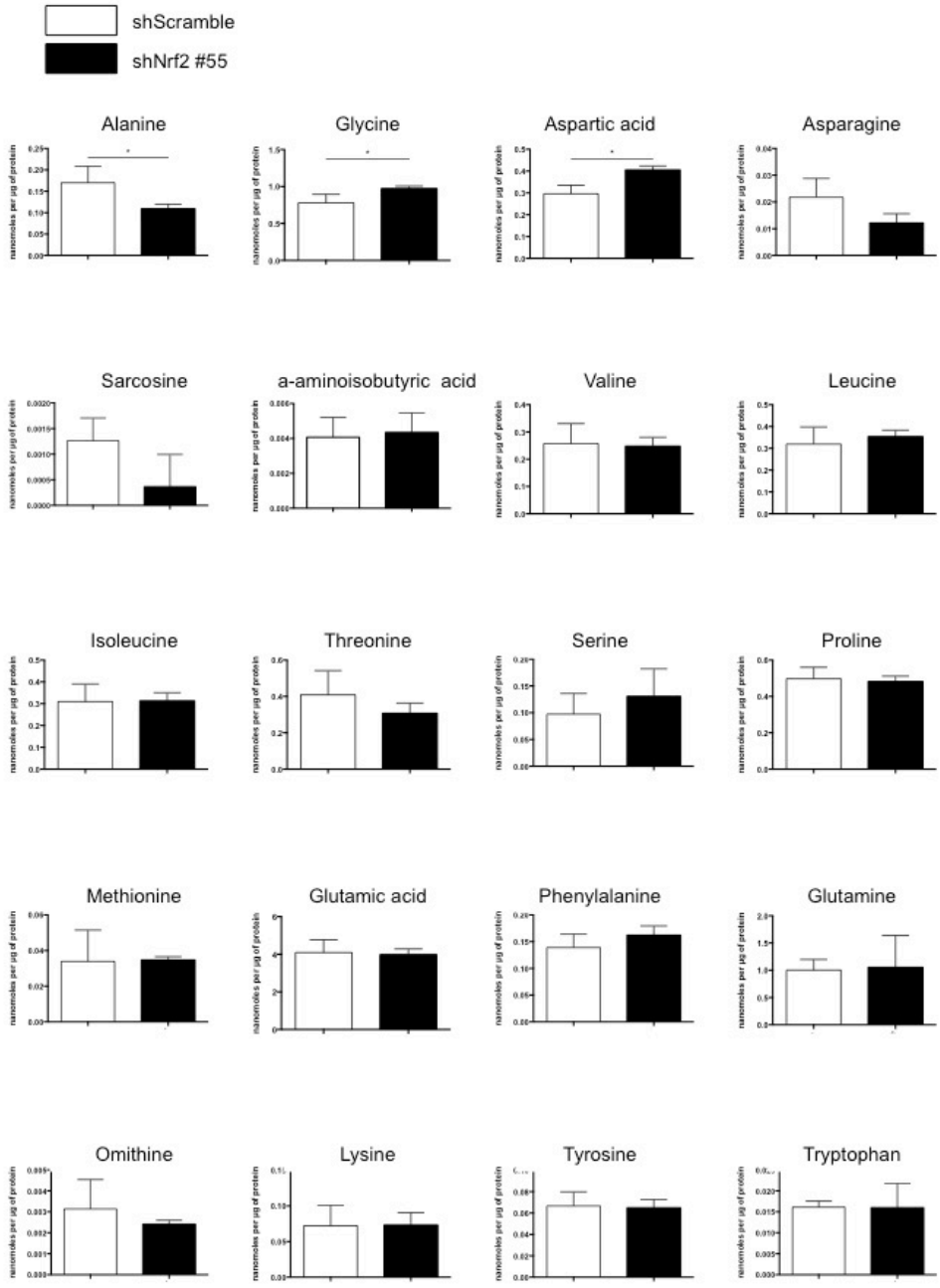

Figure 4.14 Effects of Nrf2 suppression on amino acid metabolism.
Concentrations of 20 amino acids were measured by University of Michigan Metabolomic Core. Concentrations were further normalized by total protein amount per sample. Graphic data are mean ± SEM; results are representative of at least three independent triplicates experiments.

Gly/TCA/Nucleolide	shScramble/shNrf2 #55 fold change
NAD	1.29
NADP	1.59
AMP	0.27
ATP	1.50
SUC	0.70
FAD	0.68
MAL	0.67
6PG	2.12
ADP	1.44
aCOA	1.24
FBP	1.34
CIT/ICIT	0.77
2PG/3PG	1.81
F6P/G6P	1.05

Table 4.1 Loss of Nrf2 redirected cell metabolism from PPP to glycolysis.
Contents in glycolysis, TCA, and nucleolide were measured by University of Michigan Metabolomic Core. Data presented as folder change.

Chapter 5

Conclusion and future directions

The first part of the thesis emphasizes the therapeutic potential of downregulating IRS proteins by NT157. NT157 was studied as mono- and combination therapy in various breast cancer models. In addition, we, for the first time, reveal that NT157 also targeted ERα in ERα+ breast cancer cells. Targeting IRS protein could be useful alone or in combination with other therapies in many different subtypes of breast cancer. Further work needs to be performed to evaluate growth inhibitory effects of NT157 compound in breast cancer xenograft models. The compound itself also needs to be modified to improve potency.

The data presented in the third chapter of the thesis reveals that IGF-I regulates oxidative stress and thereby promotes proliferation by stimulating xC^- transporter function in an IRS-1 dependent mechanism. xC^- transporter expression level could be a promising biomarker to indicate tumor metabolic status to oxidative stress. xC^- transporter could also be a target to enhance anti-IGF-IR therapy, chemotherapy, and radiotherapy in multiple subtypes of breast cancer.

Our ongoing research also observed that IGF-I stimulated the message, protein, and cell surface expressions of heavy chain of the xC^- transporter (CD98hc) in ER positive breast cancer cells (Figure 5.1). CD98hc has been reported to mediate β-intergin signaling [165], cell adhesion [166], and cell proliferation [167] in various cancers. CD98hc also forms L-type amino acid transporter-1 (LAT1) with the light chain *SLC7A5* [168, 169]. Interestingly, in our preliminary experiments IGF-I also regulated of *SLC7A5* gene expression. Cellular uptake of neutral branched amino acids through LAT1 has been reported to stimulate mammalian target of rapamycin (mTOR) in cancer cells [170]. Both CD98hc and *SLC7A5* expression has been included in an immunohistochemical predictor of breast cancer outcome [171, 172]. It will be worthy and interesting to further study the roles of CD98hc and SLC7A5 in mediating IGF-I regulated cancer behaviors.

Efforts have been made to treat human gliomas and lymphomas by inhibiting xC^- function with the FDA approved drug SASP [173]. However due to the low potency and

metabolic instability (SASP is designed to be metabolized by azoreductases to sulfapyridine and 5-aminosalicylic acid, which do not have xC^- inhibitory activities [174]) of the drug *in vivo*, those studies results were disappointing. To date, the structural basis of SASP interaction with xC^- remains unsolved. It is insoluble in aqueous solutions and needs further modification to characterize the interaction with xC^- [175]. Besides xC^-, other pathways could be targeted to inhibit amino acid uptake. Glutaminase generates cellular glutamate from glutamine and its inhibition is an indirect target for inhibiting xC^- transporter as xC^- requires intracellular glutamate concentration for exchange of extracellular cysteine (Figure 5.1). Studies have shown evidences that targeting glutaminase by the inhibitor CB-968, CB-839, (Calithera Biosicences), and BPTES (Sigma-Aldrich) significantly suppressed TNBC tumor growth [176]. Another group also reported that the small molecule erastin is a potent selective inhibitor of xC^- [177, 178]. Recent work from our and other laboratories suggest that xC^- transporter is a compelling drug target either alone or in combination with IGF-IR targeted therapy, radio-, or chemotherapy in treating a broad spectrum of breast cancers. These findings suggest a new direction for rapid drug development as well as research direction to characterize the importance of amino acid transport on cancer cell behaviors in cancer.

The last part of this thesis investigates Nrf2 as a mono- or adjuvant therapeutic target in ER+, tamoxifen resistant, and TNBC/basal-like breast cancer subtypes. Nrf2 is a direct regulator of xCT gene expression. Our data suggest IGF signaling also controls Nrf2 expression and function in ER+ breast cancer cells. Consistent with the regulation of IGF-I on xCT mRNA expression, PI3K-AKT signaling also positively regulates Nrf2 expression and function, which further emphasizes PI3K inhibitors' value in cancer treatment. Nrf2 controls cellular redox status via metabolic reprogramming to generate NADPH and directly regulate of GSH biosynthesis, thereby promotes tumor growth, maintains stem cell population, and contributing to radio-resistance. Future investigation directed toward understanding the crosstalk between Nrf2 and cellular amino acid metabolism will help to reveal hidden function of this powerful molecule. On the other hand, accumulation of Nrf2 in TNBC/basal-like breast cancer cells may due to

inactivation of Nrf2 inhibitory molecule Keap1. Sequencing for Keap1 loss-of-function mutation could help to predict prognosis and also stratify patients for ROS-manipulating therapies.

Although preclinical evidence provides strong rationale for clinically targeting IGF/insulin signaling, the withdrawal of figitumumab from phase III clinical trials raised significant concerns about the clinical utility of targeting IGF-IR with a monoclonal antibody. However, we still believe that IGF-IR antibodies can be clinically beneficial in a subset of breast cancer patients through the use of appropriate predictive biomarkers and adjuvant therapies, and coupled with cautious monitoring of insulin levels during the therapy. Other drugs affecting IGF/insulin signaling such as TKIs, ligand neutralizers, and mTOR inhibitors show promise, most likely in combination with conventional and novel agents. A more insightful understanding of IGF/insulin system and its crosstalk with other critical signaling pathways in breast cancer cells is needed to optimize the targeting of the IGF/insulin system in breast cancer.

Acknowledgements

The authors thank the assistance of the Flow Cytometry shared resource of the Masonic Cancer Center (P30 CA077598).

Funding

Chapter 2: This study was supported by Komen for the Cure SAC110039 (DY), Mayo Clinic SPORE in Breast Cancer (NIH/NCI P50CA116201-06A1 - Ingle), and NIH/NCI Cancer Center Support Grant (2P30-CA077598 - Yee).

Chapter 3: This study was supported by R01CA74285 to D.Y., the Komen for the Cure grant (SAC 110039) to D.Y., and P30-CA077598.

Chapter 4: The work on this chapter utilized Metabolomics Core Services supported by grant U24 DK097153 of NIH Common Funds Project to the University of Michigan.

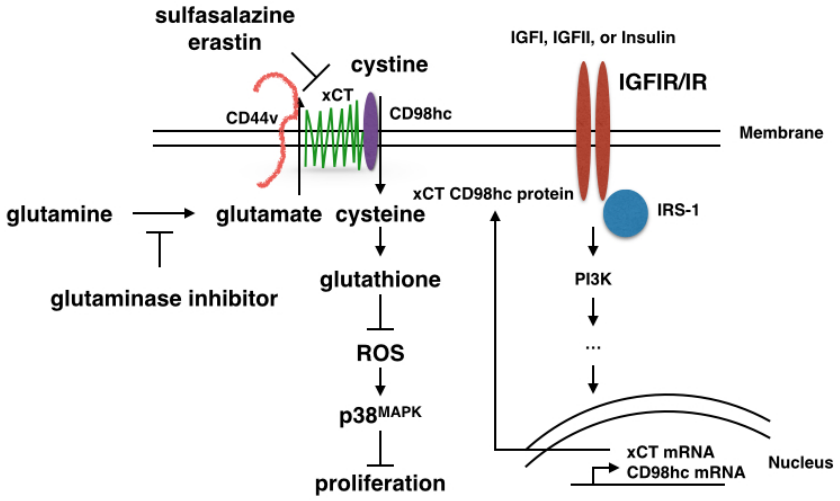

Figure 5.1 Schematic diagram showing the function and regulation of the plasma membrane cystine-glutamate transporter xC$^-$.
The transporter is composed of two subunits linked by a disulfide bond: CD98hc serves as anchorage to the plasma membrane; xCT is the functional subunit imports cystine into cell while exporting glutamate to the extracellular environment with a stoichiometry of 1:1. In TNBC cells, CD44v stabilizes xCT membrane expression and therefore facilitates the uptake of cystine to generate intracellular GSH. GSH further reduces cellular redox and sequentially promotes cell proliferation. In ER positive breast cancer cells, growth factors such as IGF-I, IGF-II, and insulin stimulate xCT and CD98hc mRNA and protein expression through IGF-I receptors and IRS-1 protein. The up-regulated plasma membrane expression of xC$^-$ transporters ultimately promotes cancer cell proliferation. The negative regulation of xC$^-$ transporter function could be achieved by direct inhibition with sulfazalazine and erastin or indirect suppression with a glutaminase inhibitor.

Bibliography

1. Osborne CK. Tamoxifen in the treatment of breast cancer. N Engl J Med. 1998; 339**:** 1609-1618.
2. Gianni L, Dafni U, Gelber RD, Azambuja E, Muehlbauer S, Goldhirsch A, Untch M, Smith I, Baselga J, Jackisch C, Cameron D, Mano M *et al*. Treatment with trastuzumab for 1 year after adjuvant chemotherapy in patients with her2-positive early breast cancer: A 4-year follow-up of a randomised controlled trial. Lancet Oncol. 2011; 12**:** 236-244.
3. Piccart-Gebhart MJ, Procter M, Leyland-Jones B, Goldhirsch A, Untch M, Smith I, Gianni L, Baselga J, Bell R, Jackisch C, Cameron D, Dowsett M *et al*. Trastuzumab after adjuvant chemotherapy in her2-positive breast cancer. N Engl J Med. 2005; 353**:** 1659-1672.
4. Garcia-Closas M, Hall P, Nevanlinna H, Pooley K, Morrison J, Richesson DA, Bojesen SE, Nordestgaard BG, Axelsson CK, Arias JI, Milne RL, Ribas G *et al*. Heterogeneity of breast cancer associations with five susceptibility loci by clinical and pathological characteristics. PLoS Genet. 2008; 4**:** e1000054.
5. Sachdev D. Regulation of breast cancer metastasis by igf signaling. J Mammary Gland Biol Neoplasia. 2008; 13**:** 431-441.
6. Pollak M. The insulin and insulin-like growth factor receptor family in neoplasia: An update. Nat Rev Cancer. 2012; 12**:** 159-169.
7. Favoni RE, de Cupis A, Ravera F, Cantoni C, Pirani P, Ardizzoni A, Noonan D, Biassoni R. Expression and function of the insulin-like growth factor i system in human non-small-cell lung cancer and normal lung cell lines. Int J Cancer. 1994; 56**:** 858-866.
8. Arteaga CL, Kitten LJ, Coronado EB, Jacobs S, Kull FC, Jr., Allred DC, Osborne CK. Blockade of the type i somatomedin receptor inhibits growth of human breast cancer cells in athymic mice. J Clin Invest. 1989; 84**:** 1418-1423.
9. Kaleko M, Rutter WJ, Miller AD. Overexpression of the human insulinlike growth factor i receptor promotes ligand-dependent neoplastic transformation. Mol Cell Biol. 1990; 10**:** 464-473.
10. Kim HJ, Litzenburger BC, Cui X, Delgado DA, Grabiner BC, Lin X, Lewis MT, Gottardis MM, Wong TW, Attar RM, Carboni JM, Lee AV. Constitutively active type i insulin-like growth factor receptor causes transformation and xenograft growth of immortalized mammary epithelial cells and is accompanied by an epithelial-to-mesenchymal transition mediated by nf-kappab and snail. Mol Cell Biol. 2007; 27**:** 3165-3175.
11. Sachdev D, Hartell JS, Lee AV, Zhang X, Yee D. A dominant negative type i insulin-like growth factor receptor inhibits metastasis of human cancer cells. J Biol Chem. 2004; 279**:** 5017-5024.
12. Sachdev D, Li SL, Hartell JS, Fujita-Yamaguchi Y, Miller JS, Yee D. A chimeric humanized single-chain antibody against the type i insulin-like growth factor (igf) receptor renders breast cancer cells refractory to the mitogenic effects of igf-i. Cancer Res. 2003; 63**:** 627-635.
13. Burtrum D, Zhu Z, Lu D, Anderson DM, Prewett M, Pereira DS, Bassi R, Abdullah R, Hooper AT, Koo H, Jimenez X, Johnson D *et al*. A fully human monoclonal antibody to

the insulin-like growth factor i receptor blocks ligand-dependent signaling and inhibits human tumor growth in vivo. Cancer Res. 2003; 63**:** 8912-8921.
14. Arteaga CL, Osborne CK. Growth inhibition of human breast cancer cells in vitro with an antibody against the type i somatomedin receptor. Cancer Res. 1989; 49**:** 6237-6241.
15. Tanno S, Tanno S, Mitsuuchi Y, Altomare DA, Xiao GH, Testa JR. Akt activation up-regulates insulin-like growth factor i receptor expression and promotes invasiveness of human pancreatic cancer cells. Cancer Res. 2001; 61**:** 589-593.
16. Ciampolillo A, De Tullio C, Giorgino F. The igf-i/igf-i receptor pathway: Implications in the pathophysiology of thyroid cancer. Curr Med Chem. 2005; 12**:** 2881-2891.
17. Frasca F, Pandini G, Scalia P, Sciacca L, Mineo R, Costantino A, Goldfine ID, Belfiore A, Vigneri R. Insulin receptor isoform a, a newly recognized, high-affinity insulin-like growth factor ii receptor in fetal and cancer cells. Mol Cell Biol. 1999; 19**:** 3278-3288.
18. Belfiore A, Frasca F, Pandini G, Sciacca L, Vigneri R. Insulin receptor isoforms and insulin receptor/insulin-like growth factor receptor hybrids in physiology and disease. Endocr Rev. 2009; 30**:** 586-623.
19. Hanahan D, Weinberg RA. Hallmarks of cancer: The next generation. Cell. 2011; 144**:** 646-674.
20. Weichhaus M, Broom J, Wahle K, Bermano G. A novel role for insulin resistance in the connection between obesity and postmenopausal breast cancer. Int J Oncol. 2012; 41**:** 745-752.
21. Algire C, Amrein L, Zakikhani M, Panasci L, Pollak M. Metformin blocks the stimulative effect of a high-energy diet on colon carcinoma growth in vivo and is associated with reduced expression of fatty acid synthase. Endocr Relat Cancer. 2010; 17**:** 351-360.
22. Gunter MJ, Hoover DR, Yu H, Wassertheil-Smoller S, Rohan TE, Manson JE, Li J, Ho GY, Xue X, Anderson GL, Kaplan RC, Harris TG *et al*. Insulin, insulin-like growth factor-i, and risk of breast cancer in postmenopausal women. J Natl Cancer Inst. 2009; 101**:** 48-60.
23. Ferguson RD, Novosyadlyy R, Fierz Y, Alikhani N, Sun H, Yakar S, Leroith D. Hyperinsulinemia enhances c-myc-mediated mammary tumor development and advances metastatic progression to the lung in a mouse model of type 2 diabetes. Breast Cancer Res. 2012; 14**:** R8.
24. Guevara-Aguirre J, Balasubramanian P, Guevara-Aguirre M, Wei M, Madia F, Cheng CW, Hwang D, Martin-Montalvo A, Saavedra J, Ingles S, de Cabo R, Cohen P *et al*. Growth hormone receptor deficiency is associated with a major reduction in pro-aging signaling, cancer, and diabetes in humans. Sci Transl Med. 2011; 3**:** 70ra13.
25. Szereday Z, Schally AV, Varga JL, Kanashiro CA, Hebert F, Armatis P, Groot K, Szepeshazi K, Halmos G, Busto R. Antagonists of growth hormone-releasing hormone inhibit the proliferation of experimental non-small cell lung carcinoma. Cancer Res. 2003; 63**:** 7913-7919.

26. Yin D, Vreeland F, Schaaf LJ, Millham R, Duncan BA, Sharma A. Clinical pharmacodynamic effects of the growth hormone receptor antagonist pegvisomant: Implications for cancer therapy. Clin Cancer Res. 2007; 13**:** 1000-1009.
27. Gao J, Chesebrough JW, Cartlidge SA, Ricketts SA, Incognito L, Veldman-Jones M, Blakey DC, Tabrizi M, Jallal B, Trail PA, Coats S, Bosslet K *et al*. Dual igf-i/ii-neutralizing antibody medi-573 potently inhibits igf signaling and tumor growth. Cancer Res. 2011; 71**:** 1029-1040.
28. Jogie-Brahim S, Feldman D, Oh Y. Unraveling insulin-like growth factor binding protein-3 actions in human disease. Endocr Rev. 2009; 30**:** 417-437.
29. Alami N, Page V, Yu Q, Jerome L, Paterson J, Shiry L, Leyland-Jones B. Recombinant human insulin-like growth factor-binding protein 3 inhibits tumor growth and targets the akt pathway in lung and colon cancer models. Growth Horm IGF Res. 2008; 18**:** 487-496.
30. Jerome L, Alami N, Belanger S, Page V, Yu Q, Paterson J, Shiry L, Pegram M, Leyland-Jones B. Recombinant human insulin-like growth factor binding protein 3 inhibits growth of human epidermal growth factor receptor-2-overexpressing breast tumors and potentiates herceptin activity in vivo. Cancer Res. 2006; 66**:** 7245-7252.
31. Papa V, Pezzino V, Costantino A, Belfiore A, Giuffrida D, Frittitta L, Vannelli GB, Brand R, Goldfine ID, Vigneri R. Elevated insulin receptor content in human breast cancer. J Clin Invest. 1990; 86**:** 1503-1510.
32. Mathieu MC, Clark GM, Allred DC, Goldfine ID, Vigneri R. Insulin receptor expression and clinical outcome in node-negative breast cancer. Proc Assoc Am Physicians. 1997; 109**:** 565-571.
33. Haluska P, Shaw HM, Batzel GN, Yin D, Molina JR, Molife LR, Yap TA, Roberts ML, Sharma A, Gualberto A, Adjei AA, de Bono JS. Phase i dose escalation study of the anti insulin-like growth factor-i receptor monoclonal antibody cp-751,871 in patients with refractory solid tumors. Clin Cancer Res. 2007; 13**:** 5834-5840.
34. Avnet S, Sciacca L, Salerno M, Gancitano G, Cassarino MF, Longhi A, Zakikhani M, Carboni JM, Gottardis M, Giunti A, Pollak M, Vigneri R *et al*. Insulin receptor isoform a and insulin-like growth factor ii as additional treatment targets in human osteosarcoma. Cancer Res. 2009; 69**:** 2443-2452.
35. Pandini G, Wurch T, Akla B, Corvaia N, Belfiore A, Goetsch L. Functional responses and in vivo anti-tumour activity of h7c10: A humanised monoclonal antibody with neutralising activity against the insulin-like growth factor-1 (igf-1) receptor and insulin/igf-1 hybrid receptors. Eur J Cancer. 2007; 43**:** 1318-1327.
36. Sachdev D, Yee D. Disrupting insulin-like growth factor signaling as a potential cancer therapy. Mol Cancer Ther. 2007; 6**:** 1-12.
37. Zeng X, Sachdev D, Zhang H, Gaillard-Kelly M, Yee D. Sequencing of type i insulin-like growth factor receptor inhibition affects chemotherapy response in vitro and in vivo. Clin Cancer Res. 2009; 15**:** 2840-2849.
38. Sachdev D, Zhang X, Matise I, Gaillard-Kelly M, Yee D. The type i insulin-like growth factor receptor regulates cancer metastasis independently of primary tumor growth by promoting invasion and survival. Oncogene. 2010; 29**:** 251-262.

39. Atzori F, Tabernero J, Cervantes A, Prudkin L, Andreu J, Rodriguez-Braun E, Domingo A, Guijarro J, Gamez C, Rodon J, Di Cosimo S, Brown H *et al*. A phase i pharmacokinetic and pharmacodynamic study of dalotuzumab (mk-0646), an anti-insulin-like growth factor-1 receptor monoclonal antibody, in patients with advanced solid tumors. Clin Cancer Res. 2011; 17**:** 6304-6312.
40. Fagan DH, Uselman RR, Sachdev D, Yee D. Acquired resistance to tamoxifen is associated with loss of the type i insulin-like growth factor receptor: Implications for breast cancer treatment. Cancer Res. 2012; 72**:** 3372-3380.
41. Belfiore A, Malaguarnera R. Insulin receptor and cancer. Endocr Relat Cancer. 2011; 18**:** R125-147.
42. Qiu J, Yang R, Rao Y, Du Y, Kalembo FW. Risk factors for breast cancer and expression of insulin-like growth factor-2 (igf-2) in women with breast cancer in wuhan city, china. PLoS One. 2012; 7**:** e36497.
43. Ward A, Bates P, Fisher R, Richardson L, Graham CF. Disproportionate growth in mice with igf-2 transgenes. Proc Natl Acad Sci U S A. 1994; 91**:** 10365-10369.
44. Mitsiades CS, Mitsiades NS, McMullan CJ, Poulaki V, Shringarpure R, Akiyama M, Hideshima T, Chauhan D, Joseph M, Libermann TA, Garcia-Echeverria C, Pearson MA *et al*. Inhibition of the insulin-like growth factor receptor-1 tyrosine kinase activity as a therapeutic strategy for multiple myeloma, other hematologic malignancies, and solid tumors. Cancer Cell. 2004; 5**:** 221-230.
45. Garcia-Echeverria C, Pearson MA, Marti A, Meyer T, Mestan J, Zimmermann J, Gao J, Brueggen J, Capraro HG, Cozens R, Evans DB, Fabbro D *et al*. In vivo antitumor activity of nvp-aew541-a novel, potent, and selective inhibitor of the igf-ir kinase. Cancer Cell. 2004; 5**:** 231-239.
46. Carboni JM, Wittman M, Yang Z, Lee F, Greer A, Hurlburt W, Hillerman S, Cao C, Cantor GH, Dell-John J, Chen C, Discenza L *et al*. Bms-754807, a small molecule inhibitor of insulin-like growth factor-1r/ir. Mol Cancer Ther. 2009; 8**:** 3341-3349.
47. Hou X, Huang F, Macedo LF, Harrington SC, Reeves KA, Greer A, Finckenstein FG, Brodie A, Gottardis MM, Carboni JM, Haluska P. Dual igf-1r/insr inhibitor bms-754807 synergizes with hormonal agents in treatment of estrogen-dependent breast cancer. Cancer Res. 2011; 71**:** 7597-7607.
48. Durfort T, Tkach M, Meschaninova MI, Rivas MA, Elizalde PV, Venyaminova AG, Schillaci R, Francois JC. Small interfering rna targeted to igf-ir delays tumor growth and induces proinflammatory cytokines in a mouse breast cancer model. PLoS One. 2012; 7**:** e29213.
49. Whitehead KA, Langer R, Anderson DG. Knocking down barriers: Advances in sirna delivery. Nat Rev Drug Discov. 2009; 8**:** 129-138.
50. Jones RA, Campbell CI, Wood GA, Petrik JJ, Moorehead RA. Reversibility and recurrence of igf-ir-induced mammary tumors. Oncogene. 2009; 28**:** 2152-2162.
51. Shen K, Liang Q, Xu K, Cui D, Jiang L, Yin P, Lu Y, Li Q, Liu J. Mir-139 inhibits invasion and metastasis of colorectal cancer by targeting the type i insulin-like growth factor receptor. Biochem Pharmacol. 2012; 84**:** 320-330.

52. Kong KL, Kwong DL, Chan TH, Law SY, Chen L, Li Y, Qin YR, Guan XY. Microrna-375 inhibits tumour growth and metastasis in oesophageal squamous cell carcinoma through repressing insulin-like growth factor 1 receptor. Gut. 2012; 61**:** 33-42.
53. Kalebic T, Blakesley V, Slade C, Plasschaert S, Leroith D, Helman LJ. Expression of a kinase-deficient igf-i-r suppresses tumorigenicity of rhabdomyosarcoma cells constitutively expressing a wild type igf-i-r. Int J Cancer. 1998; 76**:** 223-227.
54. Becker MA, Ibrahim YH, Cui X, Lee AV, Yee D. The igf pathway regulates eralpha through a s6k1-dependent mechanism in breast cancer cells. Mol Endocrinol. 2011; 25**:** 516-528.
55. Liu H, Scholz C, Zang C, Schefe JH, Habbel P, Regierer AC, Schulz CO, Possinger K, Eucker J. Metformin and the mtor inhibitor everolimus (rad001) sensitize breast cancer cells to the cytotoxic effect of chemotherapeutic drugs in vitro. Anticancer Res. 2012; 32**:** 1627-1637.
56. Noh WC, Mondesire WH, Peng J, Jian W, Zhang H, Dong J, Mills GB, Hung MC, Meric-Bernstam F. Determinants of rapamycin sensitivity in breast cancer cells. Clin Cancer Res. 2004; 10**:** 1013-1023.
57. Rivera VM, Squillace RM, Miller D, Berk L, Wardwell SD, Ning Y, Pollock R, Narasimhan NI, Iuliucci JD, Wang F, Clackson T. Ridaforolimus (ap23573; mk-8669), a potent mtor inhibitor, has broad antitumor activity and can be optimally administered using intermittent dosing regimens. Mol Cancer Ther. 2011; 10**:** 1059-1071.
58. Yu K, Toral-Barza L, Discafani C, Zhang WG, Skotnicki J, Frost P, Gibbons JJ. Mtor, a novel target in breast cancer: The effect of cci-779, an mtor inhibitor, in preclinical models of breast cancer. Endocr Relat Cancer. 2001; 8**:** 249-258.
59. Bachelot T, Bourgier C, Cropet C, Ray-Coquard I, Ferrero JM, Freyer G, Abadie-Lacourtoisie S, Eymard JC, Debled M, Spaeth D, Legouffe E, Allouache D *et al*. Randomized phase ii trial of everolimus in combination with tamoxifen in patients with hormone receptor-positive, human epidermal growth factor receptor 2-negative metastatic breast cancer with prior exposure to aromatase inhibitors: A gineco study. J Clin Oncol. 2012; 30**:** 2718-2724.
60. Baselga J, Campone M, Piccart M, Burris HA, 3rd, Rugo HS, Sahmoud T, Noguchi S, Gnant M, Pritchard KI, Lebrun F, Beck JT, Ito Y *et al*. Everolimus in postmenopausal hormone-receptor-positive advanced breast cancer. N Engl J Med. 2012; 366**:** 520-529.
61. Harrington LS, Findlay GM, Gray A, Tolkacheva T, Wigfield S, Rebholz H, Barnett J, Leslie NR, Cheng S, Shepherd PR, Gout I, Downes CP *et al*. The tsc1-2 tumor suppressor controls insulin-pi3k signaling via regulation of irs proteins. J Cell Biol. 2004; 166**:** 213-223.
62. Shi Y, Yan H, Frost P, Gera J, Lichtenstein A. Mammalian target of rapamycin inhibitors activate the akt kinase in multiple myeloma cells by up-regulating the insulin-like growth factor receptor/insulin receptor substrate-1/phosphatidylinositol 3-kinase cascade. Mol Cancer Ther. 2005; 4**:** 1533-1540.
63. Clark AS, West K, Streicher S, Dennis PA. Constitutive and inducible akt activity promotes resistance to chemotherapy, trastuzumab, or tamoxifen in breast cancer cells. Mol Cancer Ther. 2002; 1**:** 707-717.

64. Casa AJ, Potter AS, Malik S, Lazard Z, Kuiatse I, Kim HT, Tsimelzon A, Creighton CJ, Hilsenbeck SG, Brown PH, Oesterreich S, Lee AV. Estrogen and insulin-like growth factor-i (igf-i) independently down-regulate critical repressors of breast cancer growth. Breast Cancer Res Treat. 2012; 132**:** 61-73.
65. Brachmann SM, Hofmann I, Schnell C, Fritsch C, Wee S, Lane H, Wang S, Garcia-Echeverria C, Maira SM. Specific apoptosis induction by the dual pi3k/mtor inhibitor nvp-bez235 in her2 amplified and pik3ca mutant breast cancer cells. Proc Natl Acad Sci U S A. 2009; 106**:** 22299-22304.
66. O'Reilly KE, Rojo F, She QB, Solit D, Mills GB, Smith D, Lane H, Hofmann F, Hicklin DJ, Ludwig DL, Baselga J, Rosen N. Mtor inhibition induces upstream receptor tyrosine kinase signaling and activates akt. Cancer Res. 2006; 66**:** 1500-1508.
67. Wan X, Harkavy B, Shen N, Grohar P, Helman LJ. Rapamycin induces feedback activation of akt signaling through an igf-1r-dependent mechanism. Oncogene. 2007; 26**:** 1932-1940.
68. Leung E, Kim JE, Rewcastle GW, Finlay GJ, Baguley BC. Comparison of the effects of the pi3k/mtor inhibitors nvp-bez235 and gsk2126458 on tamoxifen-resistant breast cancer cells. Cancer Biol Ther. 2011; 11**:** 938-946.
69. Cho DC, Cohen MB, Panka DJ, Collins M, Ghebremichael M, Atkins MB, Signoretti S, Mier JW. The efficacy of the novel dual pi3-kinase/mtor inhibitor nvp-bez235 compared with rapamycin in renal cell carcinoma. Clin Cancer Res. 2010; 16**:** 3628-3638.
70. Hamelers IH, Steenbergh PH. Interactions between estrogen and insulin-like growth factor signaling pathways in human breast tumor cells. Endocr Relat Cancer. 2003; 10**:** 331-345.
71. Tremblay GB, Tremblay A, Copeland NG, Gilbert DJ, Jenkins NA, Labrie F, Giguere V. Cloning, chromosomal localization, and functional analysis of the murine estrogen receptor beta. Mol Endocrinol. 1997; 11**:** 353-365.
72. Campbell RA, Bhat-Nakshatri P, Patel NM, Constantinidou D, Ali S, Nakshatri H. Phosphatidylinositol 3-kinase/akt-mediated activation of estrogen receptor alpha: A new model for anti-estrogen resistance. J Biol Chem. 2001; 276**:** 9817-9824.
73. Martin MB, Franke TF, Stoica GE, Chambon P, Katzenellenbogen BS, Stoica BA, McLemore MS, Olivo SE, Stoica A. A role for akt in mediating the estrogenic functions of epidermal growth factor and insulin-like growth factor i. Endocrinology. 2000; 141**:** 4503-4511.
74. Lee AV, Darbre P, King RJ. Processing of insulin-like growth factor-ii (igf-ii) by human breast cancer cells. Mol Cell Endocrinol. 1994; 99**:** 211-220.
75. Lee AV, Jackson JG, Gooch JL, Hilsenbeck SG, Coronado-Heinsohn E, Osborne CK, Yee D. Enhancement of insulin-like growth factor signaling in human breast cancer: Estrogen regulation of insulin receptor substrate-1 expression in vitro and in vivo. Mol Endocrinol. 1999; 13**:** 787-796.
76. Huynh H, Yang X, Pollak M. Estradiol and antiestrogens regulate a growth inhibitory insulin-like growth factor binding protein 3 autocrine loop in human breast cancer cells. J Biol Chem. 1996; 271**:** 1016-1021.
77. Mathieu M, Vignon F, Capony F, Rochefort H. Estradiol down-regulates the mannose-6-phosphate/insulin-like growth factor-ii receptor gene and induces cathepsin-d

in breast cancer cells: A receptor saturation mechanism to increase the secretion of lysosomal proenzymes. Mol Endocrinol. 1991; 5**:** 815-822.
78. Song RX, Chen Y, Zhang Z, Bao Y, Yue W, Wang JP, Fan P, Santen RJ. Estrogen utilization of igf-1-r and egf-r to signal in breast cancer cells. J Steroid Biochem Mol Biol. 2010; 118**:** 219-230.
79. Drury SC, Detre S, Leary A, Salter J, Reis-Filho J, Barbashina V, Marchio C, Lopez-Knowles E, Ghazoui Z, Habben K, Arbogast S, Johnston S *et al*. Changes in breast cancer biomarkers in the igf1r/pi3k pathway in recurrent breast cancer after tamoxifen treatment. Endocr Relat Cancer. 2011; 18**:** 565-577.
80. Tan M, Yu D. Molecular mechanisms of erbb2-mediated breast cancer chemoresistance. Adv Exp Med Biol. 2007; 608**:** 119-129.
81. Nahta R, Yuan LX, Zhang B, Kobayashi R, Esteva FJ. Insulin-like growth factor-i receptor/human epidermal growth factor receptor 2 heterodimerization contributes to trastuzumab resistance of breast cancer cells. Cancer Res. 2005; 65**:** 11118-11128.
82. Slamon DJ, Clark GM, Wong SG, Levin WJ, Ullrich A, McGuire WL. Human breast cancer: Correlation of relapse and survival with amplification of the her-2/neu oncogene. Science. 1987; 235**:** 177-182.
83. Carter P, Presta L, Gorman CM, Ridgway JB, Henner D, Wong WL, Rowland AM, Kotts C, Carver ME, Shepard HM. Humanization of an anti-p185her2 antibody for human cancer therapy. Proc Natl Acad Sci U S A. 1992; 89**:** 4285-4289.
84. Esteva FJ, Valero V, Booser D, Guerra LT, Murray JL, Pusztai L, Cristofanilli M, Arun B, Esmaeli B, Fritsche HA, Sneige N, Smith TL *et al*. Phase ii study of weekly docetaxel and trastuzumab for patients with her-2-overexpressing metastatic breast cancer. J Clin Oncol. 2002; 20**:** 1800-1808.
85. Albanell J, Baselga J. Unraveling resistance to trastuzumab (herceptin): Insulin-like growth factor-i receptor, a new suspect. J Natl Cancer Inst. 2001; 93**:** 1830-1832.
86. Browne BC, Crown J, Venkatesan N, Duffy MJ, Clynes M, Slamon D, O'Donovan N. Inhibition of igf1r activity enhances response to trastuzumab in her-2-positive breast cancer cells. Ann Oncol. 2011; 22**:** 68-73.
87. Rowe DL, Ozbay T, Bender LM, Nahta R. Nordihydroguaiaretic acid, a cytotoxic insulin-like growth factor-i receptor/her2 inhibitor in trastuzumab-resistant breast cancer. Mol Cancer Ther. 2008; 7**:** 1900-1908.
88. Zeng X, Zhang H, Oh A, Zhang Y, Yee D. Enhancement of doxorubicin cytotoxicity of human cancer cells by tyrosine kinase inhibition of insulin receptor and type i igf receptor. Breast Cancer Res Treat. 2012; 133**:** 117-126.
89. Ma J, Giovannucci E, Pollak M, Leavitt A, Tao Y, Gaziano JM, Stampfer MJ. A prospective study of plasma c-peptide and colorectal cancer risk in men. J Natl Cancer Inst. 2004; 96**:** 546-553.
90. Yee D. Targeting insulin-like growth factor pathways. Br J Cancer. 2006; 94**:** 465-468.
91. Lee AV, Yee D. Targeting igf-1r: At a crossroad. Oncology (Williston Park). 2011; 25**:** 535-536; discussion 551.

92. Barker AD, Sigman CC, Kelloff GJ, Hylton NM, Berry DA, Esserman LJ. I-spy 2: An adaptive breast cancer trial design in the setting of neoadjuvant chemotherapy. Clin Pharmacol Ther. 2009; 86**:** 97-100.
93. Algire C, Moiseeva O, Deschenes-Simard X, Amrein L, Petruccelli L, Birman E, Viollet B, Ferbeyre G, Pollak MN. Metformin reduces endogenous reactive oxygen species and associated DNA damage. Cancer Prev Res (Phila). 2012; 5**:** 536-543.
94. Litzenburger BC, Creighton CJ, Tsimelzon A, Chan BT, Hilsenbeck SG, Wang T, Carboni JM, Gottardis MM, Huang F, Chang JC, Lewis MT, Rimawi MF *et al*. High igf-ir activity in triple-negative breast cancer cell lines and tumorgrafts correlates with sensitivity to anti-igf-ir therapy. Clin Cancer Res. 2011; 17**:** 2314-2327.
95. Huang F, Greer A, Hurlburt W, Han X, Hafezi R, Wittenberg GM, Reeves K, Chen J, Robinson D, Li A, Lee FY, Gottardis MM *et al*. The mechanisms of differential sensitivity to an insulin-like growth factor-1 receptor inhibitor (bms-536924) and rationale for combining with egfr/her2 inhibitors. Cancer Res. 2009; 69**:** 161-170.
96. Pitts TM, Tan AC, Kulikowski GN, Tentler JJ, Brown AM, Flanigan SA, Leong S, Coldren CD, Hirsch FR, Varella-Garcia M, Korch C, Eckhardt SG. Development of an integrated genomic classifier for a novel agent in colorectal cancer: Approach to individualized therapy in early development. Clin Cancer Res. 2010; 16**:** 3193-3204.
97. Carboni JM, Lee AV, Hadsell DL, Rowley BR, Lee FY, Bol DK, Camuso AE, Gottardis M, Greer AF, Ho CP, Hurlburt W, Li A *et al*. Tumor development by transgenic expression of a constitutively active insulin-like growth factor i receptor. Cancer Res. 2005; 65**:** 3781-3787.
98. Shaw LM. Identification of insulin receptor substrate 1 (irs-1) and irs-2 as signaling intermediates in the alpha6beta4 integrin-dependent activation of phosphoinositide 3-oh kinase and promotion of invasion. Mol Cell Biol. 2001; 21**:** 5082-5093.
99. Jackson JG, Zhang X, Yoneda T, Yee D. Regulation of breast cancer cell motility by insulin receptor substrate-2 (irs-2) in metastatic variants of human breast cancer cell lines. Oncogene. 2001; 20**:** 7318-7325.
100. Jackson JG, White MF, Yee D. Insulin receptor substrate-1 is the predominant signaling molecule activated by insulin-like growth factor-i, insulin, and interleukin-4 in estrogen receptor-positive human breast cancer cells. J Biol Chem. 1998; 273**:** 9994-10003.
101. Byron SA, Horwitz KB, Richer JK, Lange CA, Zhang X, Yee D. Insulin receptor substrates mediate distinct biological responses to insulin-like growth factor receptor activation in breast cancer cells. Br J Cancer. 2006; 95**:** 1220-1228.
102. Gualberto A, Hixon ML, Karp DD, Li D, Green S, Dolled-Filhart M, Paz-Ares LG, Novello S, Blakely J, Langer CJ, Pollak MN. Pre-treatment levels of circulating free igf-1 identify nsclc patients who derive clinical benefit from figitumumab. Br J Cancer. 2011; 104**:** 68-74.
103. Asmane I, Watkin E, Alberti L, Duc A, Marec-Berard P, Ray-Coquard I, Cassier P, Decouvelaere AV, Ranchere D, Kurtz JE, Bergerat JP, Blay JY. Insulin-like growth factor type 1 receptor (igf-1r) exclusive nuclear staining: A predictive biomarker for igf-1r monoclonal antibody (ab) therapy in sarcomas. Eur J Cancer. 2012.

104. Becker MA, Hou X, Harrington SC, Weroha SJ, Gonzalez SE, Jacob KA, Carboni JM, Gottardis MM, Haluska P. Igfbp ratio confers resistance to igf targeting and correlates with increased invasion and poor outcome in breast tumors. Clin Cancer Res. 2012; 18**:** 1808-1817.
105. Yang Y, Yee D. Targeting insulin and insulin-like growth factor signaling in breast cancer. J Mammary Gland Biol Neoplasia. 2012; 17**:** 251-261.
106. Yee D. A tale of two receptors: Insulin and insulin-like growth factor signaling in cancer. Clin Cancer Res. 2015; 21**:** 667-669.
107. Reuveni H, Flashner-Abramson E, Steiner L, Makedonski K, Song R, Shir A, Herlyn M, Bar-Eli M, Levitzki A. Therapeutic destruction of insulin receptor substrates for cancer treatment. Cancer Res. 2013; 73**:** 4383-4394.
108. Ibuki N, Ghaffari M, Reuveni H, Pandey M, Fazli L, Azuma H, Gleave ME, Levitzki A, Cox ME. The tyrphostin nt157 suppresses insulin receptor substrates and augments therapeutic response of prostate cancer. Mol Cancer Ther. 2014; 13**:** 2827-2839.
109. Nieman MT, Prudoff RS, Johnson KR, Wheelock MJ. N-cadherin promotes motility in human breast cancer cells regardless of their e-cadherin expression. J Cell Biol. 1999; 147**:** 631-644.
110. Mendez MG, Kojima S, Goldman RD. Vimentin induces changes in cell shape, motility, and adhesion during the epithelial to mesenchymal transition. FASEB J. 2010; 24**:** 1838-1851.
111. Tian J, Berton TR, Shirley SH, Lambertz I, Gimenez-Conti IB, DiGiovanni J, Korach KS, Conti CJ, Fuchs-Young R. Developmental stage determines estrogen receptor alpha expression and non-genomic mechanisms that control igf-1 signaling and mammary proliferation in mice. J Clin Invest. 2012; 122**:** 192-204.
112. Molloy CA, May FE, Westley BR. Insulin receptor substrate-1 expression is regulated by estrogen in the mcf-7 human breast cancer cell line. J Biol Chem. 2000; 275**:** 12565-12571.
113. Gao Q, Patani N, Dunbier AK, Ghazoui Z, Zvelebil M, Martin LA, Dowsett M. Effect of aromatase inhibition on functional gene modules in estrogen receptor-positive breast cancer and their relationship with antiproliferative response. Clin Cancer Res. 2014; 20**:** 2485-2494.
114. Yang Y, Yee D. Igf-i regulates redox status in breast cancer cells by activating the amino acid transport molecule xc. Cancer Res. 2014; 74**:** 2295-2305.
115. Wander SA, Hennessy BT, Slingerland JM. Next-generation mtor inhibitors in clinical oncology: How pathway complexity informs therapeutic strategy. J Clin Invest. 2011; 121**:** 1231-1241.
116. Vignot S, Faivre S, Aguirre D, Raymond E. Mtor-targeted therapy of cancer with rapamycin derivatives. Ann Oncol. 2005; 16**:** 525-537.
117. Tremblay F, Brule S, Hee Um S, Li Y, Masuda K, Roden M, Sun XJ, Krebs M, Polakiewicz RD, Thomas G, Marette A. Identification of irs-1 ser-1101 as a target of s6k1 in nutrient- and obesity-induced insulin resistance. Proc Natl Acad Sci U S A. 2007; 104**:** 14056-14061.
118. Gibson SL, Ma Z, Shaw LM. Divergent roles for irs-1 and irs-2 in breast cancer metastasis. Cell Cycle. 2007; 6**:** 631-637.

119. Yee D. Insulin-like growth factor receptor inhibitors: Baby or the bathwater? J Natl Cancer Inst. 2012; 104**:** 975-981.
120. Lovly CM, McDonald NT, Chen H, Ortiz-Cuaran S, Heukamp LC, Yan Y, Florin A, Ozretic L, Lim D, Wang L, Chen Z, Chen X *et al*. Rationale for co-targeting igf-1r and alk in alk fusion-positive lung cancer. Nat Med. 2014; 20**:** 1027-1034.
121. Bosch A, Li Z, Bergamaschi A, Ellis H, Toska E, Prat A, Tao JJ, Spratt DE, Viola-Villegas NT, Castel P, Minuesa G, Morse N *et al*. Pi3k inhibition results in enhanced estrogen receptor function and dependence in hormone receptor-positive breast cancer. Sci Transl Med. 2015; 7**:** 283-251.
122. http://www.oncomine.org.
123. Gyorffy B, Lanczky A, Eklund AC, Denkert C, Budczies J, Li Q, Szallasi Z. An online survival analysis tool to rapidly assess the effect of 22,277 genes on breast cancer prognosis using microarray data of 1,809 patients. Breast Cancer Res Treat. 2010; 123**:** 725-731.
124. Sachdev D, Yee D. The igf system and breast cancer. Endocr Relat Cancer. 2001; 8**:** 197-209.
125. Taniguchi CM, Emanuelli B, Kahn CR. Critical nodes in signalling pathways: Insights into insulin action. Nat Rev Mol Cell Biol. 2006; 7**:** 85-96.
126. Kaufman PA, Ferrero JM, Bourgeois H, Kennecke H, De Boer R, Jacot W, McGreivy J, Suzuki S, Loh E, Robertson J. A randomized, double-blind, placebo-controlled, phase 2 study of amg 479 with exemestane (e) or fulvestrant (f) in postmenopausal women with hormone-receptor positive (hr+) metastatic (m) or locally advanced (la) breast cancer (bc). Cancer Res. 2010; 70.
127. Yang Y, Yee D. Targeting insulin and insulin-like growth factor signaling in breast cancer. J Mammary Gland Biol Neoplasia. 2012.
128. Lo M, Wang YZ, Gout PW. The x(c)- cystine/glutamate antiporter: A potential target for therapy of cancer and other diseases. J Cell Physiol. 2008; 215**:** 593-602.
129. Vaughn AE, Deshmukh M. Glucose metabolism inhibits apoptosis in neurons and cancer cells by redox inactivation of cytochrome c. Nat Cell Biol. 2008; 10**:** 1477-1483.
130. Sartorius CA, Groshong SD, Miller LA, Powell RL, Tung L, Takimoto GS, Horwitz KB. New t47d breast cancer cell lines for the independent study of progesterone b- and a-receptors: Only antiprogestin-occupied b-receptors are switched to transcriptional agonists by camp. Cancer Res. 1994; 54**:** 3868-3877.
131. Trachootham D, Alexandre J, Huang P. Targeting cancer cells by ros-mediated mechanisms: A radical therapeutic approach? Nat Rev Drug Discov. 2009; 8**:** 579-591.
132. Cairns RA, Harris IS, Mak TW. Regulation of cancer cell metabolism. Nat Rev Cancer. 2011; 11**:** 85-95.
133. Ishimoto T, Nagano O, Yae T, Tamada M, Motohara T, Oshima H, Oshima M, Ikeda T, Asaba R, Yagi H, Masuko T, Shimizu T *et al*. Cd44 variant regulates redox status in cancer cells by stabilizing the xct subunit of system xc(-) and thereby promotes tumor growth. Cancer Cell. 2011; 19**:** 387-400.
134. Trachootham D, Lu W, Ogasawara MA, Nilsa RD, Huang P. Redox regulation of cell survival. Antioxid Redox Signal. 2008; 10**:** 1343-1374.

135. Schneider BL, Kulesz-Martin M. Destructive cycles: The role of genomic instability and adaptation in carcinogenesis. Carcinogenesis. 2004; 25**:** 2033-2044.
136. Chen EI, Hewel J, Krueger JS, Tiraby C, Weber MR, Kralli A, Becker K, Yates JR, 3rd, Felding-Habermann B. Adaptation of energy metabolism in breast cancer brain metastases. Cancer Res. 2007; 67**:** 1472-1486.
137. Sullivan R, Graham CH. Chemosensitization of cancer by nitric oxide. Curr Pharm Des. 2008; 14**:** 1113-1123.
138. Sato H, Shiiya A, Kimata M, Maebara K, Tamba M, Sakakura Y, Makino N, Sugiyama F, Yagami K, Moriguchi T, Takahashi S, Bannai S. Redox imbalance in cystine/glutamate transporter-deficient mice. J Biol Chem. 2005; 280**:** 37423-37429.
139. Chen RS, Song YM, Zhou ZY, Tong T, Li Y, Fu M, Guo XL, Dong LJ, He X, Qiao HX, Zhan QM, Li W. Disruption of xct inhibits cancer cell metastasis via the caveolin-1/beta-catenin pathway. Oncogene. 2009; 28**:** 599-609.
140. Huang Y, Dai Z, Barbacioru C, Sadee W. Cystine-glutamate transporter slc7a11 in cancer chemosensitivity and chemoresistance. Cancer Res. 2005; 65**:** 7446-7454.
141. Pham AN, Blower PE, Alvarado O, Ravula R, Gout PW, Huang Y. Pharmacogenomic approach reveals a role for the x(c)- cystine/glutamate antiporter in growth and celastrol resistance of glioma cell lines. J Pharmacol Exp Ther. 2010; 332**:** 949-958.
142. Griffith OW, Meister A. Potent and specific inhibition of glutathione synthesis by buthionine sulfoximine (s-n-butyl homocysteine sulfoximine). J Biol Chem. 1979; 254**:** 7558-7560.
143. Leach JK, Van Tuyle G, Lin PS, Schmidt-Ullrich R, Mikkelsen RB. Ionizing radiation-induced, mitochondria-dependent generation of reactive oxygen/nitrogen. Cancer Res. 2001; 61**:** 3894-3901.
144. Zafarullah M, Li WQ, Sylvester J, Ahmad M. Molecular mechanisms of n-acetylcysteine actions. Cell Mol Life Sci. 2003; 60**:** 6-20.
145. Wiemer EA. Stressed tumor cell, chemosensitized cancer. Nat Med. 2011; 17**:** 1552-1554.
146. Sheridan C, Kishimoto H, Fuchs RK, Mehrotra S, Bhat-Nakshatri P, Turner CH, Goulet R, Jr., Badve S, Nakshatri H. Cd44+/cd24- breast cancer cells exhibit enhanced invasive properties: An early step necessary for metastasis. Breast Cancer Res. 2006; 8**:** R59.
147. Timmerman LA, Holton T, Yuneva M, Louie RJ, Padro M, Daemen A, Hu M, Chan DA, Ethier SP, van 't Veer LJ, Polyak K, McCormick F *et al*. Glutamine sensitivity analysis identifies the xct antiporter as a common triple-negative breast tumor therapeutic target. Cancer Cell. 2013.
148. Reuveni H, Flashner-Abramson E, Steiner L, Makedonski K, Song R, Shir A, Herlyn M, Bar-Eli M, Levitzki A. Therapeutic destruction of insulin receptor substrates for cancer treatment. Cancer Res. 2013.
149. Sachdev D, Singh R, Fujita-Yamaguchi Y, Yee D. Down-regulation of insulin receptor by antibodies against the type i insulin-like growth factor receptor: Implications for anti-insulin-like growth factor therapy in breast cancer. Cancer Res. 2006; 66**:** 2391-2402.

150. Koglin N, Mueller A, Berndt M, Schmitt-Willich H, Toschi L, Stephens AW, Gekeler V, Friebe M, Dinkelborg LM. Specific pet imaging of xc- transporter activity using a (1)(8)f-labeled glutamate derivative reveals a dominant pathway in tumor metabolism. Clin Cancer Res. 2011; 17**:** 6000-6011.
151. Baek S, Choi CM, Ahn SH, Lee JW, Gong G, Ryu JS, Oh SJ, Bacher-Stier C, Fels L, Koglin N, Hultsch C, Schatz CA *et al*. Exploratory clinical trial of (4s)-4-(3-[18f]fluoropropyl)-l-glutamate for imaging xc- transporter using positron emission tomography in patients with non-small cell lung or breast cancer. Clin Cancer Res. 2012; 18**:** 5427-5437.
152. Mitsuishi Y, Taguchi K, Kawatani Y, Shibata T, Nukiwa T, Aburatani H, Yamamoto M, Motohashi H. Nrf2 redirects glucose and glutamine into anabolic pathways in metabolic reprogramming. Cancer Cell. 2012; 22**:** 66-79.
153. Winer EP, Hudis C, Burstein HJ, Wolff AC, Pritchard KI, Ingle JN, Chlebowski RT, Gelber R, Edge SB, Gralow J, Cobleigh MA, Mamounas EP *et al*. American society of clinical oncology technology assessment on the use of aromatase inhibitors as adjuvant therapy for postmenopausal women with hormone receptor-positive breast cancer: Status report 2004. J Clin Oncol. 2005; 23**:** 619-629.
154. Vogel CL, Cobleigh MA, Tripathy D, Gutheil JC, Harris LN, Fehrenbacher L, Slamon DJ, Murphy M, Novotny WF, Burchmore M, Shak S, Stewart SJ *et al*. Efficacy and safety of trastuzumab as a single agent in first-line treatment of her2-overexpressing metastatic breast cancer. J Clin Oncol. 2002; 20**:** 719-726.
155. Gorrini C, Gang BP, Bassi C, Wakeham A, Baniasadi SP, Hao Z, Li WY, Cescon DW, Li YT, Molyneux S, Penrod N, Lupien M *et al*. Estrogen controls the survival of brca1-deficient cells via a pi3k-nrf2-regulated pathway. Proc Natl Acad Sci U S A. 2014; 111**:** 4472-4477.
156. Cook KL, Clarke PA, Parmar J, Hu R, Schwartz-Roberts JL, Abu-Asab M, Warri A, Baumann WT, Clarke R. Knockdown of estrogen receptor-alpha induces autophagy and inhibits antiestrogen-mediated unfolded protein response activation, promoting ros-induced breast cancer cell death. FASEB J. 2014; 28**:** 3891-3905.
157. Fagan DH, Yee D. Crosstalk between igf1r and estrogen receptor signaling in breast cancer. J Mammary Gland Biol Neoplasia. 2008; 13**:** 423-429.
158. Timmerman LA, Holton T, Yuneva M, Louie RJ, Padro M, Daemen A, Hu M, Chan DA, Ethier SP, van 't Veer LJ, Polyak K, McCormick F *et al*. Glutamine sensitivity analysis identifies the xct antiporter as a common triple-negative breast tumor therapeutic target. Cancer Cell. 2013; 24**:** 450-465.
159. Diehn M, Cho RW, Lobo NA, Kalisky T, Dorie MJ, Kulp AN, Qian D, Lam JS, Ailles LE, Wong M, Joshua B, Kaplan MJ *et al*. Association of reactive oxygen species levels and radioresistance in cancer stem cells. Nature. 2009; 458**:** 780-783.
160. Sasaki H, Sato H, Kuriyama-Matsumura K, Sato K, Maebara K, Wang H, Tamba M, Itoh K, Yamamoto M, Bannai S. Electrophile response element-mediated induction of the cystine/glutamate exchange transporter gene expression. J Biol Chem. 2002; 277**:** 44765-44771.

161. Wang XJ, Hayes JD, Henderson CJ, Wolf CR. Identification of retinoic acid as an inhibitor of transcription factor nrf2 through activation of retinoic acid receptor alpha. Proc Natl Acad Sci U S A. 2007; 104**:** 19589-19594.
162. Phillips TM, McBride WH, Pajonk F. The response of cd24(-/low)/cd44+ breast cancer-initiating cells to radiation. J Natl Cancer Inst. 2006; 98**:** 1777-1785.
163. Budczies J, Brockmoller SF, Muller BM, Barupal DK, Richter-Ehrenstein C, Kleine-Tebbe A, Griffin JL, Oresic M, Dietel M, Denkert C, Fiehn O. Comparative metabolomics of estrogen receptor positive and estrogen receptor negative breast cancer: Alterations in glutamine and beta-alanine metabolism. J Proteomics. 2013; 94**:** 279-288.
164. Lee GY, Kenny PA, Lee EH, Bissell MJ. Three-dimensional culture models of normal and malignant breast epithelial cells. Nat Methods. 2007; 4**:** 359-365.
165. Feral CC, Nishiya N, Fenczik CA, Stuhlmann H, Slepak M, Ginsberg MH. Cd98hc (slc3a2) mediates integrin signaling. Proc Natl Acad Sci U S A. 2005; 102**:** 355-360.
166. Ohgimoto S, Tabata N, Suga S, Nishio M, Ohta H, Tsurudome M, Komada H, Kawano M, Watanabe N, Ito Y. Molecular characterization of fusion regulatory protein-1 (frp-1) that induces multinucleated giant cell formation of monocytes and hiv gp160-mediated cell fusion. Frp-1 and 4f2/cd98 are identical molecules. J Immunol. 1995; 155**:** 3585-3592.
167. Cantor J, Browne CD, Ruppert R, Feral CC, Fassler R, Rickert RC, Ginsberg MH. Cd98hc facilitates b cell proliferation and adaptive humoral immunity. Nat Immunol. 2009; 10**:** 412-419.
168. Kanai Y, Segawa H, Miyamoto K, Uchino H, Takeda E, Endou H. Expression cloning and characterization of a transporter for large neutral amino acids activated by the heavy chain of 4f2 antigen (cd98). J Biol Chem. 1998; 273**:** 23629-23632.
169. Mastroberardino L, Spindler B, Pfeiffer R, Skelly PJ, Loffing J, Shoemaker CB, Verrey F. Amino-acid transport by heterodimers of 4f2hc/cd98 and members of a permease family. Nature. 1998; 395**:** 288-291.
170. Nicklin P, Bergman P, Zhang B, Triantafellow E, Wang H, Nyfeler B, Yang H, Hild M, Kung C, Wilson C, Myer VE, MacKeigan JP *et al*. Bidirectional transport of amino acids regulates mtor and autophagy. Cell. 2009; 136**:** 521-534.
171. Ring BZ, Seitz RS, Beck R, Shasteen WJ, Tarr SM, Cheang MC, Yoder BJ, Budd GT, Nielsen TO, Hicks DG, Estopinal NC, Ross DT. Novel prognostic immunohistochemical biomarker panel for estrogen receptor-positive breast cancer. J Clin Oncol. 2006; 24**:** 3039-3047.
172. Bartlett JM, Bloom KJ, Piper T, Lawton TJ, van de Velde CJ, Ross DT, Ring BZ, Seitz RS, Beck RA, Hasenburg A, Kieback D, Putter H *et al*. Mammostrat as an immunohistochemical multigene assay for prediction of early relapse risk in the tamoxifen versus exemestane adjuvant multicenter trial pathology study. J Clin Oncol. 2012; 30**:** 4477-4484.
173. Robe PA, Martin DH, Nguyen-Khac MT, Artesi M, Deprez M, Albert A, Vanbelle S, Califice S, Bredel M, Bours V. Early termination of isrctn45828668, a phase 1/2 prospective, randomized study of sulfasalazine for the treatment of progressing malignant gliomas in adults. BMC Cancer. 2009; 9**:** 372.

174. Chung WJ, Sontheimer H. Sulfasalazine inhibits the growth of primary brain tumors independent of nuclear factor-kappab. J Neurochem. 2009; 110**:** 182-193.
175. Shukla K, Thomas AG, Ferraris DV, Hin N, Sattler R, Alt J, Rojas C, Slusher BS, Tsukamoto T. Inhibition of xc(-) transporter-mediated cystine uptake by sulfasalazine analogs. Bioorg Med Chem Lett. 2011; 21**:** 6184-6187.
176. Gross MI, Demo SD, Dennison JB, Chen L, Chernov-Rogan T, Goyal B, Janes JR, Laidig GJ, Lewis ER, Li J, Mackinnon AL, Parlati F *et al*. Antitumor activity of the glutaminase inhibitor cb-839 in triple-negative breast cancer. Mol Cancer Ther. 2014; 13**:** 890-901.
177. Dixon SJ, Lemberg KM, Lamprecht MR, Skouta R, Zaitsev EM, Gleason CE, Patel DN, Bauer AJ, Cantley AM, Yang WS, Morrison B, 3rd, Stockwell BR. Ferroptosis: An iron-dependent form of nonapoptotic cell death. Cell. 2012; 149**:** 1060-1072.
178. Dixon SJ, Patel DN, Welsch M, Skouta R, Lee ED, Hayano M, Thomas AG, Gleason CE, Tatonetti NP, Slusher BS, Stockwell BR. Pharmacological inhibition of cystine-glutamate exchange induces endoplasmic reticulum stress and ferroptosis. Elife. 2014; 3**:** e02523.